US009585577B2

(12) **United States Patent**
Banet et al.

(10) **Patent No.: US 9,585,577 B2**
(45) **Date of Patent: *Mar. 7, 2017**

(54) **BODY-WORN SYSTEM FOR CONTINUOUS, NONINVASIVE MEASUREMENT OF CARDIAC OUTPUT, STROKE VOLUME, CARDIAC POWER, AND BLOOD PRESSURE**

(75) Inventors: **Matt Banet**, Kihei, HI (US); **Isaac Henry**, La Mesa, CA (US); **Donald Bernstein**, Rancho Santa Fe, CA (US)

(73) Assignee: **SOTERA WIRELESS, INC.**, San Diego, CA (US)

(*) Notice: Subject to any disclaimer, the term of this patent is extended or adjusted under 35 U.S.C. 154(b) by 1099 days.

This patent is subject to a terminal disclaimer.

(21) Appl. No.: **13/338,248**

(22) Filed: **Dec. 28, 2011**

(65) **Prior Publication Data**

US 2014/0249442 A1 Sep. 4, 2014

Related U.S. Application Data

(60) Provisional application No. 61/427,756, filed on Dec. 28, 2010.

(51) **Int. Cl.**

A61B 5/0295	(2006.01)
A61B 5/01	(2006.01)
A61B 5/029	(2006.01)
A61B 5/053	(2006.01)
A61B 5/08	(2006.01)

(Continued)

(52) **U.S. Cl.**

CPC ***A61B 5/0295*** (2013.01); ***A61B 5/01*** (2013.01); ***A61B 5/021*** (2013.01); ***A61B 5/029*** (2013.01); ***A61B 5/0535*** (2013.01); ***A61B 5/0816*** (2013.01); ***A61B 5/1116*** (2013.01); ***A61B 5/14551*** (2013.01); ***A61B 5/6823*** (2013.01); ***A61B 5/746*** (2013.01); *A61B 5/681* (2013.01); *A61B 5/6824* (2013.01); *A61B 5/6826* (2013.01); *A61B 5/6833* (2013.01); *A61B 5/7239* (2013.01); *A61B 2562/04* (2013.01)

(58) **Field of Classification Search**

CPC A61B 5/029; A61B 5/0295; A61B 5/0261; A61B 5/0535; A61B 5/02416

USPC 600/526; 3/526

See application file for complete search history.

(56) **References Cited**

U.S. PATENT DOCUMENTS

4,263,918	A	4/1981	Swearingen et al.
4,270,547	A	6/1981	Steffen et al.

(Continued)

FOREIGN PATENT DOCUMENTS

EP	0443267	A1	8/1991
EP	0993803	A1	4/2000

(Continued)

OTHER PUBLICATIONS

Non-Final Office Action issued by the US Patent and Trademark Office on Aug. 30, 2012 in U.S. Appl. No. 12/469,202.

(Continued)

Primary Examiner — Christopher D Koharski
Assistant Examiner — Jeremiah Kimball
(74) *Attorney, Agent, or Firm* — Acuity Law Group, PC; Michael A. Whittaker

(57) **ABSTRACT**

The invention provides methods for measuring stroke volume from a patient using a transbrachial electro-velocimetry waveform measured using an impedance sensor together with a motion waveform measured using a motion sensor.

21 Claims, 38 Drawing Sheets

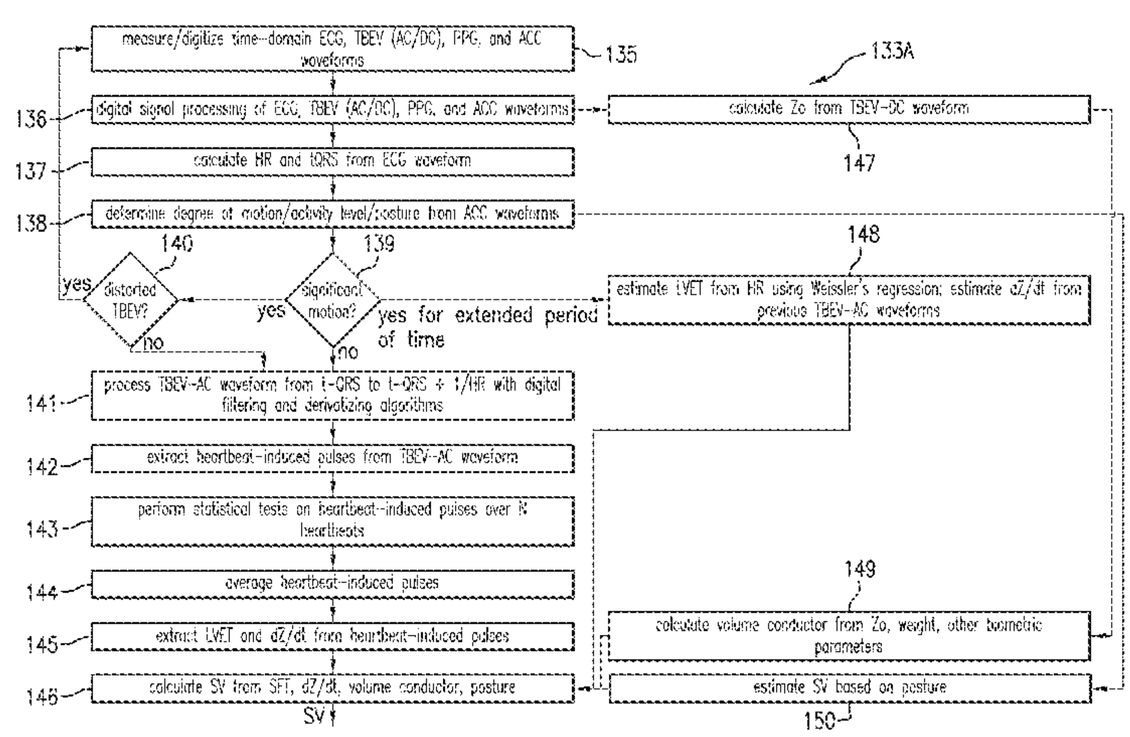

(51) **Int. Cl.**

A61B 5/11	(2006.01)
A61B 5/1455	(2006.01)
A61B 5/021	(2006.01)
A61B 5/00	(2006.01)

(56) **References Cited**

U.S. PATENT DOCUMENTS

4,305,400 A 12/1981 Logan
4,367,752 A 1/1983 Jimenez et al.
4,577,639 A 3/1986 Simon et al.
4,582,068 A 4/1986 Phillipps et al.
4,653,498 A 3/1987 New, Jr. et al.
4,710,164 A 12/1987 Levin et al.
4,722,351 A 2/1988 Phillipps et al.
4,802,486 A 2/1989 Goodman et al.
4,807,638 A 2/1989 Sramek
4,905,697 A 3/1990 Heggs et al.
5,025,791 A 6/1991 Niwa
5,140,990 A 8/1992 Jones et al.
5,190,038 A 3/1993 Polson et al.
5,197,489 A 3/1993 Conlan
5,247,931 A 9/1993 Norwood
5,316,008 A 5/1994 Suga et al.
5,339,818 A 8/1994 Baker et al.
5,435,315 A 7/1995 McPhee et al.
5,448,991 A 9/1995 Polson et al.
5,465,082 A 11/1995 Chaco
5,482,036 A 1/1996 Diab et al.
5,485,838 A 1/1996 Ukawa et al.
5,490,505 A 2/1996 Diab et al.
5,515,858 A 5/1996 Myllymaki
5,517,988 A 5/1996 Gerhard
5,524,637 A 6/1996 Erickson
5,549,650 A 8/1996 Bornzin et al.
5,575,284 A 11/1996 Athan et al.
5,577,508 A 11/1996 Medero
5,588,427 A 12/1996 Tien
5,593,431 A 1/1997 Sheldon
5,632,272 A 5/1997 Diab et al.
5,649,543 A 7/1997 Hosaka et al.
5,680,870 A 10/1997 Hood et al.
5,685,299 A 11/1997 Diab et al.
5,709,205 A 1/1998 Bukta
5,743,856 A 4/1998 Oka et al.
5,766,131 A 6/1998 Kondo et al.
5,769,785 A 6/1998 Diab et al.
5,800,349 A 9/1998 Isaacson et al.
5,820,550 A 10/1998 Polson et al.
5,848,373 A 12/1998 DeLorme et al.
5,853,370 A 12/1998 Chance et al.
5,857,975 A 1/1999 Golub
5,865,755 A 2/1999 Golub
5,865,756 A 2/1999 Peel, III
5,873,834 A 2/1999 Yanagi et al.
5,876,353 A 3/1999 Riff
5,895,359 A 4/1999 Peel, III
5,899,855 A 5/1999 Brown
5,913,827 A 6/1999 Gorman
5,919,141 A 7/1999 Money et al.
5,941,836 A 8/1999 Friedman
5,964,701 A 10/1999 Asada et al.
5,964,720 A 10/1999 Pelz
5,971,930 A 10/1999 Elghazzawi
6,002,952 A 12/1999 Diab et al.
6,011,985 A 1/2000 Athan et al.
6,018,673 A 1/2000 Chin et al.
6,036,642 A 3/2000 Diab et al.
6,041,783 A 3/2000 Gruenke
6,057,758 A 5/2000 Dempsey et al.
6,067,462 A 5/2000 Diab et al.
6,081,735 A 6/2000 Diab et al.
6,081,742 A 6/2000 Amano et al.
6,094,592 A 7/2000 Yorkey et al.
6,117,077 A 9/2000 Del Mar et al.
6,129,686 A 10/2000 Friedman
6,157,850 A 12/2000 Diab et al.
6,159,147 A 12/2000 Lichter et al.
6,160,478 A 12/2000 Jacobsen et al.
6,168,569 B1 1/2001 McEwen et al.
6,176,831 B1 1/2001 Voss et al.
6,198,394 B1 3/2001 Jacobsen et al.
6,198,951 B1 3/2001 Kosuda et al.
6,199,550 B1 3/2001 Wiesmann et al.
6,206,830 B1 3/2001 Diab et al.
6,236,872 B1 5/2001 Diab et al.
6,251,080 B1 6/2001 Henkin et al.
6,261,247 B1 7/2001 Ishikawa et al.
6,262,769 B1 7/2001 Anderson et al.
6,263,222 B1 7/2001 Diab et al.
6,287,262 B1 9/2001 Amano et al.
6,322,516 B1 11/2001 Masuda et al.
6,334,065 B1 12/2001 Al-Ali et al.
6,371,921 B1 4/2002 Caro et al.
6,388,240 B2 5/2002 Schulz et al.
RE37,852 E 9/2002 Aso et al.
6,443,890 B1 9/2002 Schulze et al.
6,480,729 B2 11/2002 Stone
6,491,647 B1 12/2002 Bridger et al.
6,503,206 B1 1/2003 Li et al.
6,514,218 B2 2/2003 Yamamoto
6,516,289 B2 2/2003 David
6,526,310 B1 2/2003 Carter et al.
6,527,729 B1 3/2003 Turcott
6,541,756 B2 4/2003 Schulz et al.
6,544,173 B2 4/2003 West et al.
6,544,174 B2 4/2003 West et al.
6,546,267 B1 4/2003 Sugiura et al.
6,551,252 B2 4/2003 Sackner et al.
6,584,336 B1 6/2003 Ali et al.
6,589,170 B1 7/2003 Flach et al.
6,595,929 B2 7/2003 Stivoric et al.
6,605,038 B1 8/2003 Teller et al.
6,606,993 B1 8/2003 Wiesmann et al.
6,616,606 B1 9/2003 Petersen et al.
6,645,154 B2 11/2003 Oka
6,650,917 B2 11/2003 Diab et al.
6,684,090 B2 1/2004 Ali et al.
6,694,177 B2 2/2004 Eggers et al.
6,699,194 B1 3/2004 Diab et al.
6,732,064 B1 5/2004 Kadtke et al.
6,745,060 B2 6/2004 Diab et al.
6,770,028 B1 8/2004 Ali et al.
6,790,178 B1 9/2004 Mault et al.
6,811,538 B2 11/2004 Westbrook et al.
6,845,256 B2 1/2005 Chin et al.
6,850,787 B2 2/2005 Weber et al.
6,879,850 B2 4/2005 Kimball
6,893,396 B2 5/2005 Schulze et al.
6,912,414 B2 6/2005 Tong
6,934,571 B2 8/2005 Wiesmann et al.
6,947,781 B2 9/2005 Asada et al.
6,976,958 B2 12/2005 Quy
6,985,078 B2 1/2006 Suzuki et al.
6,997,882 B1 2/2006 Parker et al.
7,020,508 B2 3/2006 Stivoric et al.
7,020,578 B2 3/2006 Sorensen et al.
7,029,447 B2 4/2006 Rantala
7,041,060 B2 5/2006 Flaherty et al.
7,048,687 B1 5/2006 Reuss et al.
7,115,824 B2 10/2006 Lo
7,156,809 B2 1/2007 Quy
7,184,809 B1 2/2007 Sterling et al.
7,186,966 B2 3/2007 Al-Ali
7,194,293 B2 3/2007 Baker, Jr.
7,215,984 B2 5/2007 Diab et al.
7,215,987 B1 5/2007 Sterling et al.
7,225,007 B2 5/2007 Al-Ali et al.
7,237,446 B2 7/2007 Chan et al.
7,241,265 B2 7/2007 Cummings et al.
7,257,438 B2 8/2007 Kinast
7,296,312 B2 11/2007 Menkedick et al.
7,299,159 B2 * 11/2007 Nanikashvili 702/188
7,301,451 B2 11/2007 Hastings
7,314,451 B2 1/2008 Halperin et al.

(56) **References Cited**

U.S. PATENT DOCUMENTS

7,351,206 B2 4/2008 Suzuki et al.
7,355,512 B1 4/2008 Al-Ali
7,373,191 B2 5/2008 DeLonzer et al.
7,373,912 B2 5/2008 Self et al.
7,377,794 B2 5/2008 Al-Ali et al.
7,382,247 B2 6/2008 Welch et al.
7,383,069 B2 6/2008 Ruchti et al.
7,383,070 B2 6/2008 Diab et al.
7,384,398 B2 6/2008 Gagnadre et al.
7,400,919 B2 7/2008 Petersen et al.
7,420,472 B2 9/2008 Tran
7,427,926 B2 9/2008 Sinclair et al.
7,455,643 B1 11/2008 Li et al.
7,468,036 B1 12/2008 Rulkov et al.
7,477,143 B2 1/2009 Albert
7,479,890 B2 1/2009 Lehrman et al.
7,485,095 B2 2/2009 Shusterman
7,502,643 B2 3/2009 Farringdon et al.
7,508,307 B2 3/2009 Albert
7,509,131 B2 3/2009 Krumm et al.
7,509,154 B2 3/2009 Diab et al.
7,522,035 B2 4/2009 Albert
7,530,949 B2 5/2009 Al Ali et al.
7,539,532 B2 5/2009 Tran
7,541,939 B2 6/2009 Zadesky et al.
7,542,878 B2 6/2009 Nanikashvili
7,586,418 B2 9/2009 Cuddihy et al.
7,598,878 B2 10/2009 Goldreich
7,602,301 B1 10/2009 Stirling et al.
7,616,110 B2 11/2009 Crump et al.
7,625,344 B1 12/2009 Brady et al.
7,628,071 B2 12/2009 Sasaki et al.
7,628,730 B1 12/2009 Watterson et al.
7,641,614 B2 1/2010 Asada et al.
7,648,463 B1 1/2010 Elhag et al.
7,656,287 B2 2/2010 Albert et al.
7,668,588 B2 2/2010 Kovacs
7,670,295 B2 3/2010 Sackner et al.
7,674,230 B2 3/2010 Reisfeld
7,674,231 B2 3/2010 McCombie et al.
7,678,061 B2 3/2010 Lee et al.
7,684,954 B2 3/2010 Shahabdeen et al.
7,689,437 B1 3/2010 Teller et al.
7,698,101 B2 4/2010 Alten et al.
7,698,830 B2 4/2010 Townsend et al.
7,698,941 B2 4/2010 Sasaki et al.
7,715,984 B2 5/2010 Ramakrishnan et al.
7,725,147 B2 5/2010 Li et al.
7,782,189 B2 8/2010 Spoonhower et al.
7,827,011 B2 11/2010 DeVaul et al.
7,925,022 B2 4/2011 Jung et al.
7,976,480 B2 7/2011 Grajales et al.
7,983,933 B2 7/2011 Karkanias et al.
8,047,998 B2 11/2011 Kolluri et al.
8,082,160 B2 12/2011 Collins, Jr. et al.
8,137,270 B2 3/2012 Keenan et al.
8,167,800 B2 5/2012 Ouchi et al.
2001/0004234 A1 6/2001 Petelenz et al.
2001/0007923 A1 7/2001 Yamamoto
2001/0013826 A1 8/2001 Ahmed et al.
2002/0013517 A1 1/2002 West et al.
2002/0032386 A1 3/2002 Sackner et al.
2002/0072859 A1 6/2002 Kajimoto et al.
2002/0151805 A1 10/2002 Sugo et al.
2002/0156354 A1 10/2002 Larson
2002/0170193 A1 11/2002 Townsend et al.
2002/0183627 A1 12/2002 Nishii et al.
2002/0193671 A1 12/2002 Ciurczak et al.
2002/0193692 A1 12/2002 Inukai et al.
2002/0198679 A1 12/2002 Victor et al.
2003/0004420 A1 1/2003 Narimatsu
2003/0130590 A1 7/2003 Bui et al.
2003/0135099 A1 7/2003 Al-Ali
2003/0153836 A1 8/2003 Gagnadre et al.
2003/0158699 A1 8/2003 Townsend et al.
2003/0167012 A1* 9/2003 Friedman et al. 600/506
2003/0171662 A1 9/2003 O'Conner et al.
2003/0181815 A1 9/2003 Ebner et al.
2003/0208335 A1 11/2003 Unuma et al.
2004/0019288 A1 1/2004 Kinast
2004/0030261 A1 2/2004 Rantala
2004/0034293 A1 2/2004 Kimball
2004/0034294 A1 2/2004 Kimball et al.
2004/0054821 A1 3/2004 Warren et al.
2004/0073128 A1 4/2004 Hatlestad et al.
2004/0077934 A1 4/2004 Massad
2004/0122315 A1 6/2004 Krill
2004/0133079 A1 7/2004 Mazar et al.
2004/0162466 A1 8/2004 Quy
2004/0162493 A1 8/2004 Mills
2004/0225207 A1 11/2004 Bae et al.
2004/0267099 A1 12/2004 McMahon et al.
2005/0027205 A1 2/2005 Tarassenko et al.
2005/0043598 A1 2/2005 Goode, Jr. et al.
2005/0059870 A1 3/2005 Aceti
2005/0070773 A1 3/2005 Chin et al.
2005/0113107 A1 5/2005 Meunier
2005/0113703 A1 5/2005 Farringdon et al.
2005/0119586 A1 6/2005 Coyle et al.
2005/0119833 A1 6/2005 Nanikashvili
2005/0124866 A1 6/2005 Elaz et al.
2005/0124903 A1 6/2005 Roteliuk et al.
2005/0149350 A1 7/2005 Kerr et al.
2005/0171444 A1* 8/2005 Ono et al. 600/490
2005/0187796 A1 8/2005 Rosenfeld et al.
2005/0206518 A1 9/2005 Welch et al.
2005/0209511 A1 9/2005 Heruth et al.
2005/0228296 A1 10/2005 Banet
2005/0228298 A1 10/2005 Banet et al.
2005/0228301 A1 10/2005 Banet et al.
2005/0234317 A1 10/2005 Kiani
2005/0240087 A1 10/2005 Keenan et al.
2005/0261565 A1 11/2005 Lane et al.
2005/0261593 A1 11/2005 Zhang et al.
2005/0265267 A1 12/2005 Hwang
2005/0283088 A1 12/2005 Bernstein
2006/0036141 A1 2/2006 Kamath et al.
2006/0047215 A1 3/2006 Newman et al.
2006/0074321 A1 4/2006 Kouchi et al.
2006/0074322 A1 4/2006 Nitzan
2006/0128263 A1 6/2006 Baird
2006/0142648 A1 6/2006 Banet et al.
2006/0155589 A1 7/2006 Lane et al.
2006/0178591 A1 8/2006 Hempfling
2006/0200029 A1 9/2006 Evans et al.
2006/0252999 A1 11/2006 Devaul et al.
2006/0265246 A1 11/2006 Hoag
2006/0270949 A1 11/2006 Mathie et al.
2006/0271404 A1 11/2006 Brown
2006/0281979 A1 12/2006 Kim et al.
2007/0010719 A1 1/2007 Huster et al.
2007/0055163 A1 3/2007 Asada et al.
2007/0066910 A1 3/2007 Inukai et al.
2007/0071643 A1 3/2007 Hall et al.
2007/0094045 A1 4/2007 Cobbs et al.
2007/0118056 A1 5/2007 Wang et al.
2007/0129769 A1 6/2007 Bourget et al.
2007/0142715 A1 6/2007 Banet et al.
2007/0156456 A1 7/2007 McGillin et al.
2007/0161912 A1 7/2007 Zhang et al.
2007/0185393 A1 8/2007 Zhou et al.
2007/0188323 A1 8/2007 Sinclair et al.
2007/0193834 A1 8/2007 Pai et al.
2007/0208233 A1 9/2007 Kovacs
2007/0232867 A1 10/2007 Hansmann
2007/0237719 A1 10/2007 Jones et al.
2007/0244376 A1 10/2007 Wang
2007/0250261 A1 10/2007 Soehren
2007/0252853 A1 11/2007 Park et al.
2007/0255116 A1 11/2007 Mehta et al.
2007/0260487 A1 11/2007 Bartfeld et al.
2007/0265533 A1 11/2007 Tran
2007/0265880 A1 11/2007 Bartfeld et al.
2007/0270671 A1 11/2007 Gal

(56) **References Cited**

U.S. PATENT DOCUMENTS

2007/0276261 A1 11/2007 Banet et al.
2007/0282208 A1 12/2007 Jacobs et al.
2007/0287386 A1 12/2007 Agrawal et al.
2007/0293770 A1 12/2007 Bour et al.
2007/0293781 A1 12/2007 Sims et al.
2008/0004500 A1 1/2008 Cazares et al.
2008/0004507 A1 1/2008 Williams, Jr. et al.
2008/0004904 A1 1/2008 Tran
2008/0027341 A1 1/2008 Sackner et al.
2008/0033255 A1 2/2008 Essenpreis et al.
2008/0039731 A1 2/2008 McCombie et al.
2008/0077027 A1 3/2008 Allgeyer
2008/0082001 A1 4/2008 Hatlestad et al.
2008/0101160 A1 5/2008 Besson
2008/0103405 A1 5/2008 Banet et al.
2008/0114220 A1 5/2008 Banet et al.
2008/0132106 A1 6/2008 Burnes et al.
2008/0139955 A1 6/2008 Hansmann et al.
2008/0146887 A1 6/2008 Rao et al.
2008/0146892 A1 6/2008 LeBoeuf et al.
2008/0161707 A1 7/2008 Farringdon et al.
2008/0162496 A1 7/2008 Postrel
2008/0167535 A1 7/2008 Stivoric et al.
2008/0171927 A1 7/2008 Yang et al.
2008/0194918 A1 8/2008 Kulik et al.
2008/0195735 A1 8/2008 Hodges et al.
2008/0204254 A1 8/2008 Kazuno
2008/0208013 A1 8/2008 Zhang et al.
2008/0208273 A1 8/2008 Owen et al.
2008/0214963 A1 9/2008 Guillemaud et al.
2008/0221399 A1 9/2008 Zhou et al.
2008/0221404 A1 9/2008 Tso
2008/0262362 A1 10/2008 Kolluri et al.
2008/0275349 A1 11/2008 Halperin et al.
2008/0281168 A1 11/2008 Gibson et al.
2008/0281310 A1 11/2008 Dunning et al.
2008/0287751 A1 11/2008 Stivoric et al.
2008/0294019 A1 11/2008 Tran
2008/0319282 A1 12/2008 Tran
2008/0319327 A1 12/2008 Banet et al.
2009/0018408 A1 1/2009 Ouchi et al.
2009/0018409 A1 1/2009 Banet et al.
2009/0018453 A1 1/2009 Banet et al.
2009/0040041 A1 2/2009 Janetis et al.
2009/0054752 A1 2/2009 Jonnalagadda et al.
2009/0069642 A1 3/2009 Gao et al.
2009/0076363 A1 3/2009 Bly et al.
2009/0076397 A1 3/2009 Libbus et al.
2009/0076398 A1 3/2009 Li et al.
2009/0076405 A1 3/2009 Amurthur et al.
2009/0082681 A1 3/2009 Yokoyama et al.
2009/0099424 A1* 4/2009 O'Brien et al. 600/301
2009/0112072 A1 4/2009 Banet et al.
2009/0112281 A1 4/2009 Miyazawa et al.
2009/0112630 A1 4/2009 Collins, Jr. et al.
2009/0118590 A1 5/2009 Teller et al.
2009/0118626 A1 5/2009 Moon et al.
2009/0131759 A1 5/2009 Sims et al.
2009/0187085 A1 7/2009 Pav
2009/0192366 A1 7/2009 Mensinger et al.
2009/0198139 A1 8/2009 Lewicke et al.
2009/0221937 A1 9/2009 Smith et al.
2009/0222119 A1 9/2009 Plahey et al.
2009/0227877 A1 9/2009 Tran
2009/0233770 A1 9/2009 Vincent et al.
2009/0259113 A1 10/2009 Liu et al.
2009/0262074 A1 10/2009 Nasiri et al.
2009/0264712 A1 10/2009 Baldus et al.
2009/0287067 A1 11/2009 Dorogusker et al.
2009/0295541 A1 12/2009 Roof
2009/0306485 A1 12/2009 Bell
2009/0306487 A1 12/2009 Crowe et al.
2009/0306524 A1 12/2009 Muhlsteff et al.
2009/0312973 A1 12/2009 Hatlestad et al.
2009/0318779 A1 12/2009 Tran
2009/0322513 A1 12/2009 Hwang et al.
2009/0326349 A1 12/2009 McGonigle et al.
2010/0010380 A1 1/2010 Panken et al.
2010/0030034 A1 2/2010 Schulhauser et al.
2010/0030085 A1 2/2010 Rojas Ojeda et al.
2010/0056881 A1 3/2010 Libbus et al.
2010/0056886 A1 3/2010 Hurtubise et al.
2010/0113948 A1 5/2010 Yang et al.
2010/0125188 A1 5/2010 Schilling et al.
2010/0130811 A1 5/2010 Leuthardt et al.
2010/0160793 A1 6/2010 Lee et al.
2010/0160794 A1 6/2010 Banet et al.
2010/0160795 A1 6/2010 Banet et al.
2010/0160796 A1 6/2010 Banet et al.
2010/0160797 A1 6/2010 Banet et al.
2010/0160798 A1 6/2010 Banet et al.
2010/0168589 A1 7/2010 Banet et al.
2010/0210930 A1 8/2010 Saylor
2010/0217099 A1 8/2010 LeBoeuf et al.
2010/0222649 A1 9/2010 Schoenberg
2010/0234693 A1 9/2010 Srinivasan et al.
2010/0234786 A1 9/2010 Fulkerson et al.
2010/0241011 A1 9/2010 McCombie et al.
2010/0268518 A1* 10/2010 Sugo 703/2
2010/0280440 A1 11/2010 Skelton et al.
2010/0298650 A1 11/2010 Moon et al.
2010/0298651 A1 11/2010 Moon et al.
2010/0298652 A1 11/2010 McCombie et al.
2010/0298653 A1 11/2010 McCombie et al.
2010/0298654 A1 11/2010 McCombie et al.
2010/0298655 A1 11/2010 McCombie et al.
2010/0298656 A1 11/2010 McCombie et al.
2010/0298657 A1 11/2010 McCombie et al.
2010/0298658 A1 11/2010 McCombie et al.
2010/0298659 A1 11/2010 McCombie et al.
2010/0298660 A1 11/2010 McCombie et al.
2010/0298661 A1 11/2010 McCombie et al.
2010/0312115 A1 12/2010 Dentinger
2010/0324384 A1 12/2010 Moon et al.
2010/0324385 A1 12/2010 Moon et al.
2010/0324386 A1 12/2010 Moon et al.
2010/0324387 A1 12/2010 Moon et al.
2010/0324388 A1 12/2010 Moon et al.
2010/0324389 A1 12/2010 Moon et al.
2010/0331640 A1 12/2010 Medina
2011/0066006 A1 3/2011 Banet et al.
2011/0066007 A1 3/2011 Banet et al.
2011/0066008 A1 3/2011 Banet et al.
2011/0066009 A1 3/2011 Moon et al.
2011/0066010 A1 3/2011 Moon et al.
2011/0066037 A1 3/2011 Banet et al.
2011/0066038 A1 3/2011 Banet et al.
2011/0066039 A1 3/2011 Banet et al.
2011/0066043 A1 3/2011 Banet et al.
2011/0066044 A1 3/2011 Moon et al.
2011/0066045 A1 3/2011 Moon et al.
2011/0066050 A1 3/2011 Moon et al.
2011/0066051 A1 3/2011 Moon et al.
2011/0066062 A1 3/2011 Banet et al.
2011/0070829 A1 3/2011 Griffin et al.
2011/0076942 A1 3/2011 Taveau et al.
2011/0093281 A1 4/2011 Plummer et al.
2011/0105862 A1 5/2011 Gies et al.
2011/0125207 A1* 5/2011 Nabutovsky et al. 607/6
2011/0144456 A1 6/2011 Muhlsteff et al.
2011/0152632 A1 6/2011 Le Neel et al.
2011/0178375 A1 7/2011 Forster
2011/0224498 A1 9/2011 Banet et al.
2011/0224499 A1 9/2011 Banet et al.
2011/0224500 A1 9/2011 Banet et al.
2011/0224506 A1 9/2011 Moon et al.
2011/0224507 A1 9/2011 Banet et al.
2011/0224508 A1 9/2011 Moon
2011/0224556 A1 9/2011 Moon et al.
2011/0224557 A1 9/2011 Banet et al.
2011/0224564 A1 9/2011 Moon et al.
2011/0257489 A1 10/2011 Banet et al.
2011/0257551 A1 10/2011 Banet et al.
2011/0257552 A1 10/2011 Banet et al.

(56) **References Cited**

U.S. PATENT DOCUMENTS

2011/0257554	A1	10/2011	Banet et al.
2011/0257555	A1	10/2011	Banet et al.
2011/0275907	A1	11/2011	Inciardi et al.
2012/0065525	A1	3/2012	Douniama et al.
2012/0123232	A1	5/2012	Najarian et al.

FOREIGN PATENT DOCUMENTS

GB	2329250	A	3/1999
WO	9932030	A1	7/1999
WO	2006005169	A1	1/2006
WO	2007024777	A2	3/2007
WO	2007143535	A2	12/2007
WO	2008037820	A1	4/2008
WO	2008110788	A1	9/2008
WO	2009009761	A1	1/2009
WO	2010135516	A2	11/2010
WO	2010135518	A1	11/2010
WO	2010148205	A1	12/2010
WO	2011032132	A2	3/2011
WO	2011034881	A1	3/2011
WO	2011082341	A1	7/2011
WO	2011112782	A1	9/2011
WO	2011133582	A1	10/2011

OTHER PUBLICATIONS

Non-Final Office Action issued by the US Patent and Trademark Office on Sep. 17, 2012 in U.S. Appl. No. 12/650,354.
Non-Final Office Action issued by the US Patent and Trademark Office on Sep. 21, 2012 in U.S. Appl. No. 12/469,115.
Response to Non-Final Office Action issued in U.S. Appl. No. 12/469,236 dated Sep. 27, 2012.
Response to Non-Final Office Action issued in U.S. Appl. No. 12/487,283 dated Sep. 27, 2012.
Non-Final Office Action issued by the US Patent and Trademark Office on Sep. 28, 2012 in U.S. Appl. No. 12/560,087.
Response to Non-Final Office Action issued in U.S. Appl. No. 12/762,836 dated Oct. 9, 2012.
Response to Non-Final Office Action issued in U.S. Appl. No. 12/559,429 dated Oct. 12, 2012.
Response to Non-Final Office Action issued in U.S. Appl. No. 12/559,430 dated Oct. 12, 2012.
Response to Non-Final Office Action issued in U.S. Appl. No. 12/559,435 dated Oct. 23, 2012.
Final Office Action issued by the US Patent and Trademark Office on Oct. 24, 2012 in U.S. Appl. No. 12/599,429.
Final Office Action issued by the US Patent and Trademark Office on Oct. 24, 2012 in U.S. Appl. No. 12/599,430.
Non-Final Office Action issued by the US Patent and Trademark Office on Oct. 23, 2012 in U.S. Appl. No. 12/762,944.
Response to Non-Final Office Action issued in U.S. Appl. No. 12/762,733 dated Oct. 25, 2012.
Final Office Action issued by the US Patent and Trademark Office on Oct. 26, 2012 in U.S. Appl. No. 12/762,836.
Non-Final Office Action issued by the US Patent and Trademark Office on Oct. 24, 2012 in U.S. Appl. No. 12/559,403.
Non Final Office Action issued by the United States Patent and Trademark Office in U.S. Appl. No. 12/559,413 on Nov. 9, 2012.
Response to Office Action issued in U.S. Appl. No. 12/762,846 dated Nov. 13, 2012.
Response to Office Action issued in U.S. Appl. No. 12/762,874 dated Nov. 13, 2012.
Response to Office Action issued in U.S. Appl. No. 12/560,111 dated Nov. 26, 2012.
Response to Office Action issued in U.S. Appl. No. 11/930,881 dated Nov. 26, 2012.
Final Rejection issued by the United States Patent and Trademark Office in U.S. Appl. No. 12/559,419 on Nov. 16, 2012.
Non Final Office Action issued by the United States Patent and Trademark Office in U.S. Appl. No. 12/559,408 on Nov. 23, 2012.
Response to Office Action issued in U.S. Appl. No. 12/138,199 dated Nov. 29, 2012.
Response to Office Action issued in U.S. Appl. No. 12/650,383 dated Dec. 7, 2012.
Response to Office Action issued in U.S. Appl. No. 12/650,392 dated Dec. 7, 2012.
Final Rejection issued by the United States Patent and Trademark Office in U.S. Appl. No. 12/559,435 on Dec. 12, 2012.
Final Rejection issued by the United States Patent and Trademark Office in U.S. Appl. No. 12/560,111 on Dec. 12, 2012.
Clifford et al., Measuring Tilt with Low-g Accelerometers. Freescale Semiconductor, Inc., 2005:8 pages.
McKneely et al., Plug-and-Play and Network-Capable Medical Instrumentation and Database with a Complete Healthcare Technology Suite: MediCAN. Joint Workshop on High Confidence Medical Devices, Software, and Systems and Medical Device Plug-and-Play Interoperability. 2007:122-129.
Montgomery et al., Lifeguard—A Personal Physiological Monitor for Extreme Environments. Conf Proc IEEE Eng Med Biol Soc. 2004;3:2192-2195.
Thongpithoonrat et al., Networking and Plug-and-Play of Bedside Medical Instruments. Conf Proc IEEE Eng Med Biol Soc. 2008;2008:1514-1517.
Yang et al., Research on Multi-Parameter Physiological Monitor Based on CAN Bus. IFMBE Proceed. 2008;19:417-419.
Zeltwanger, Controller Area Network and CANopen in Medical Equipment. Bus Briefing: Med Dev Manuf Technol. 2002:34-37.
Zitzmann and Schumann, Interoperable Medical Devices Due to Standardized CANopen Interfaces. Joint Workshop on High Confidence Medical Devices, Software, and Systems and Medical Device Plug-and-Play Interoperability. 2007:97-103.
Non Final Office Action issued by the United States Patent and Trademark Office in U.S. Appl. No. 13/432,976 on Dec. 14, 2012.
Final Rejection issued by the United States Patent and Trademark Office in U.S. Appl. No. 12/762,733 on Dec. 20, 2012.
Final Rejection issued by the United States Patent and Trademark Office in U.S. Appl. No. 12/762,846 on Dec. 20, 2012.
Final Rejection issued by the United States Patent and Trademark Office in U.S. Appl. No. 12/650,392 on Jan. 3, 2013.
Final Rejection issued by the United States Patent and Trademark Office in U.S. Appl. No. 12/487,283 on Jan. 3, 2013.
Non Final Office Action issued by the United States Patent and Trademark Office in U.S. Appl. No. 13/292,923 on Jan. 14, 2013.
Notice of Allowance issued by the United States Patent and Trademark Office in U.S. Appl. No. 11/470,708 on Jan. 18, 2013.
International Search Report and Written Opinion issued in PCT/US2012/064302 on Jan. 15, 2013.
Non-Final Office Action issued by the US Patent and Trademark Office on Jul. 18, 2012 in U.S. Appl. No. 12/650,389.
Chan et al., Noninvasive and Cuffless Measurements of Blood Pressure for Telemedicine. Proceedings of the 23rd Annual International Conference of the IEEE Engineering in Medicine and Biology Society 2001:3 pages.
Fung, Advisory System for Administration of Phenylephrine Following Spinal Anesthesia for Cesarean Section. Master's Thesis. University of British Columbia 2002: 119 pages.
Liu et al., The Changes in Pulse Transit Time at Specific Cuff Pressures during Inflation and Deflation. Proceedings of the 28th IEEE EMBS Annual International Conference New York City, USA, Aug. 30-Sep. 3, 2006:6404-6405.
Nitzan et al., Effects of External Pressure on Arteries Distal to the Cuff During Sphygmomanometry. IEEE Transactions on Biomedical Engineering, Jun. 2005;52(6):1120-1127.
USB 2.0 Specification Engineering Change Notice. Oct. 20, 2000.
Yan and Zhang, A Novel Calibration Method for Noninvasive Blood Pressure Measurement Using Pulse Transit Time. Proceedings of the 4th IEEE-EMBS International Summer School and Symposium on Medical Devices and Biosensors St Catharine's College,Cambridge, UK, Aug. 19-22, 2007.
Zislin et al., Ways of Improving the Accuracy of Arterial Pressure Oscillometry. Biomedical Engineering 2005;39 (4):174-178.

(56) **References Cited**

OTHER PUBLICATIONS

International Search Report and Written Opinion dated May 29, 2012 issued in PCT/US2012/025648.
Non-Final Office Action issued by the US Patent and Trademark Office on Aug. 3, 2012 in U.S. Appl. No. 12/762,925.
Non-Final Office Action issued by the US Patent and Trademark Office on Aug. 3, 2012 in U.S. Appl. No. 12/762,963.
Non-Final Office Action issued by the US Patent and Trademark Office on Aug. 20, 2012 in U.S. Appl. No. 12/762,777.
Non-Final Office Action issued by the US Patent and Trademark Office on Aug. 21, 2012 in U.S. Appl. No. 12/469,107.
Non-Final Office Action issued by the US Patent and Trademark Office on Aug. 24, 2012 in U.S. Appl. No. 12/762,936.
Non-Final Office Action issued by the US Patent and Trademark Office on Jun. 11, 2012 in U.S. Appl. No. 12/469,222.
Non-Final Office Action issued by the US Patent and Trademark Office on Jun. 8, 2012 in U.S. Appl. No. 12/650,383.
Non-Final Office Action issued by the US Patent and Trademark Office on Jun. 8, 2012 in U.S. Appl. No. 12/650,392.
Non-Final Office Action issued by the US Patent and Trademark Office on Jun. 20, 2012 in U.S. Appl. No. 12/762,751.
International Search Report and Written Opinion dated Jun. 29, 2012 issued in PCT/US2012/025640.
Non-Final Office Action issued by the US Patent and Trademark Office on Jul. 5, 2012 in U.S. Appl. No. 12/560,138.
"Signal Strength." Oct. 6, 2008. http://web.archive.org/web/20081 06200523/http:/!en.wikipedia.org/wiki/Signal_strength.
Non-Final Office Action issued by the US Patent and Trademark Office on May 24, 2012 in U.S. Appl. No. 12/560,111.
Restriction Requirement issued by the US Patent and Trademark Office on Apr. 24, 2012 in U.S. Appl. No. 12/469,107.
Response to Restriction Requirement submitted Jun. 14, 2012 in U.S. Appl. No. 12/469,107.
Final Office Action issued by the United States Patent and Trademark Office in U.S. Appl. No. 12/469,236 dated Jul. 8, 2013.
Non-Final Office Action issued by the United States Patent and Trademark Office in U.S. Appl. No. 12/560,111 dated Jul. 8, 2013.
Scanaill et al., A Review of Approaches to Mobility Telemonitoring of the Elderly in Their Living Environment. Annals of Biomed Engineer. Apr. 2006;34(4):547-563.
Notice of Allowance issued by the United States Patent and Trademark Office in U.S. Appl. No. 12/762,733 dated Jul. 24, 2013.
Final Office Action issued by the United States Patent and Trademark Office in U.S. Appl. No. 12/762,944 dated Aug. 2, 2013.
Response to Office Action issued by the United States Patent and Trademark Office in U.S. Appl. No. 12/559,039 dated Aug. 9, 2013.
Sifil et al., Evaluation of the Harmonized Alert Sensing Technology Device for Hemodynamic Monitoring in Chronic Hemodialysis Patients. ASAIO J. Nov.-Dec. 2003;49(6):667-672.
Weinhold et al., Buprenorphine alone and in combination with naloxone in non-dependent humans. Drug Alcohol Depend. Aug. 1992;30(3):263-274.
Final Office Action issued by the United States Patent and Trademark Office in U.S. Appl. No. 12/762,726 dated Aug. 15, 2013.
Extended European Search Report and Written Opinion issued in application No. EP 10817733 dated Aug. 29, 2013.
Extended European Search Report and Written Opinion issued in application No. EP 08770884 dated Sep. 17, 2013.
Non-Final Office Action issued by the US Patent and Trademark Office on Aug. 31, 2012 in U.S. Appl. No. 12/469,213.
Non-Final Office Action issued by the US Patent and Trademark Office on Sep. 14, 2012 in U.S. Appl. No. 12/650,374.
Drinnan et al., Relation between heart rate and pulse transit time during paced respiration. Physiol. Meas. Aug. 2001;22(3):425-432.
Flash et al., The Coordination of Arm Movements: An Experimentally Confirmed Mathematical Model. J Neurosci. Jul. 1985;5(7):1688-1703.
Ma and Zhang, A Correlation Study on the Variabilities in Pulse Transit Time, Blood Pressure, and Heart Rate Recorded Simultaneously from Healthy Subjects. Conf Proc IEEE Eng Med Biol Soc. 2005;1:996-999.
Non-Final Office Action issued by the US Patent and Trademark Office on Sep. 17, 2012 in U.S. Appl. No. 12/469,192.
Gallagher, Comparison of Radial and Femoral Arterial Blood Pressure in Children after Cardiopulmonary Bypass. J Clin Monit. Jul. 1985;1(3):168-171.
Park et al., Direct Blood Pressure Measurements in Brachial and Femoral Arteries in Children. Circulation Feb. 1970; 41(2)231-237.
Talkowski, Quantifying Physical Activity in Community Dwelling Older Adults Using Accelerometry. University of Pittsburgh (Dissertation) 2008:1-91.
Non-Final Office Action issued by the US Patent and Trademark Office on Sep. 26, 2012 in U.S. Appl. No. 12/560,104.
Packet Definition. The Linux Information Project Jan. 8, 2006 http://www.linfo.org/packet.html.
RS-232. Wikipedia Dec. 5, 2008 http:I/web.archive.org/web/ 20081205160754/http:/len.wikipedia.org/wiki/RS-232.
Non-Final Office Action issued by the US Patent and Trademark Office on Oct. 9, 2012 in U.S. Appl. No. 12/762,726.
Final Office Action issued by the US Patent and Trademark Office on Oct. 22, 2012 in U.S. Appl. No. 12/762,822.
Final Office Action issued by the US Patent and Trademark Office on Oct. 25, 2012 in U.S. Appl. No. 12/599,426.
Alves et al., CAN Protocol: A Laboratory Prototype for Fieldbus Applications. XIX IMEKO World Congress Fundamental and Applied Metrology Sep. 6-11, 2009 Lisbon, Portugal. 4 pages :454-457 ISBN 978-963-88410-0-1.
Benefits of Digital Sensors. Gems Sensors. Feb. 14, 2008. http:// web.archive.org/web/20080214122230/http://www.sensorland. com/HowPage054.html.
Final Office Action issued by the US Patent and Trademark Office on Oct. 25, 2012 in U.S. Appl. No. 12/762,790.
Non-Final Office Action issued by the US Patent and Trademark Office on Oct. 30, 2012 in U.S. Appl. No. 12/559,386.
Non-Final Office Action issued by the US Patent and Trademark Office on Nov. 6, 2012 in U.S. Appl. No. 12/559,379.
Non-Final Office Action issued by the US Patent and Trademark Office on Nov. 6, 2012 in U.S. Appl. No. 12/650,370.
Poon and Zhang, Cuff-Less and Noninvasive Measurements of Arterial Blood Pressure by Pulse Transit Time. Conf Proc IEEE Eng Med Biol Soc. 2005;6:5877-5880.
Non-Final Office Action issued by the US Patent and Trademark Office on Nov. 7, 2012 in U.S. Appl. No. 12/559,392.
International Search Report and Written Opinion dated Jul. 22, 2011 issued in PCT/US2011/027843.
International Search Report and Written Opinion dated Jul. 20, 2011 issued in PCT/US2011/033100.
Non-Final Office Action issued by the US Patent and Trademark Office on May 26, 2011 in U.S. Appl. No. 12/469,151.
Response to Non-Final Office Action submitted Nov. 25, 2011 in U.S. Appl. No. 12/469,151.
Notice of Allowance issued by the US Patent and Trademark Office on Feb. 1, 2012 in U.S. Appl. No. 12/469,151.
Non-Final Office Action issued by the US Patent and Trademark Office on Aug. 4, 2011 in U.S. Appl. No. 12/469,182.
Response to Non-Final Office Action submitted Nov. 25, 2011 in U.S. Appl. No. 12/469,182.
Notice of Allowance issued by the US Patent and Trademark Office on Dec. 28, 2011 in U.S. Appl. No. 12/469,182.
International Search Report and Written Opinion dated Oct. 15, 2010 issued in PCT/US2010/035550.
Non-Final Office Action issued by the US Patent and Trademark Office on Apr. 12, 2012 in U.S. Appl. No. 12/559,429.
Non-Final Office Action issued by the US Patent and Trademark Office on Apr. 12, 2012 in U.S. Appl. No. 12/559,430.
Non-Final Office Action issued by the US Patent and Trademark Office on Apr. 24, 2012 in U.S. Appl. No. 12/559,435.
Non-Final Office Action issued by the US Patent and Trademark Office on Apr. 25, 2012 in U.S. Appl. No. 12/762,733.

(56) **References Cited**

OTHER PUBLICATIONS

Non-Final Office Action issued by the US Patent and Trademark Office on Apr. 27, 2012 in U.S. Appl. No. 12/762,822.
Non-Final Office Action issued by the US Patent and Trademark Office on Mar. 27, 2012 in U.S. Appl. No. 12/559,422.
Mathie, Monitoring and Interpreting Human Movement Patterns using a Triaxial Accelerometer. Faculty of Engineering. The University of New South Wales. PhD Dissertation. Aug. 2003: part1 pp. 1-256.
Mathie, Monitoring and Interpreting Human Movement Patterns using a Triaxial Accelerometer. Faculty of Engineering. The University of New South Wales. PhD Dissertation. Aug. 2003: part2 pp. 256-512.
International Search Report and Written Opinion dated Apr. 27, 2012 as reported in PCT/US2011/067441.
Non-Final Office Action issued by the US Patent and Trademark Office on May 7, 2012 in U.S. Appl. No. 12/469,115.
Non-Final Office Action issued by the US Patent and Trademark Office on May 9, 2012 in U.S. Appl. No. 12/762,836.
Non-Final Office Action issued by the US Patent and Trademark Office on May 10, 2012 in U.S. Appl. No. 12/559,419.
Jackson, Digital Filter Design and Synthesis Using High-Level Modeling Tools. Virginia Polytechnic Institute and State University Thesis. Dec. 1999.
Kim et al., Two Algorithms for Detecting Respiratory Rate from ECG Signal. IFMBE Proceedings 2007;14(6) JC27:4069-4071.
O'Haver, Peak Finding and Measurement, Version 1.6 Oct. 26, 2006. http://web.archive.org/web/20090205162604/http://terpconnect.umd.edu/-toh/spectrum/PeakFindingandMeasurement.htm.
Reinvuo et al., Measurement of Respiratory Rate with High-Resolution Accelerometer and EMFit Pressure Sensor. Proceedings of the 2006 IEEE Sensors Applications Symposium Feb. 7-9, 2006:192-195.
Non-Final Office Action issued by the US Patent and Trademark Office on May 11, 2012 in U.S. Appl. No. 12/762,846.
Non-Final Office Action issued by the US Patent and Trademark Office on May 11, 2012 in U.S. Appl. No. 12/762,874.
Allen et al., Classification of a known sequence of motions and postures from accelerometry data using adapted Gaussian mixture models. Physiol. Meas. 2006;27:935-951.
Asada et al., Active Noise Cancellation Using MEMS Accelerometers for Motion-Tolerant Wearable Bio-Sensors. Proceedings of the 26th Annual International Conference of the IEEE Embs. San Francisco, CA, USA. Sep. 1-5, 2004:2157-2160.
Bowers et al., Respiratory Rate Derived from Principal Component Analysis of Single Lead Electrocardiogram. Computers in Cardiology Conference Proceedings Sep. 2008;35:437-440.
Bussmann et al., Measuring daily behavior using ambulatory accelerometry: The Activity Monitor. Behav Res Methods Instrum Comput. Aug. 2001;33(3):349-356.
Cretikos et al., The Objective Medical Emergency Team Activation Criteria: a case-control study. Resuscitation Apr. 2007;73(1):62-72.
Espina et al., Wireless Body Sensor Network for Continuous Cuff-less Blood Pressure Monitoring. Proceedings of the 3rd IEEE-EMBS. International Summer School and Symposium on Medical Devices and Biosensors. MIT, Boston, USA, Sep. 4-6, 2006:11-15.
Fieselmann et al., Respiratory rate predicts cardiopulmonary arrest for internal medicine patients. J Gen Intern Med Jul. 1993;8(7):354-360.
Goldhill et al., A physiologically-based early warning score for ward patients: the association between score and outcome. Anaesthesia Jun. 2005;60(6):547-553.
Hung et al., Estimation of Respiratory Waveform Using an Accelerometer. 5th IEEE International Symposium on Biomedical Imaging: From Nano to Macro, May 14-17, 2008:1493-1496.
Jin, A Respiration Monitoring System Based on a Tri-Axial Accelerometer and an Air-Coupled Microphone. Technische Universiteit Eindhoven, University of Technology. Master's Graduation Paper, Electrical Engineering Aug. 25, 2009.
Karantonis et al., Implementation of a Real-Time Human Movement Classifier Using a Triaxial Accelerometer for Ambulatory Monitoring. IEEE Transactions on Information Technology in Biomedicine. Jan. 2006;10(1):156-167.
Khambete et al., Movement artefact rejection in impedance pneumography using six strategically placed electrodes. Physiol. Meas. 2000;21:79-88.
Khan et al., Accelerometer Signal-based Human Activity Recognition Using Augmented Autoregressive Model Coefficients and Artificial w Neural Nets. 30th Annual International Conference of the IEEE Engineering in Medicine and Biology Society. Aug. 20-24, 2008:5172-5175.
Mason, Signal Processing Methods for Non-Invasive Respiration Monitoring. Department of Engineering Science, University of Oxford 2002.
Mathie et al., Classification of basic daily movements using a triaxial accelerometer. Med Biol Eng Comput. Sep. 2004;42(5):679-687.
Otto et al., System Architecture of a Wireless Body Area Sensor Network for Ubiquitous Health Monitoring. Journal of Mobile Multimedia Jan. 10, 2006;1(4):307-326.
Park et al., An improved algorithm for respiration signal extraction from electrocardiogram measured by conductive textile electrodes using instantaneous frequency estimation. Med Bio Eng Comput 2008;46:147-158.
PDF-Pro for iPhone & iPod touch User Manual. ePapyrus Jul. 2009;1:1-25 http://epapyrus.com/en/files/PDFPro%.
Seo et al., Performance Improvement of Pulse Oximetry-Based Respiration Detection by Selective Mode Bandpass Filtering. Ergonomics and Health Aspects of Work with Computers Lecture Notes in Computer Science, 2007;4566:300-308.
Soh et al., An investigation of respiration while wearing back belts. Applied Ergonomics 1997; 28(3):189-192.
Subbe et al., Effect of introducing the Modified Early Warning score on clinical outcomes, cardiopulmonary arrests and intensive care utilization in acute medical admissions. Anaesthesia Aug. 2003;58(8):797-802.
Vuorela et al., Two portable long-term measurement devices for ECG and bioimpedance. Second International Conference on Pervasive Computing Technologies for Healthcare.. Jan. 30-Feb. 1, 2008: 169-172.
Wolf et al., Development of a Fall Detector and Classifier based on a Triaxial Accelerometer Demo Board. 2007:210-213.
Non-Final Office Action issued by the US Patent and Trademark Office on Apr. 30, 2012 in U.S. Appl. No. 12/762,790.
Non-Final Office Action issued by the US Patent and Trademark Office on Mar. 30, 2012 in U.S. Appl. No. 12/469,236.
Non-Final Office Action issued by the US Patent and Trademark Office on Apr. 3, 2012 in U.S. Appl. No. 12/469,094.
Restriction Requirement issued by the US Patent and Trademark Office on Feb. 2, 2012 in U.S. Appl. No. 12/469,222.
Non-Final Office Action issued by the US Patent and Trademark Office on Mar. 27, 2012 in U.S. Appl. No. 12/559,426.
Non-Final Office Action issued by the US Patent and Trademark Office on Apr. 3, 2012 in U.S. Appl. No. 12/559,039.
Non-Final Office Action issued by the US Patent and Trademark Office on Dec. 29, 2011 in U.S. Appl. No. 12/559,080.
Response to Non-Final Office Action submitted Mar. 19, 2012 in U.S. Appl. No. 12/559,080.
Notice of Allowance issued by the US Patent and Trademark Office on Apr. 2, 2012 in U.S. Appl. No. 12/559,080.
Non-Final Office Action issued by the US Patent and Trademark Office on Dec. 15, 2011 in U.S. Appl. No. 12/560,077.
Non-Final Office Action issued by the US Patent and Trademark Office on Mar. 8, 2012 in U.S. Appl. No. 12/560,093.
Restriction Requirement issued by the US Patent and Trademark Office on Dec. 14, 2012 in U.S. Appl. No. 12/560,093.
Response to Restriction Requirement submitted Feb. 15, 2012 in U.S. Appl. No. 12/560,093.
Non-Final Office Action issued by the US Patent and Trademark Office on Mar. 1, 2012 in U.S. Appl. No. 12/560,104.
Restriction Requirement issued by the US Patent and Trademark Office on Jan. 19, 2012 in U.S. Appl. No. 12/469,115.

(56) **References Cited**

OTHER PUBLICATIONS

Response to Restriction Requirement submitted Feb. 15, 2012 in U.S. Appl. No. 12/469,115.
Restriction Requirement issued by the US Patent and Trademark Office on Nov. 14, 2011 in U.S. Appl. No. 12/469,127.
Response to Restriction Requirement submitted Feb. 15, 2012 in U.S. Appl. No. 12/469,127.
Non-Final Office Action issued by the US Patent and Trademark Office on Mar. 9, 2012 in U.S. Appl. No. 12/469,127.
Non-Final Office Action issued by the US Patent and Trademark Office on Apr. 3, 2012 in U.S. Appl. No. 12/469,137.
International Preliminary Report on Patentability dated Dec. 1, 2011 issued in PCT/US2010/035554.
International Search Report and Written Opinion dated Sep. 23, 2010 issued in PCT/US2010/035554.
International Preliminary Report on Patentability dated Jan. 5, 2012 issued in PCT/US2010/039000.
International Search Report and Written Opinion dated Sep. 7, 2010 issued in PCT/US2010/039000.
International Search Report and Written Opinion dated Nov. 3, 2010 issued in PCT/US2010/048729.
International Search Report and Written Opinion dated Nov. 5, 2010 issued in PCT/US2010/048866.
International Search Report and Written Opinion dated Mar. 3, 2011 issued in PCT/US2010/062564.
Henry et al., "Stroke Volume Obtained from the Brachial Artery Using Transbrachial Electrical Bioimpedance Velocimetry", 34th Annual International Conference of the IEEE EMBS, San Diego, California USA, Aug. 28- Sep. 1, 2012, pp. 142-145.

* cited by examiner

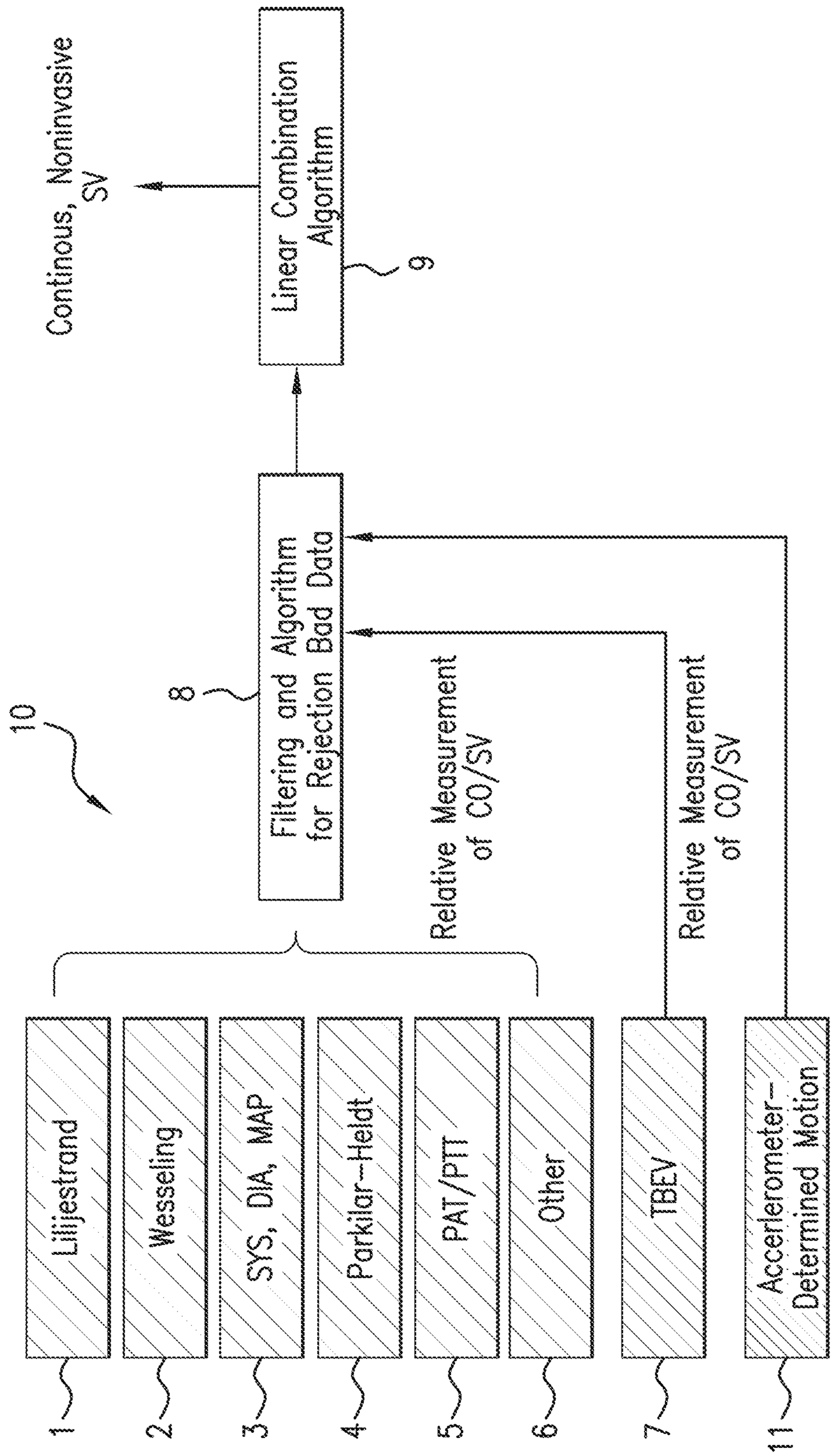
10
Continous, Noninvasive SV
Linear Combination Algorithm
9
Filtering and Algorithm for Rejection Bad Data
8
Relative Measurement of CO/SV
Relative Measurement of CO/SV
Lilljestrand
Wesseling
SYS, DIA, MAP
Parkilar--Heldt
PAT/PTT
Other
TBEV
Accerlerometer-Determined Motion
1
2
3
4
5
6
7
11

FIG. 1

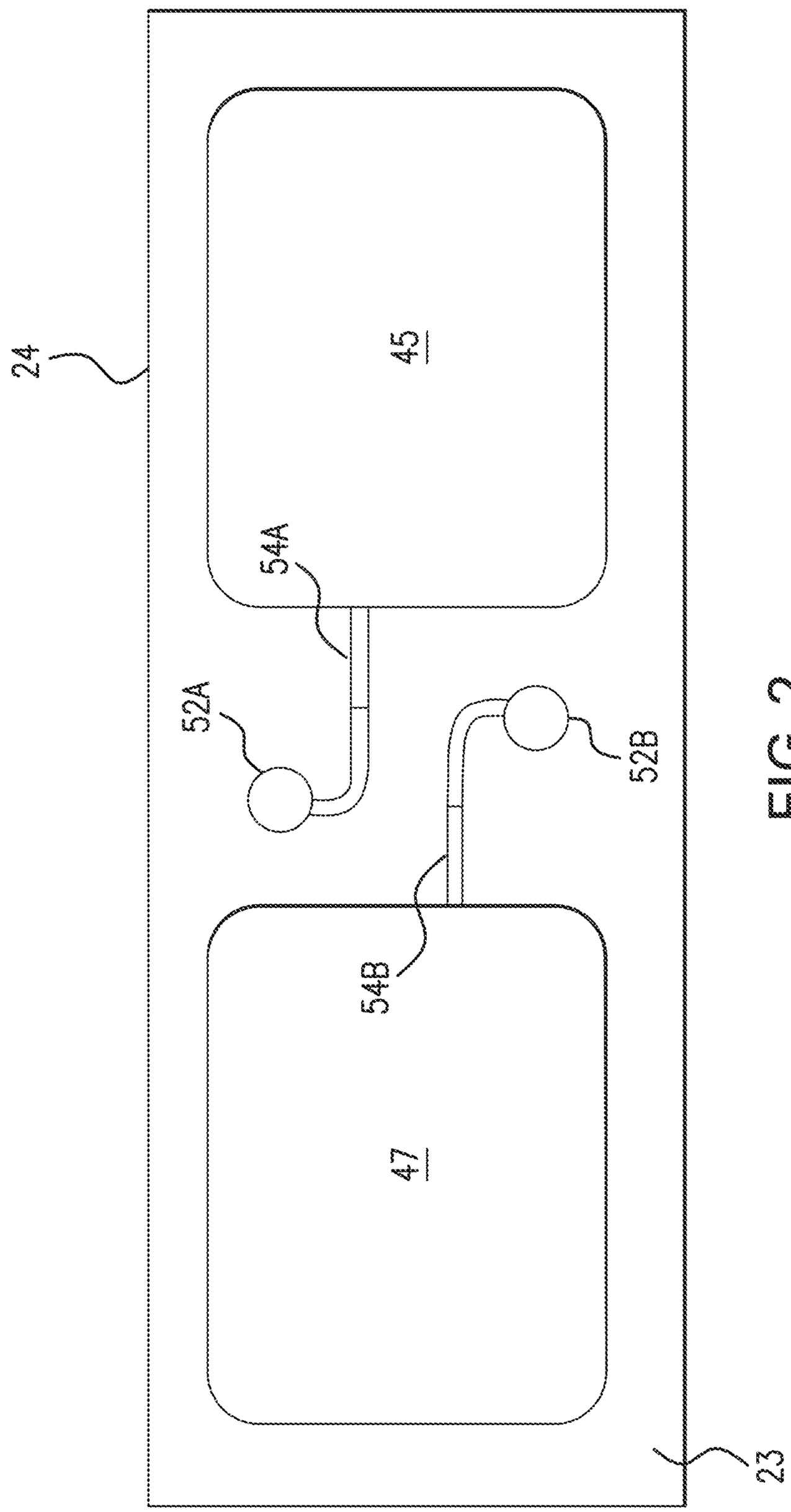

FIG. 2

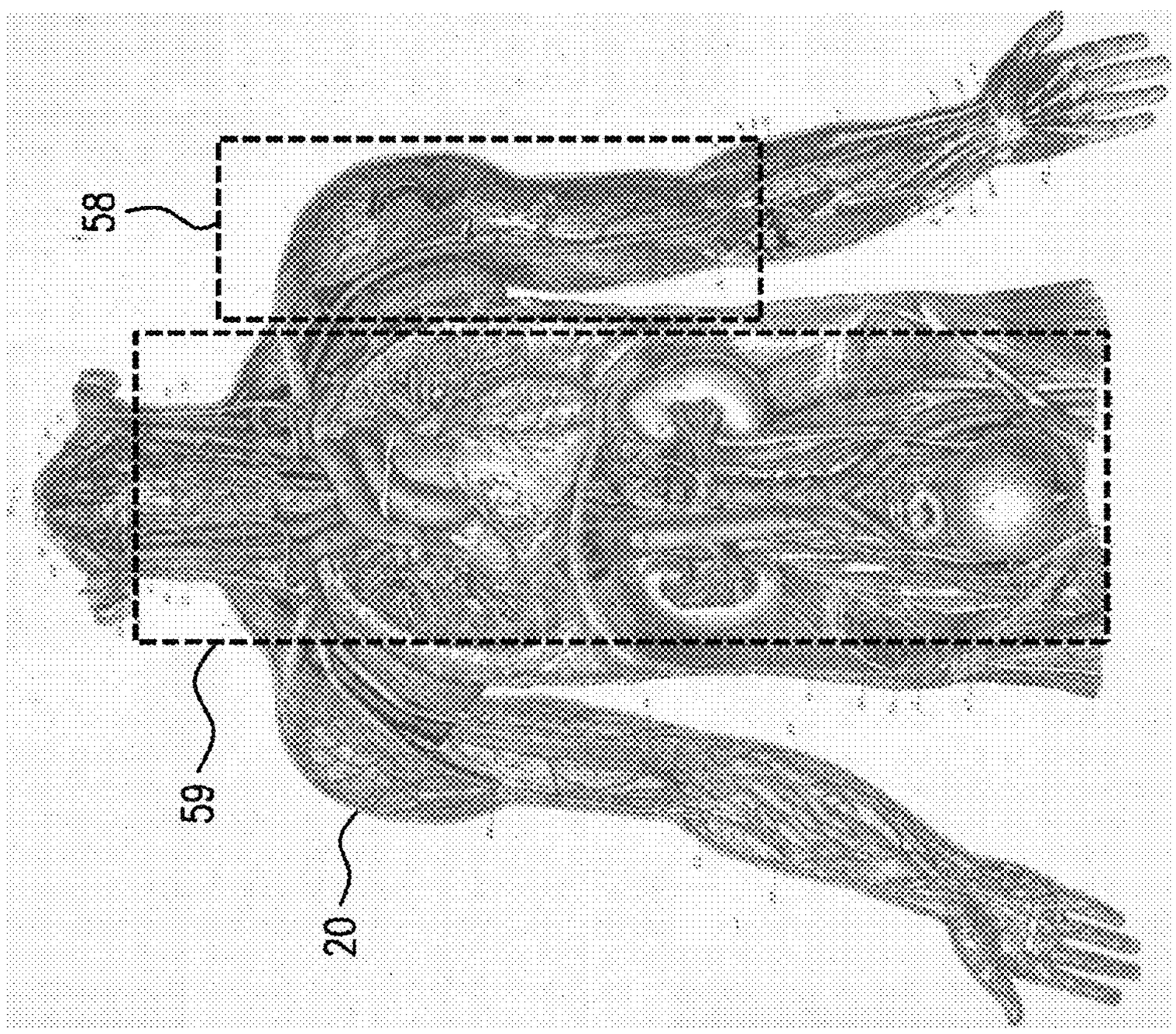

FIG.3

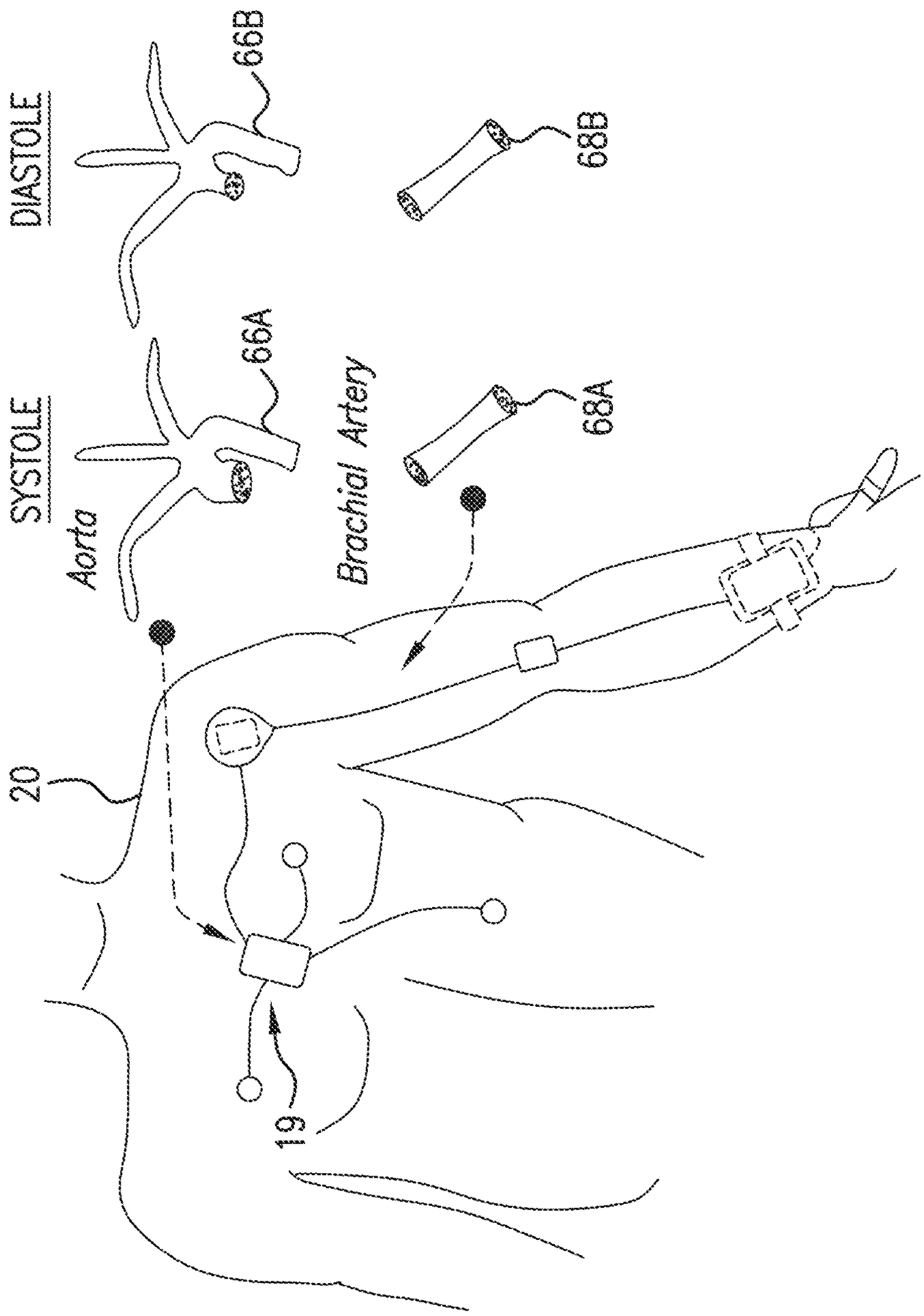
DIASTOLE
66B
68B
SYSTOLE
66A
68A
Aorta
Brachial Artery
20
19

FIG. 4

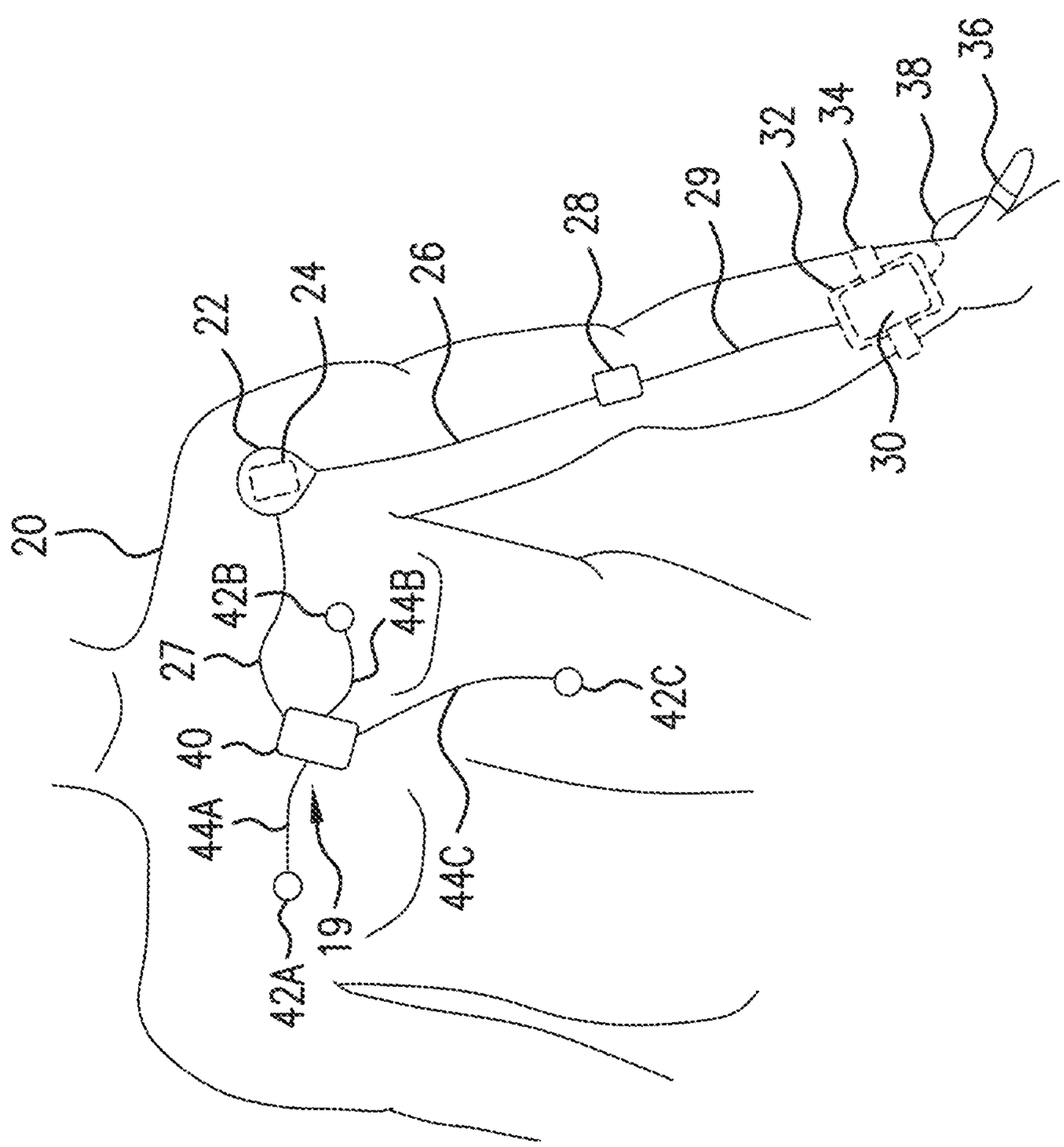

FIG. 5

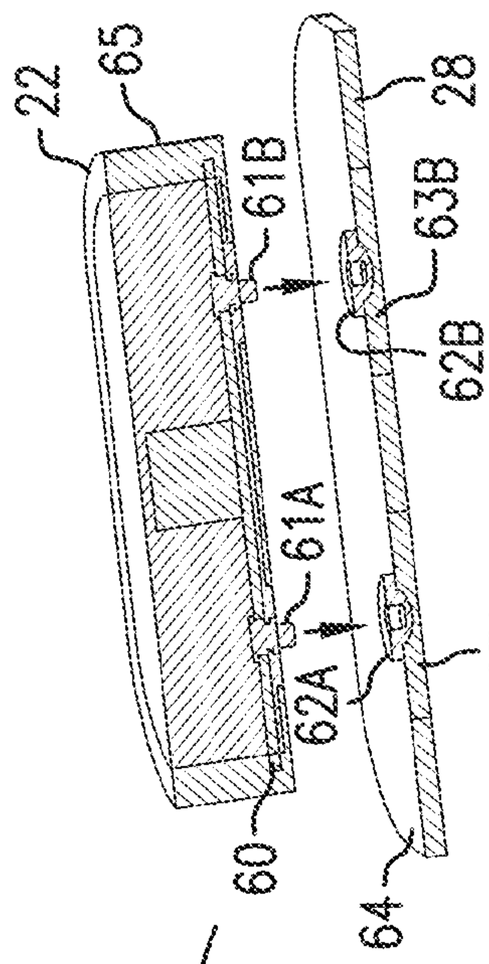
22
65
61B
28
63B
62B
61A
63A
62A
60
64

FIG.6B

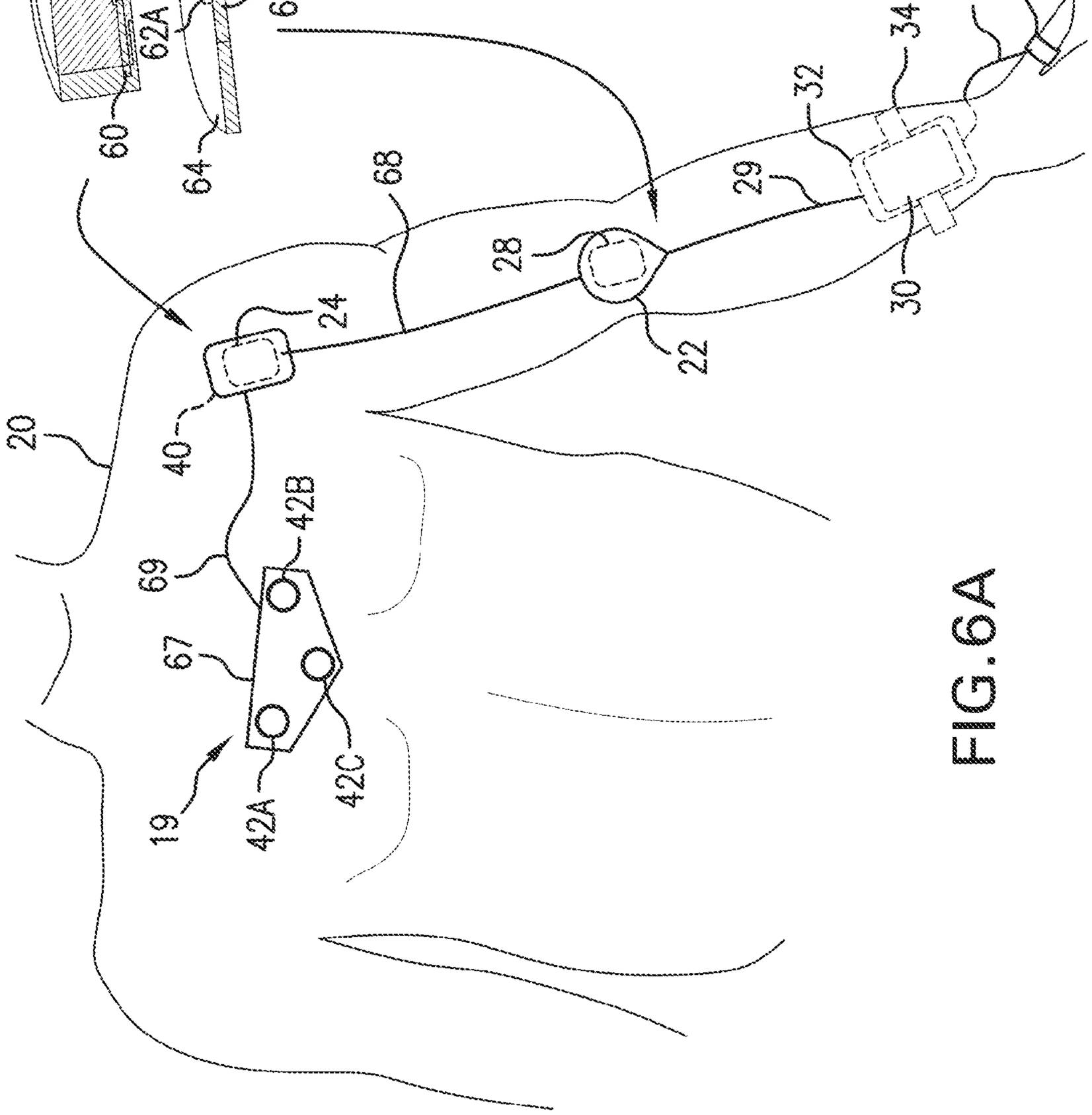
68
29
32
34
38
36
28
24
22
30
20
40
42B
69
67
19
42A
42C

FIG.6A

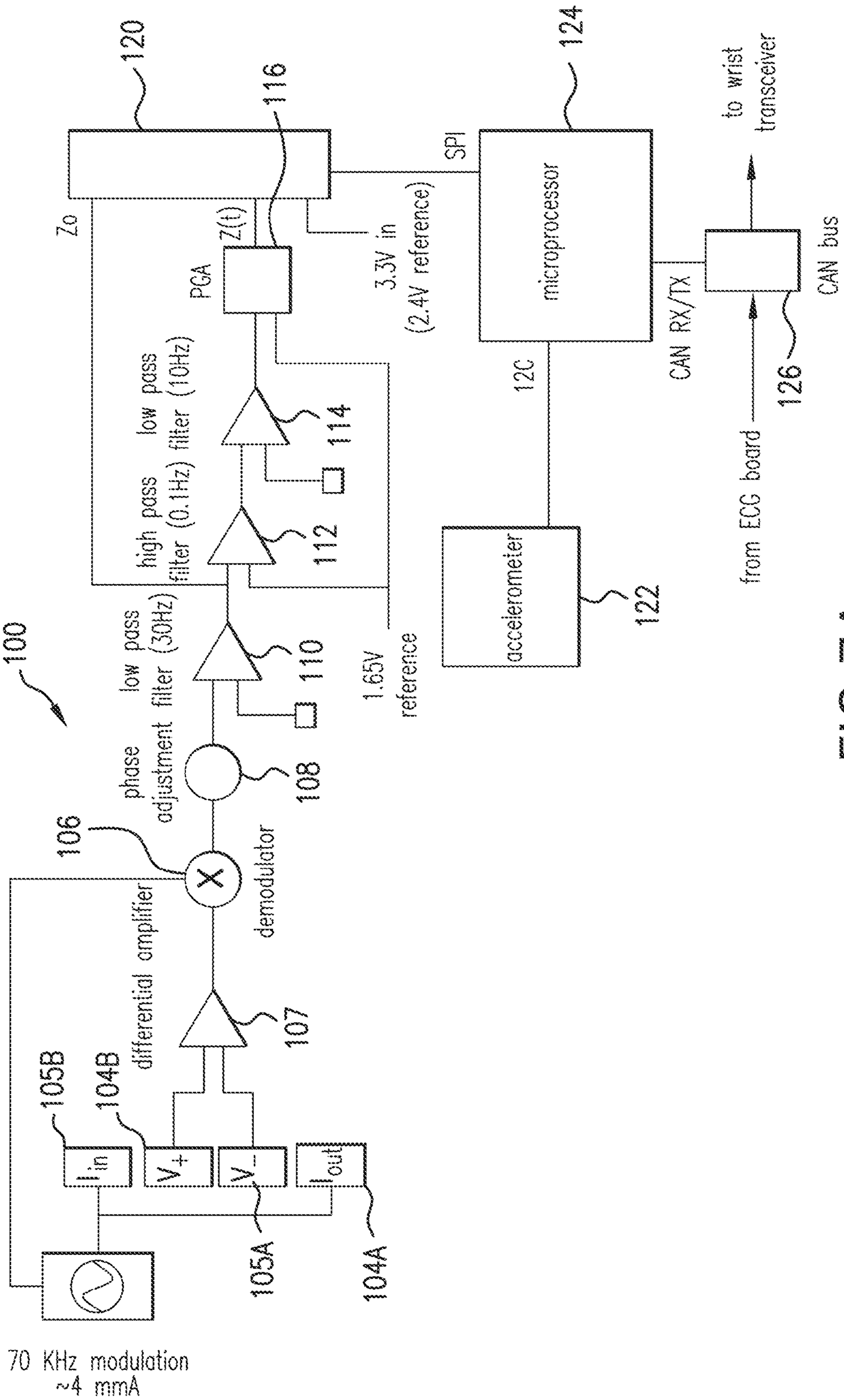
100
120
116
124
Zo
Z(t)
PGA
SPI
microprocessor
3.3V in
(2.4V reference)
to wrist
transceiver
CAN bus
CAN RX/TX
126
12C
high pass
filter (0.1Hz)
low pass
filter (10Hz)
114
112
low pass
filter (30Hz)
110
1.65V
reference
accelerometer
122
from ECG board
phase
adjustment
108
106
differential amplifier
demodulator
107
105B
104B
I_{in}
V_+
V_-
I_{out}
105A
104A
70 KHz modulation
~4 mmA

FIG. 7A

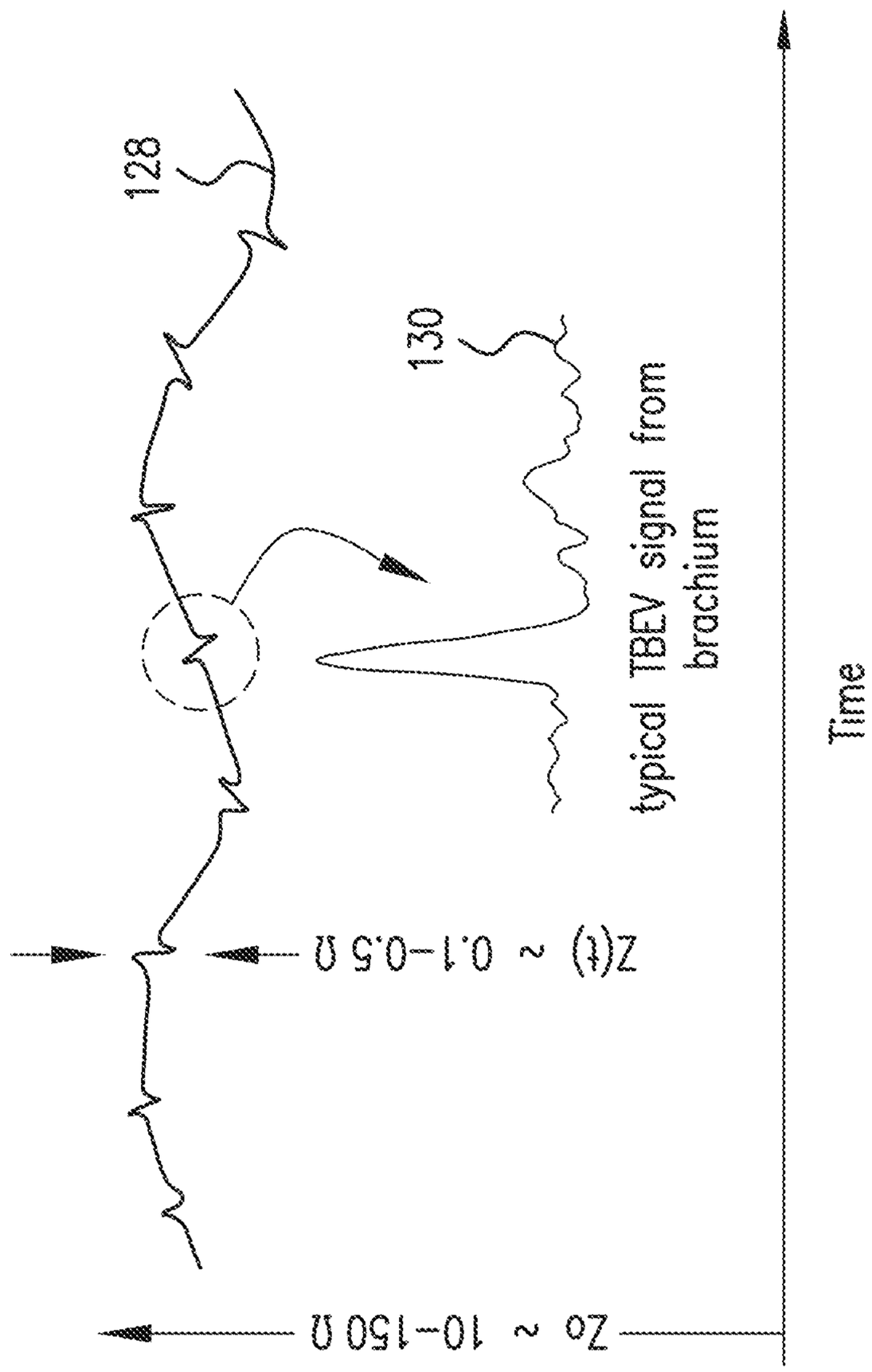
128
130
typical TBEV signal from brachium
Z(t) ~ 0.1-0.5 Ω
Zo ~ 10-150 Ω
Time

FIG. 7B

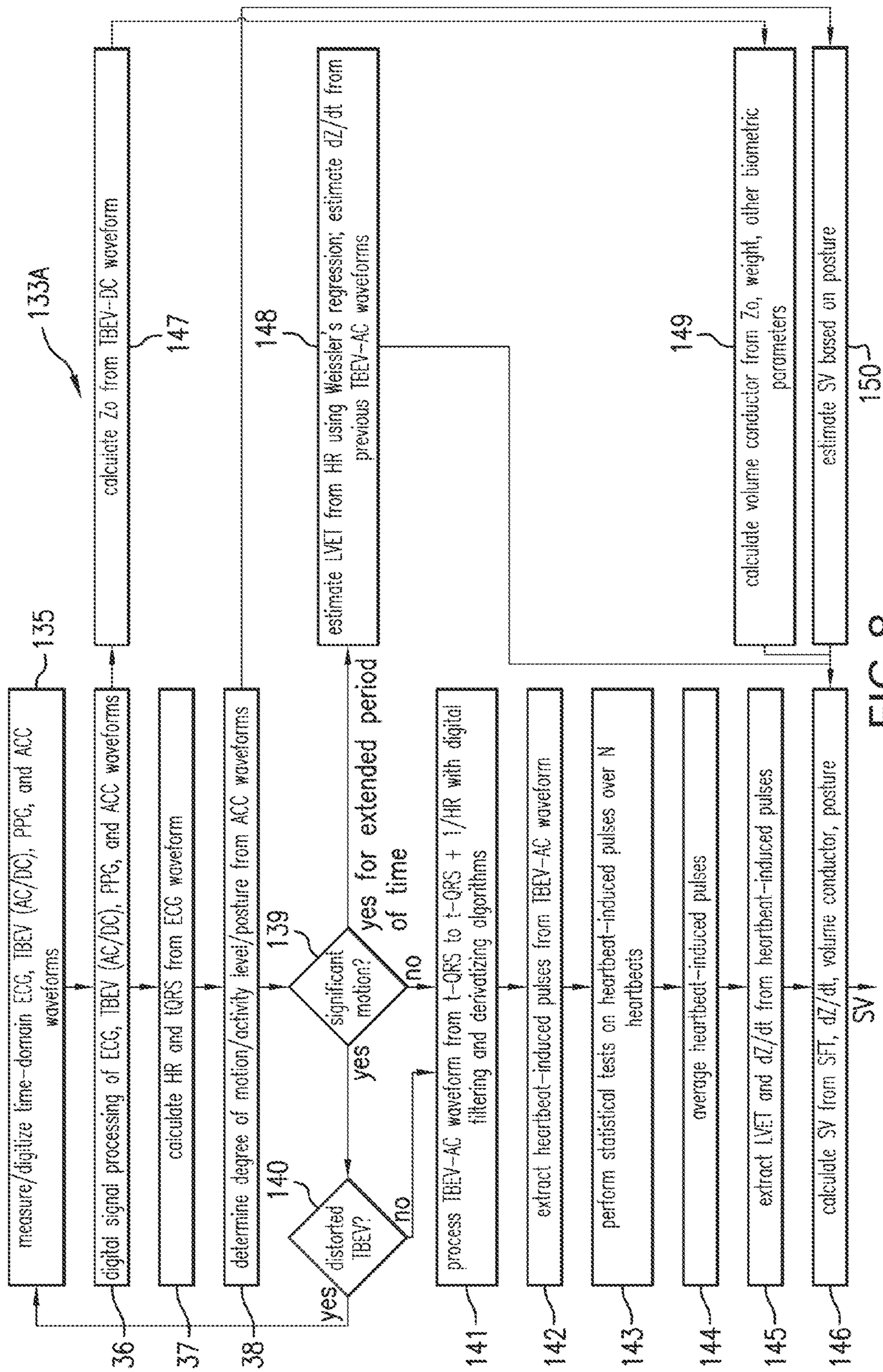
133A
135
measure/digitize time-domain ECG, TBEV (AC/DC), PPG, and ACC waveforms
136
digital signal processing of ECG, TBEV (AC/DC), PPG, and ACC waveforms
137
calculate HR and tQRS from ECG waveform
138
determine degree of motion/activity level/posture from ACC waveforms
139
significant motion?
yes
no
140
distorted TBEV?
yes
no
calculate Zo from TBEV-DC waveform
147
148
estimate LVET from HR using Weissler's regression; estimate dZ/dt from previous TBEV-AC waveforms
149
calculate volume conductor from Zo, weight, other biometric parameters
150
estimate SV based on posture
process TBEV-AC waveform from t-QRS to t-QRS + 1/HR with digital filtering and derivatizing algorithms
141
extract heartbeat-induced pulses from TBEV-AC waveform
142
perform statistical tests on heartbeat-induced pulses over N heartbeats
143
average heartbeat-induced pulses
144
extract LVET and dZ/dt from heartbeat-induced pulses
145
calculate SV from SFT, dZ/dt, volume conductor, posture
146
SV

FIG.8

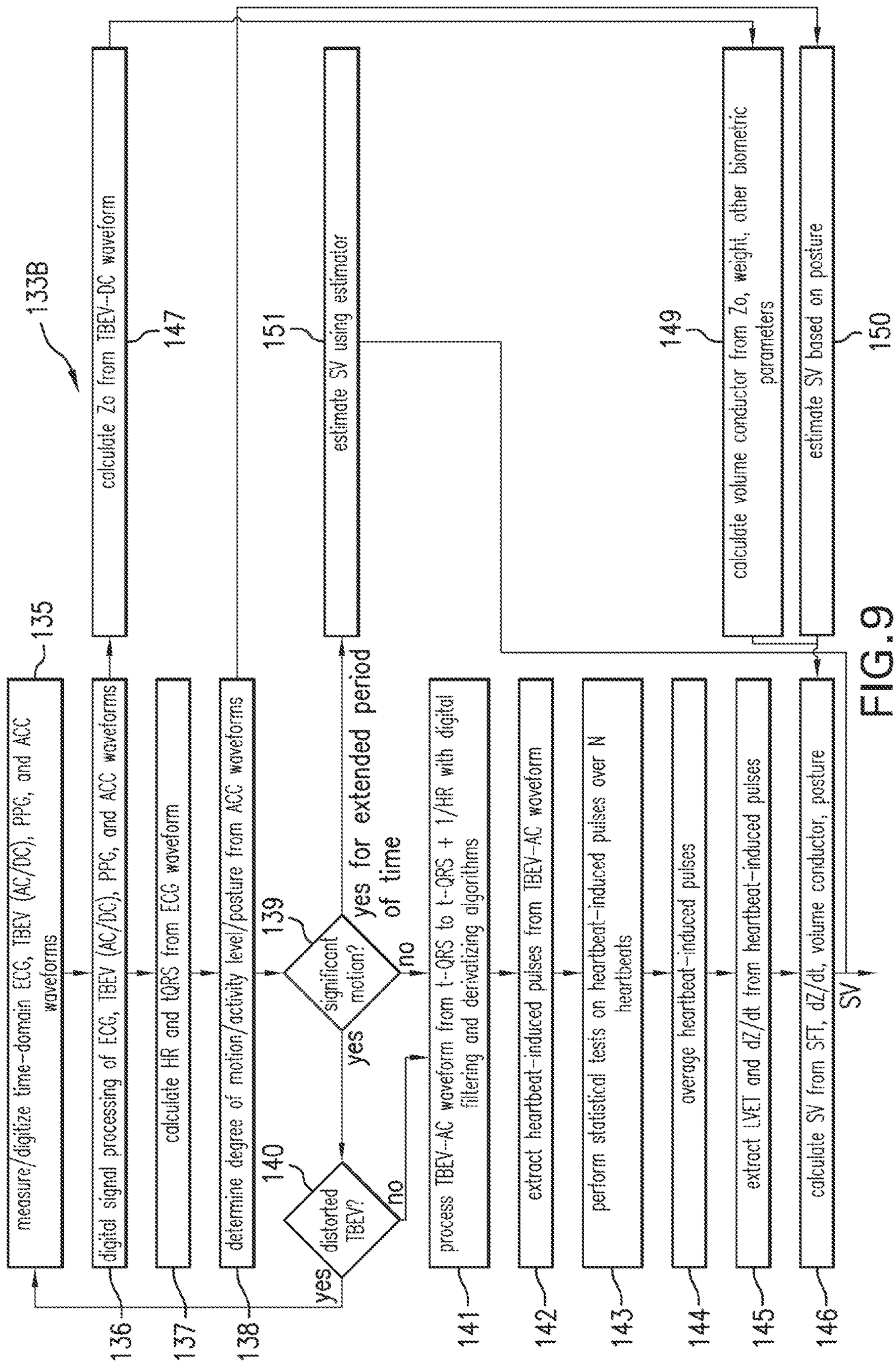
133B
135
measure/digitize time-domain ECG, TBEV (AC/DC), PPG, and ACC waveforms
136
digital signal processing of ECG, TBEV (AC/DC), PPG, and ACC waveforms
137
calculate HR and tQRS from ECG waveform
138
determine degree of motion/activity level/posture from ACC waveforms
139
significant motion?
yes
no
140
distorted TBEV?
yes
no
141
process TBEV-AC waveform from t-QRS to t-QRS + 1/HR with digital filtering and derivatizing algorithms
142
extract heartbeat-induced pulses from TBEV-AC waveform
143
perform statistical tests on heartbeat-induced pulses over N heartbeats
144
average heartbeat-induced pulses
145
extract LVET and dZ/dt from heartbeat-induced pulses
146
calculate SV from SFT, dZ/dt, volume conductor, posture
SV
147
calculate Zo from TBEV-DC waveform
151
estimate SV using estimator
yes
of time
149
calculate volume conductor from Zo, weight, other biometric parameters
150
estimate SV based on posture

FIG. 9

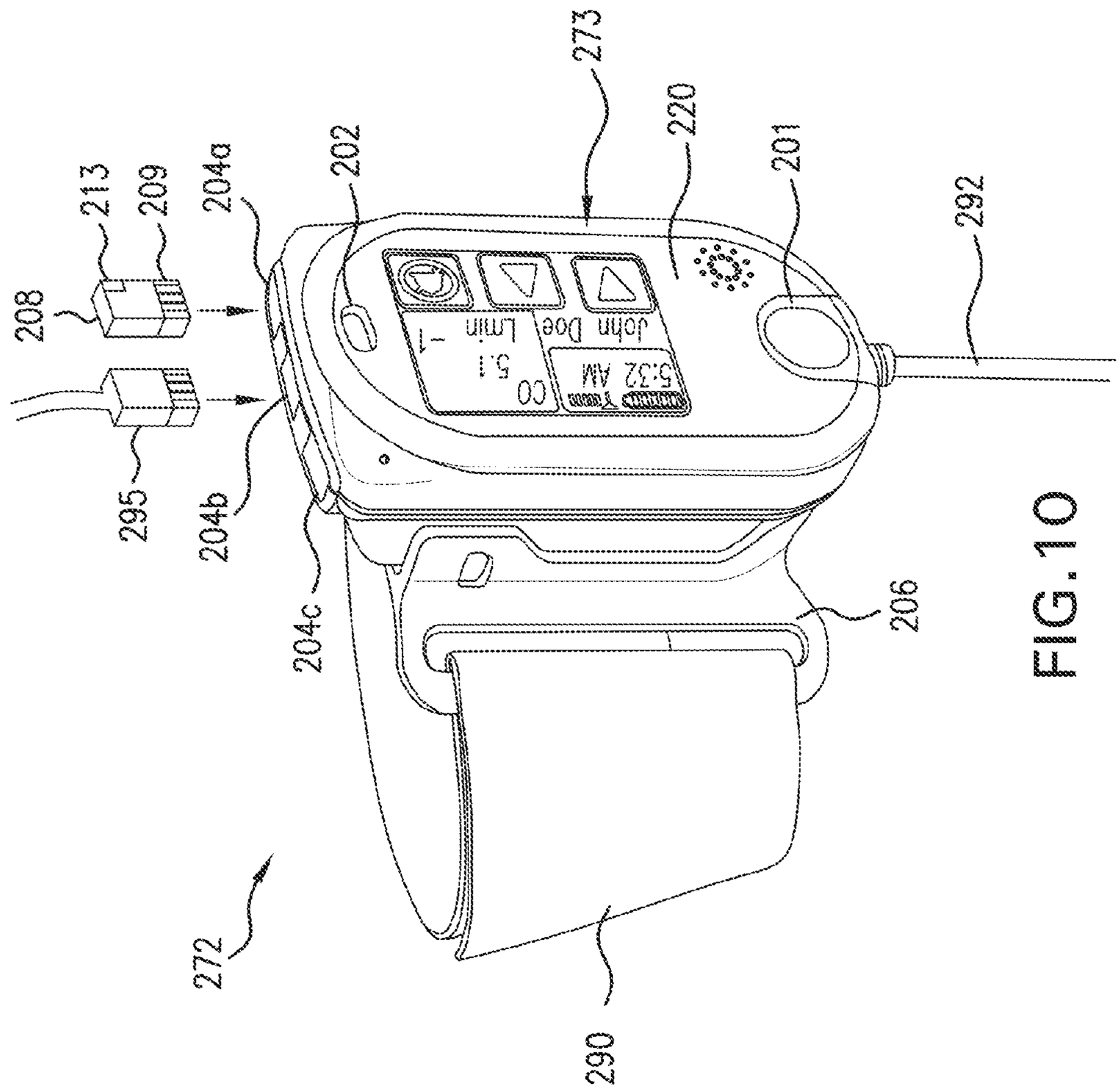
273
220
201
292
202
204a
213
209
208
295
204b
204c
206
272
290
5:32 AM
CO 5.1
Lmin -1
John Doe

FIG. 10

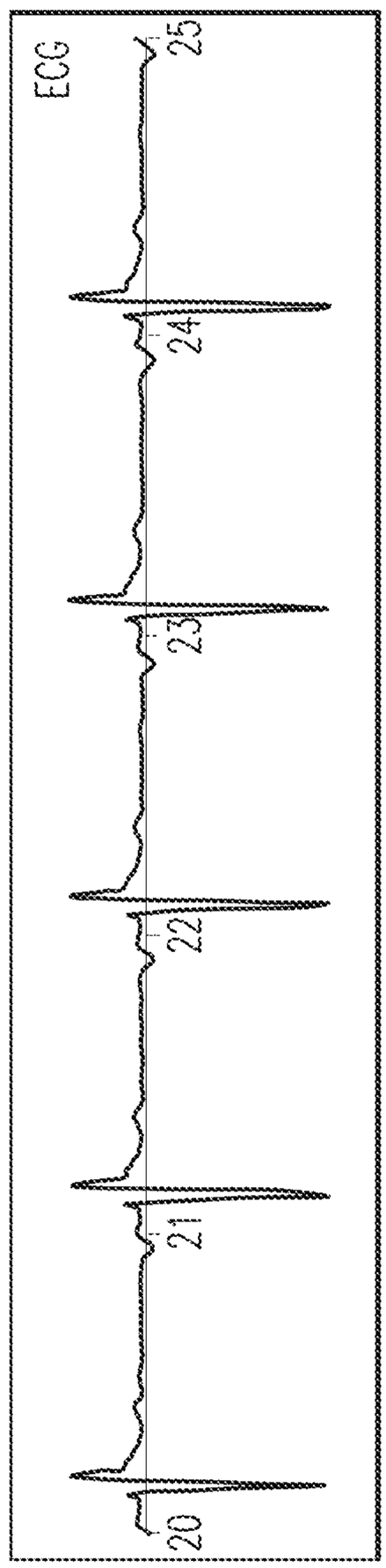

FIG. 11A

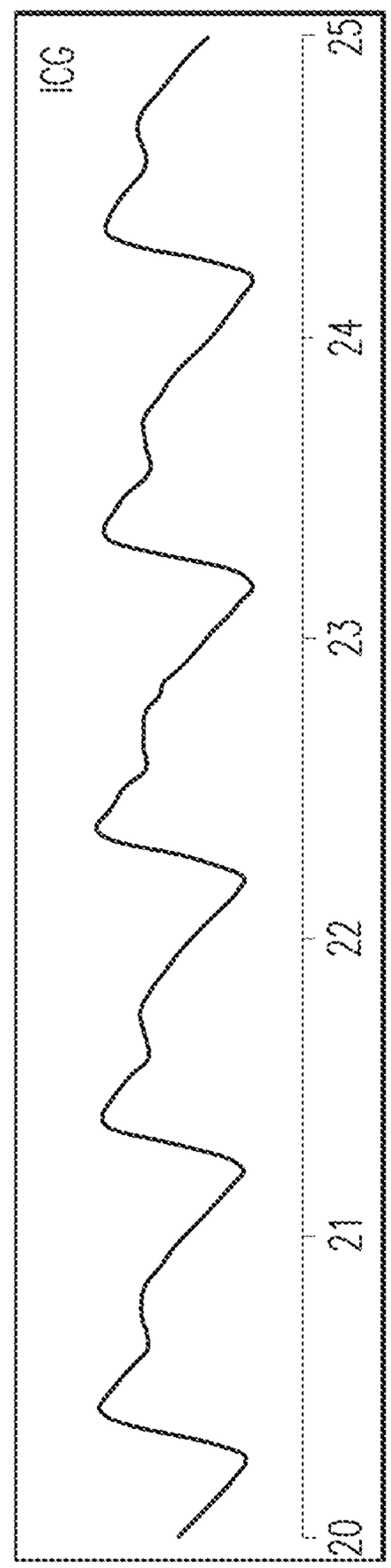

FIG. 11B

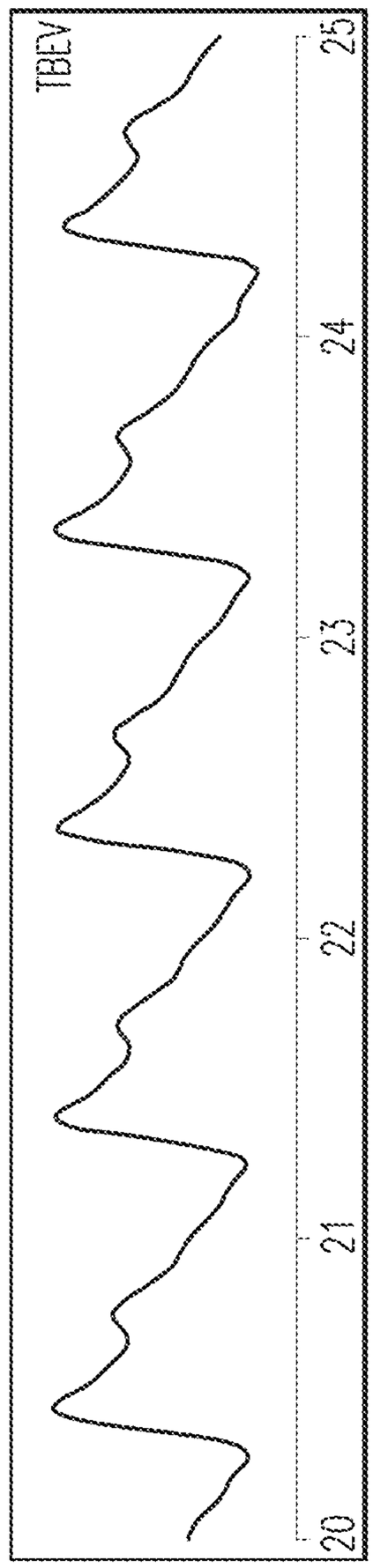

FIG.11C

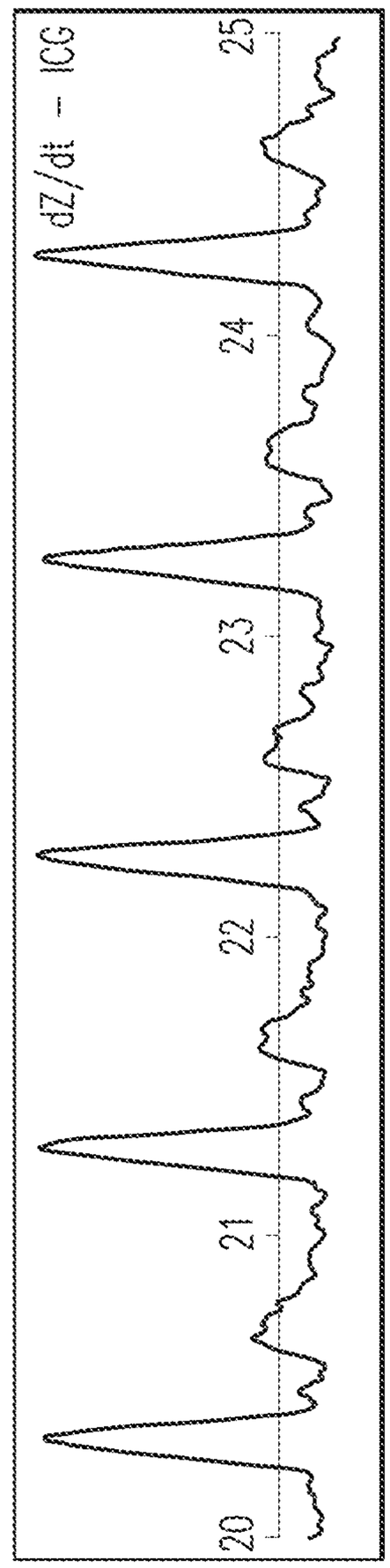

FIG.11D

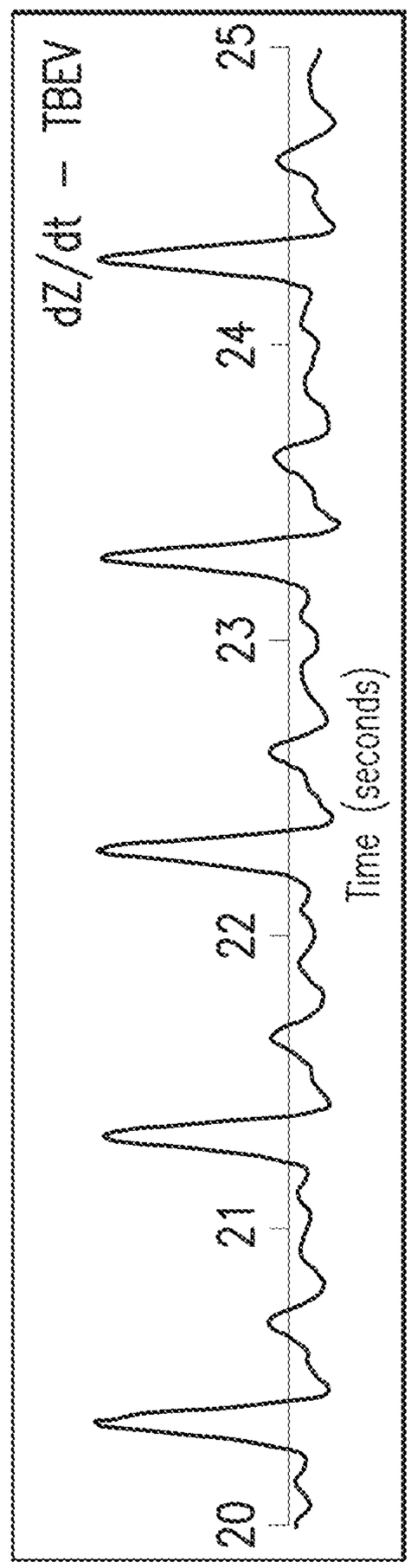

FIG. 11E

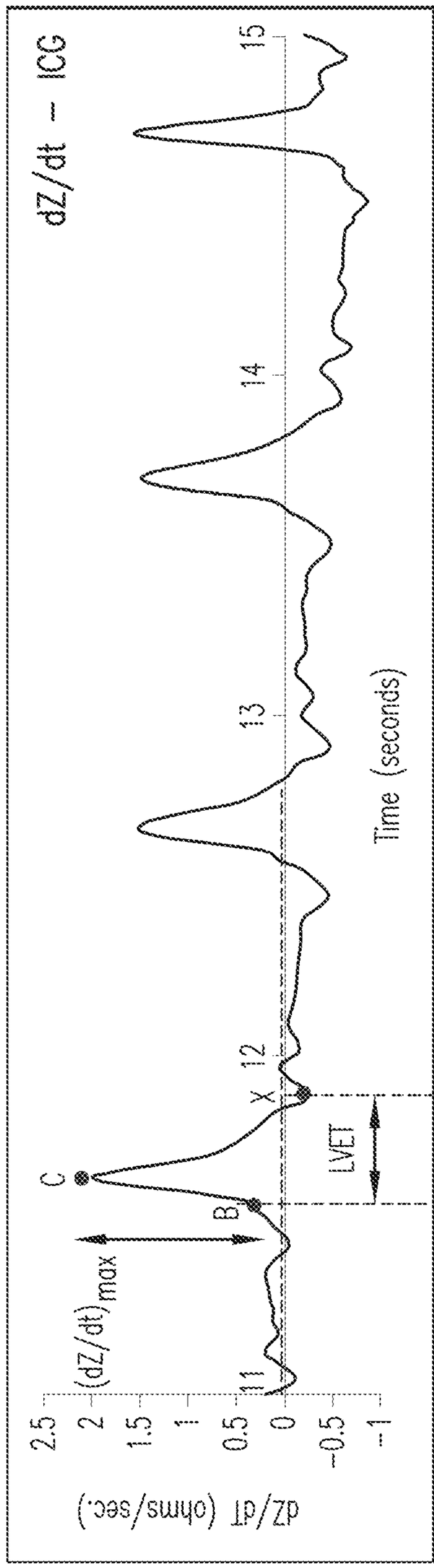

FIG. 12A

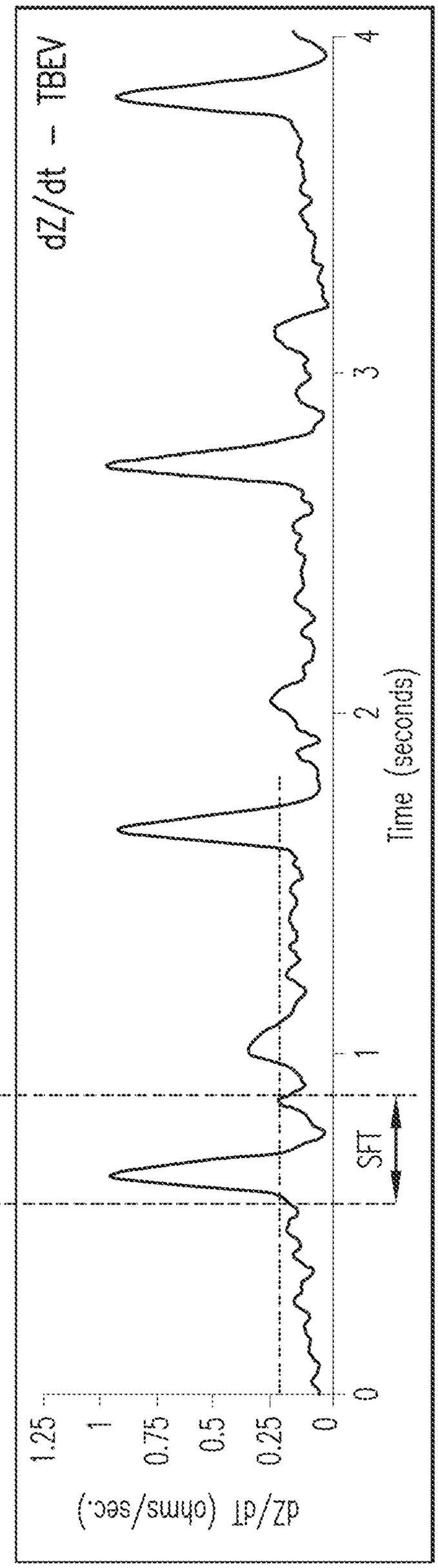

FIG. 12B

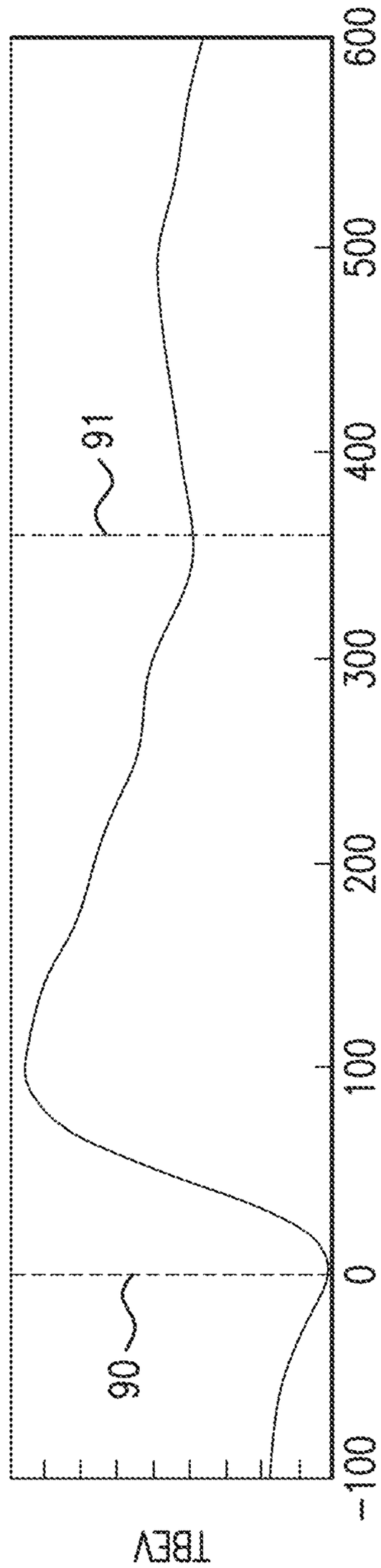

FIG. 13A

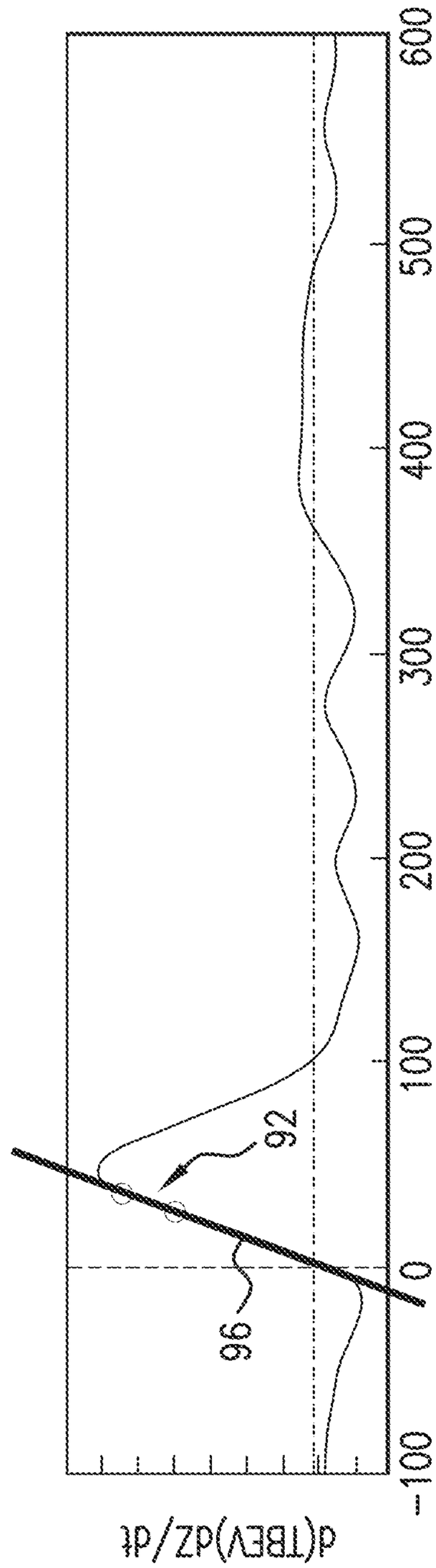

FIG. 13B

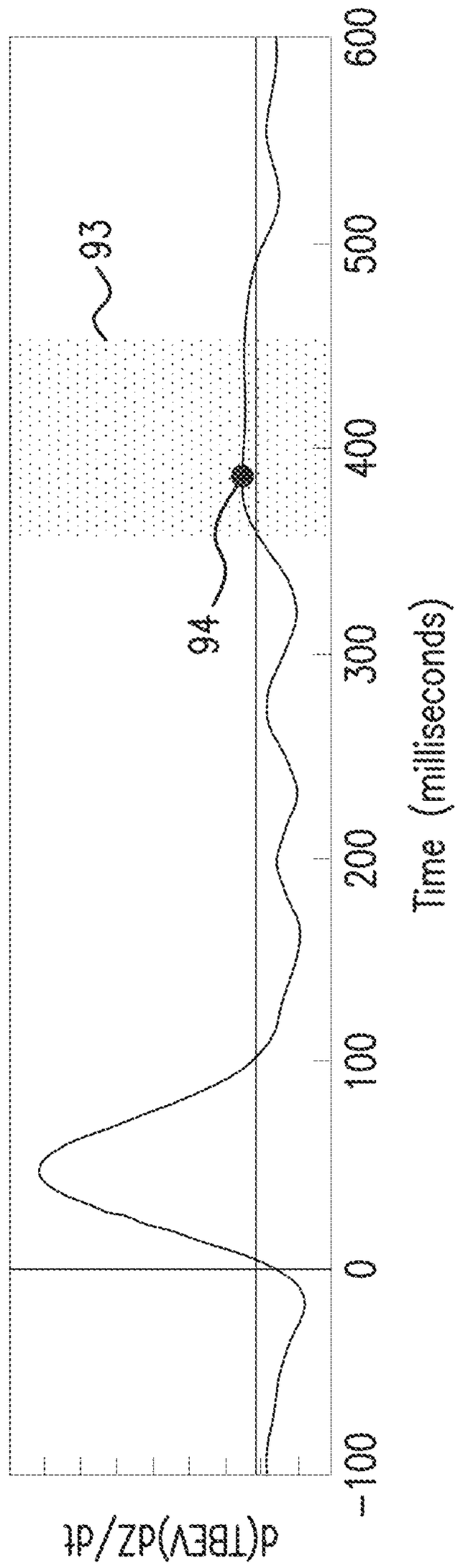

FIG. 13C

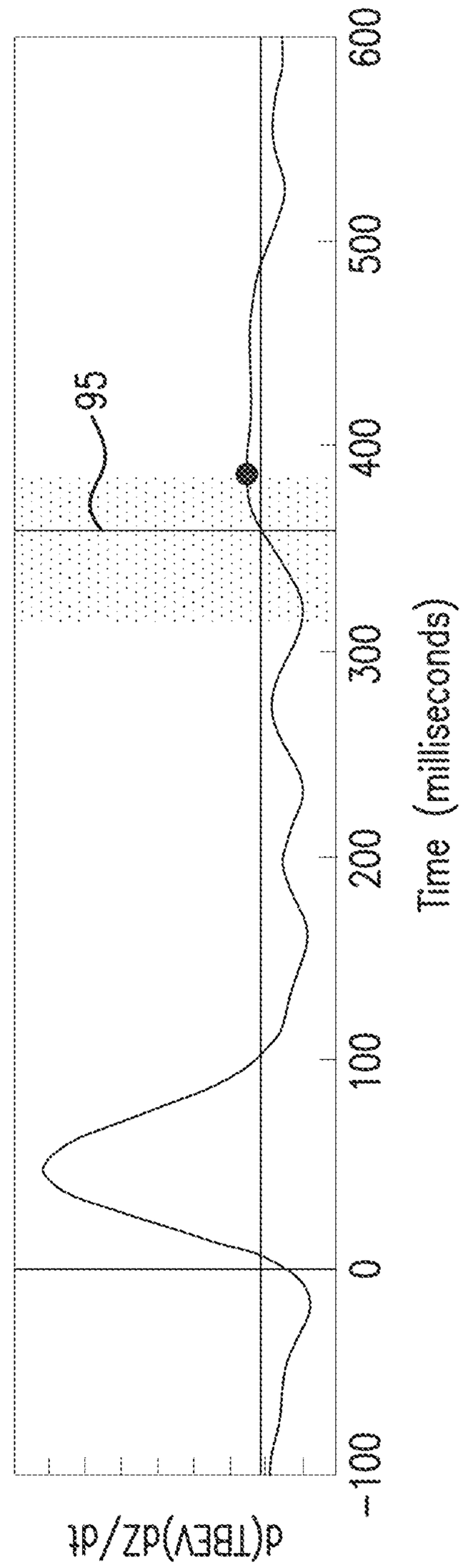

FIG. 13D

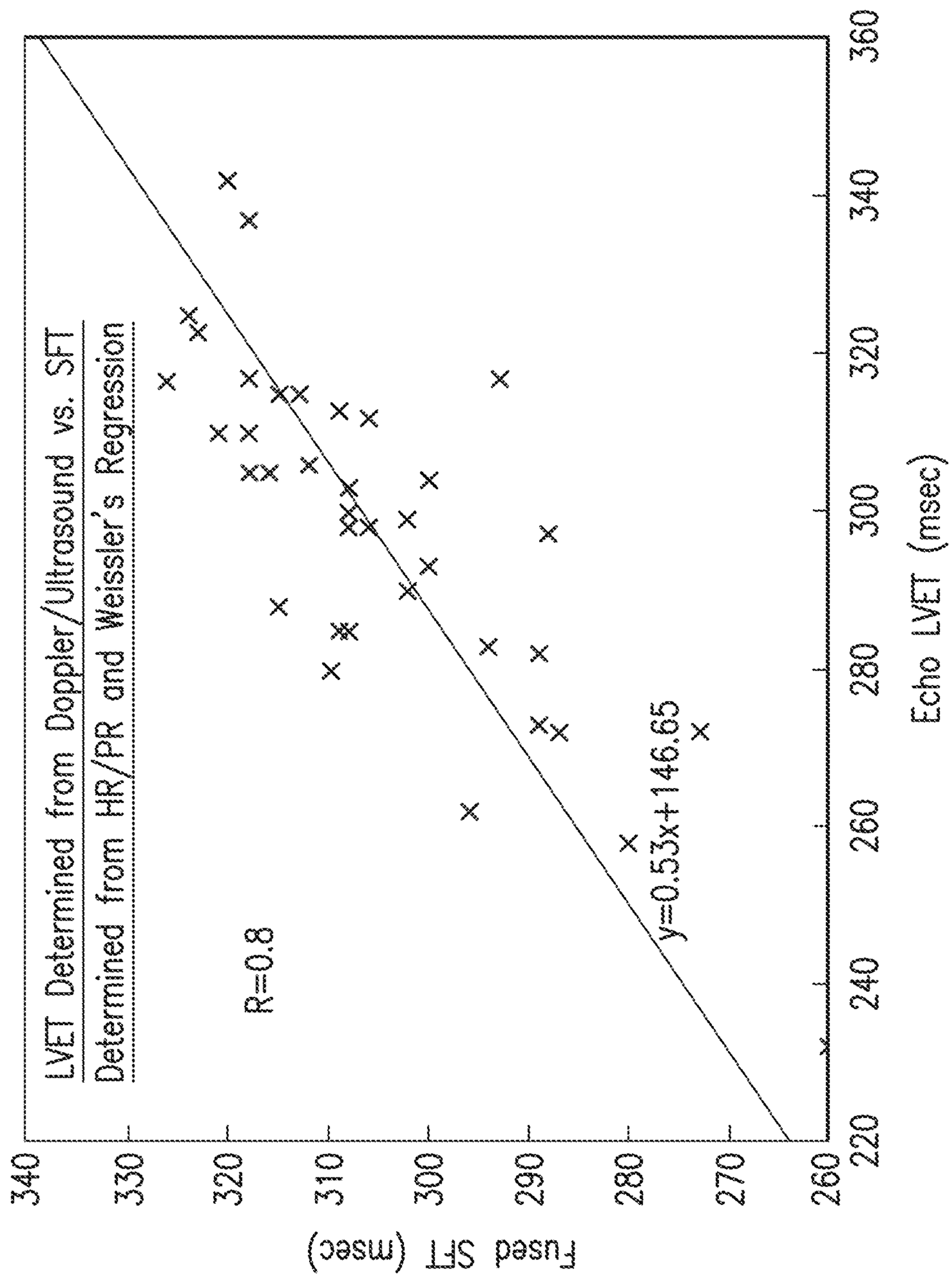
LVET Determined from Doppler/Ultrasound vs. SFT
Determined from HR/PR and Weissler's Regression
R=0.8
y=0.53x+146.65
Fused SFT (msec)
Echo LVET (msec)
340
330
320
310
300
290
280
270
260
220
240
260
280
300
320
340
360

FIG. 14

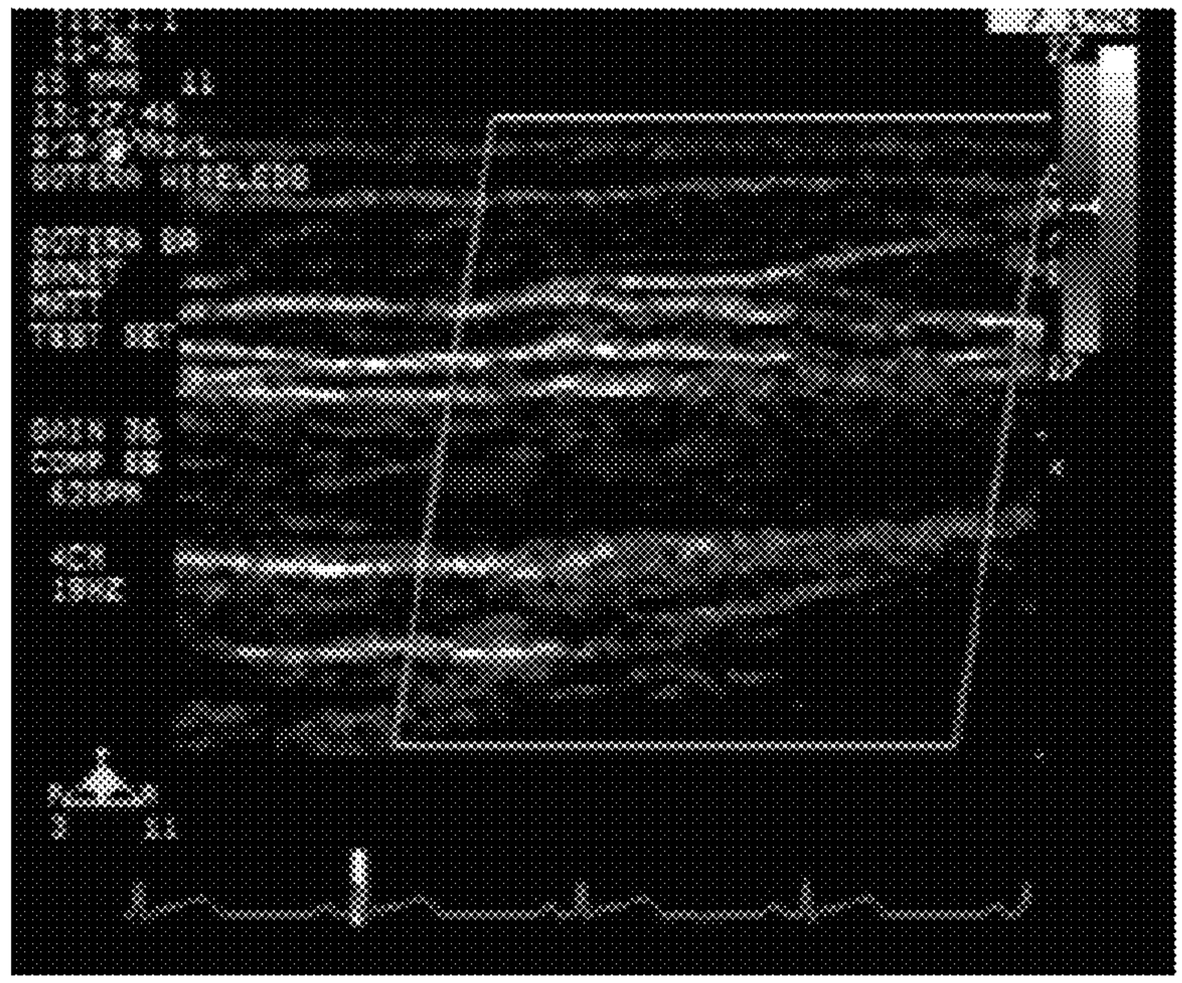

FIG. 15A

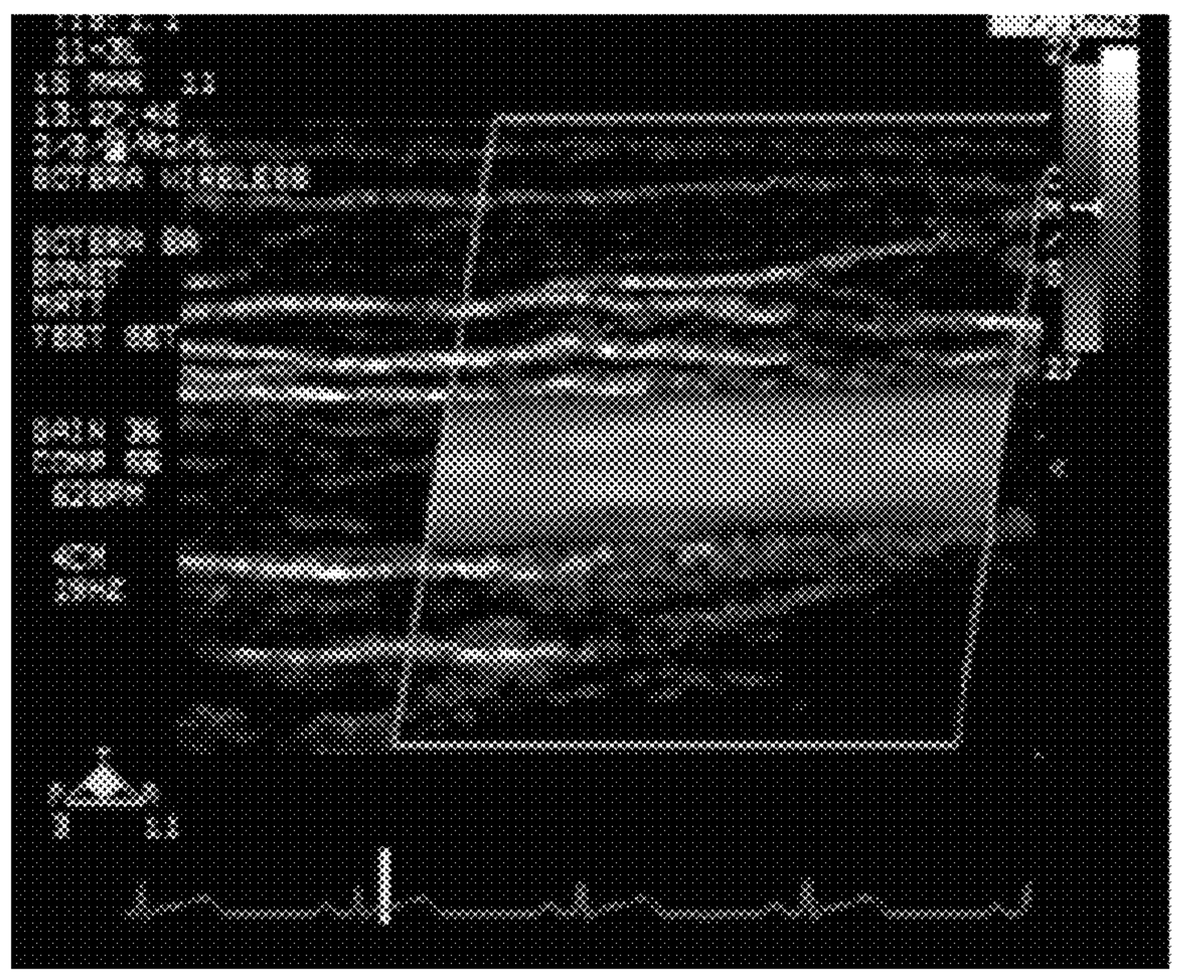

FIG. 15B

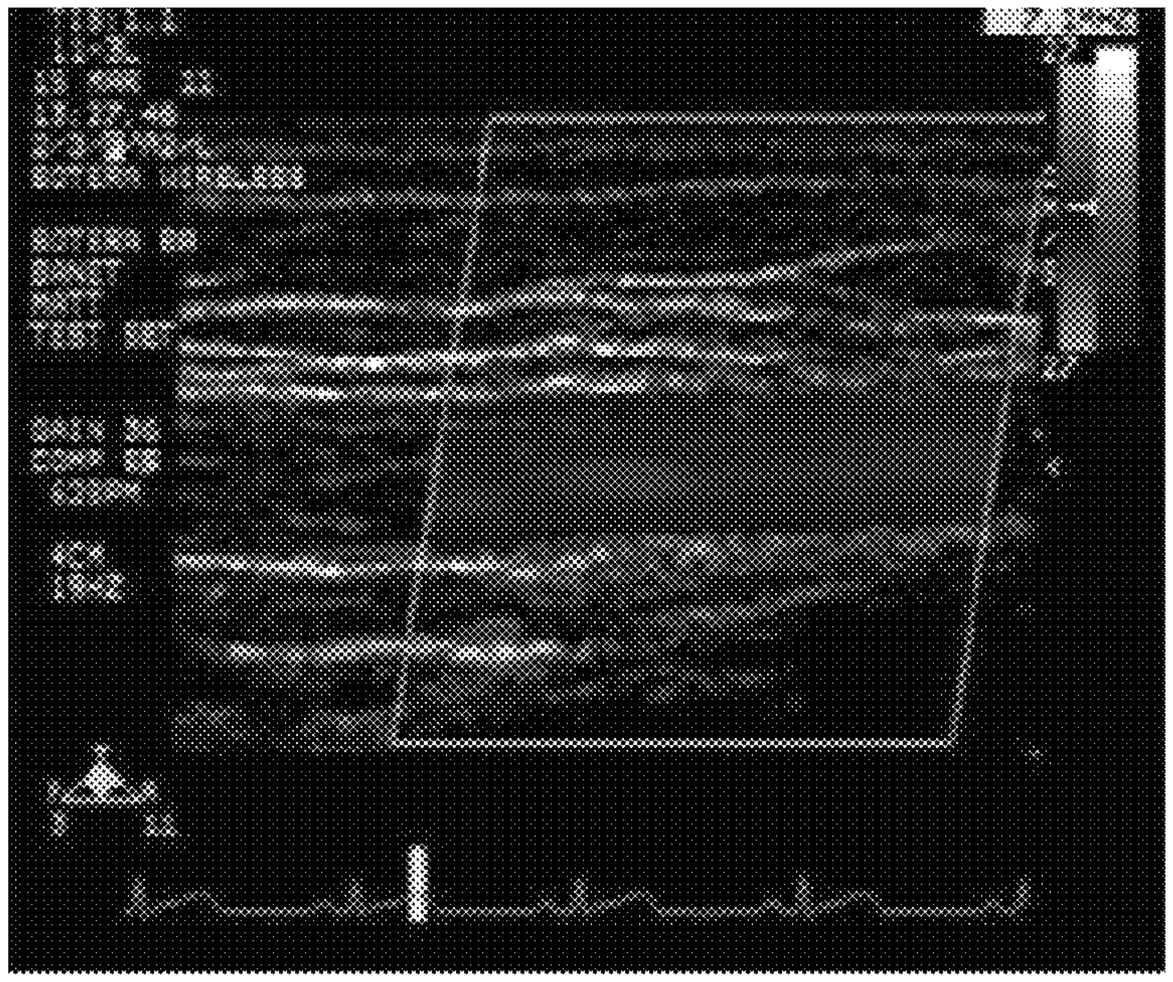

FIG. 15C

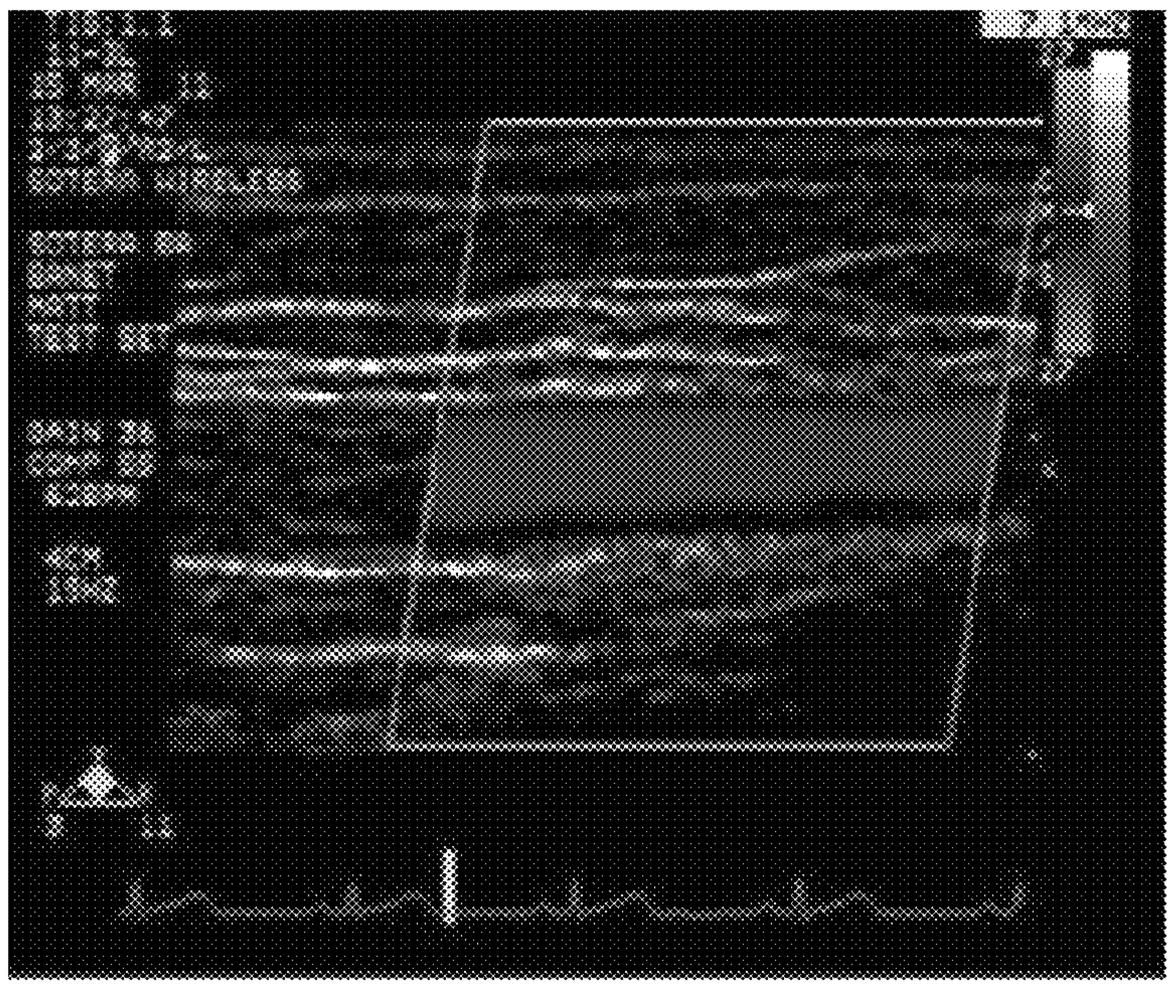

FIG. 15D

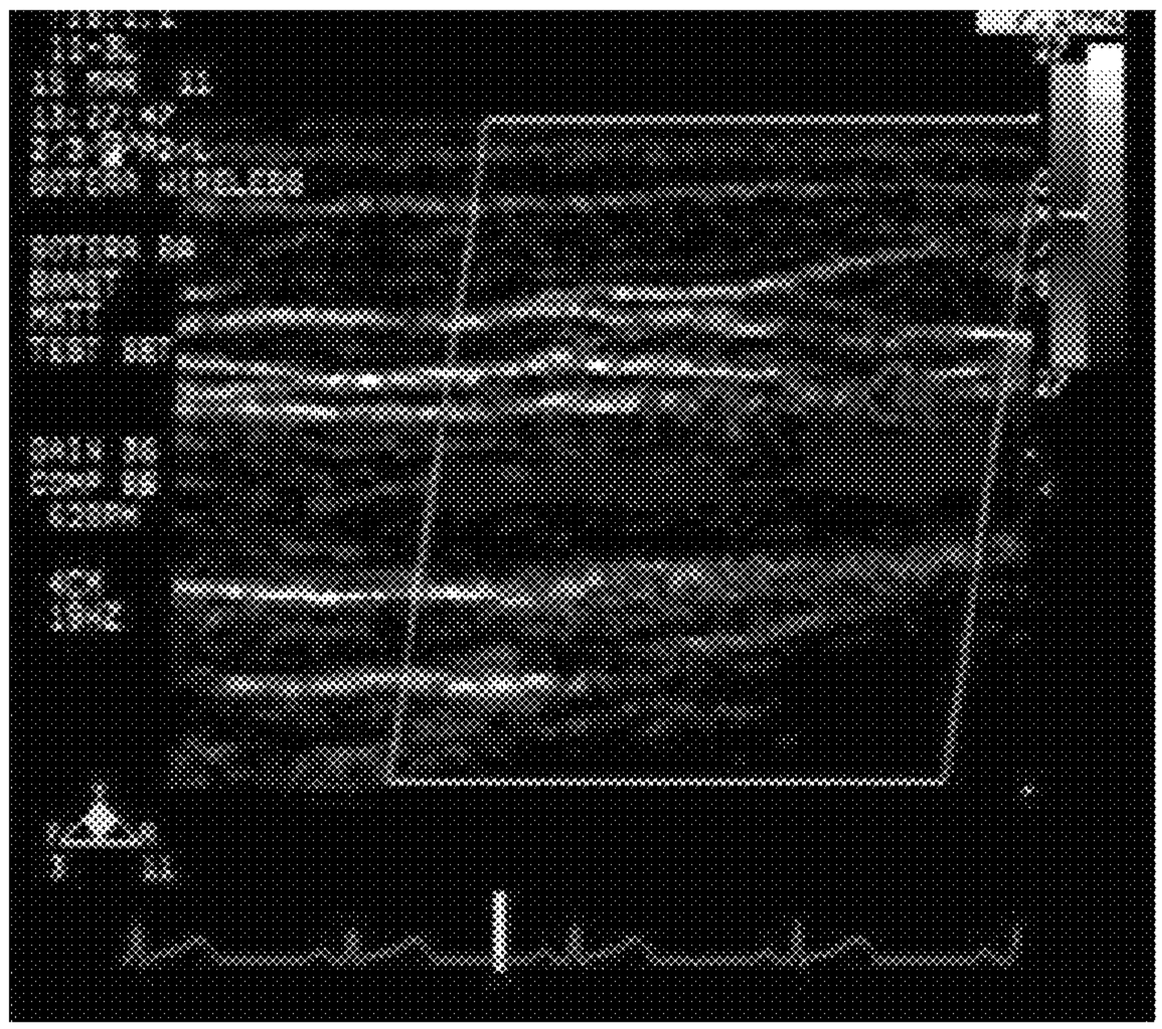

FIG.15E

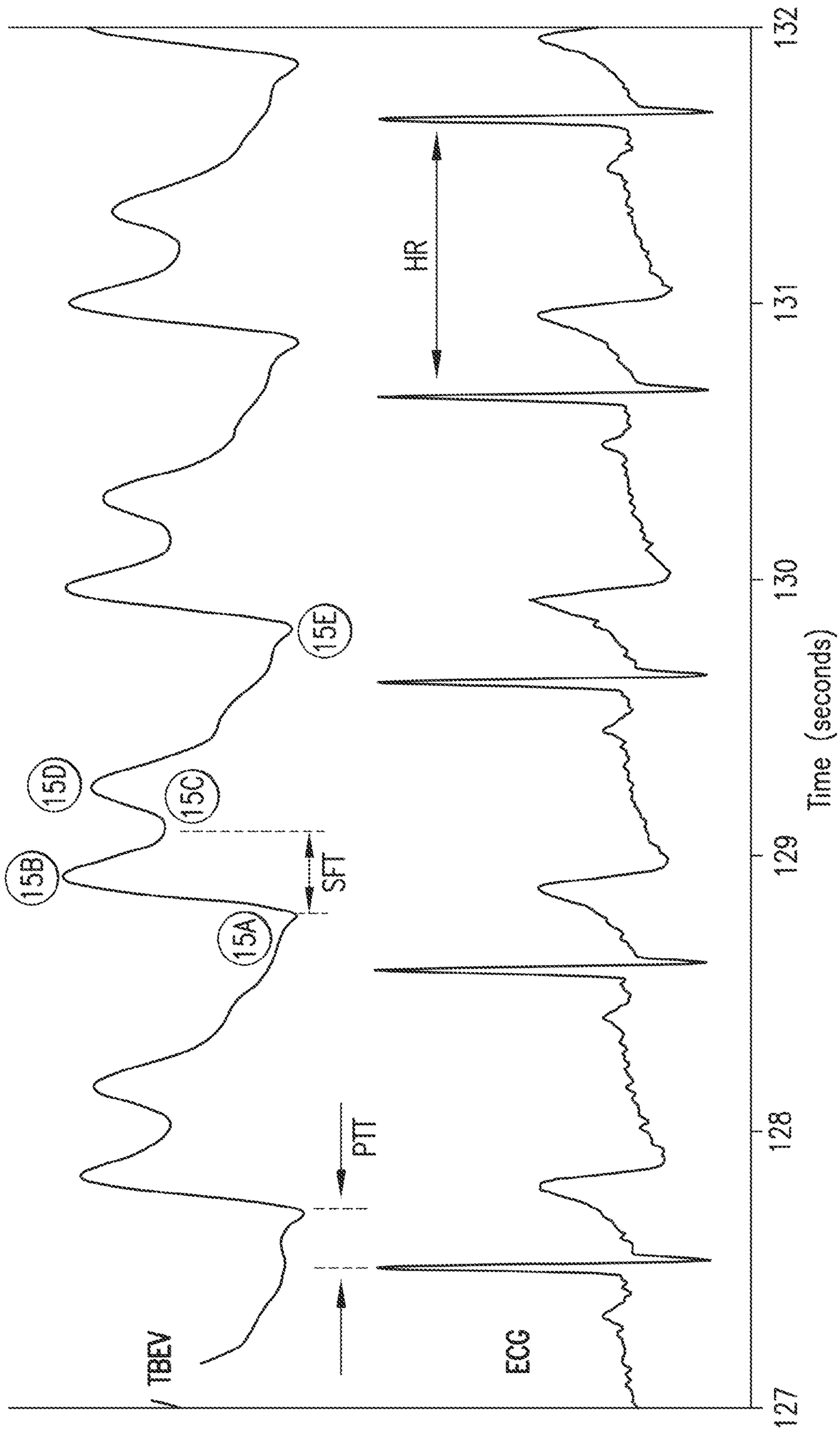
TBEV
ECG
PTT
HR
SFT
15A
15B
15C
15D
15E
127
128
129
130
131
132
Time (seconds)

FIG. 15F

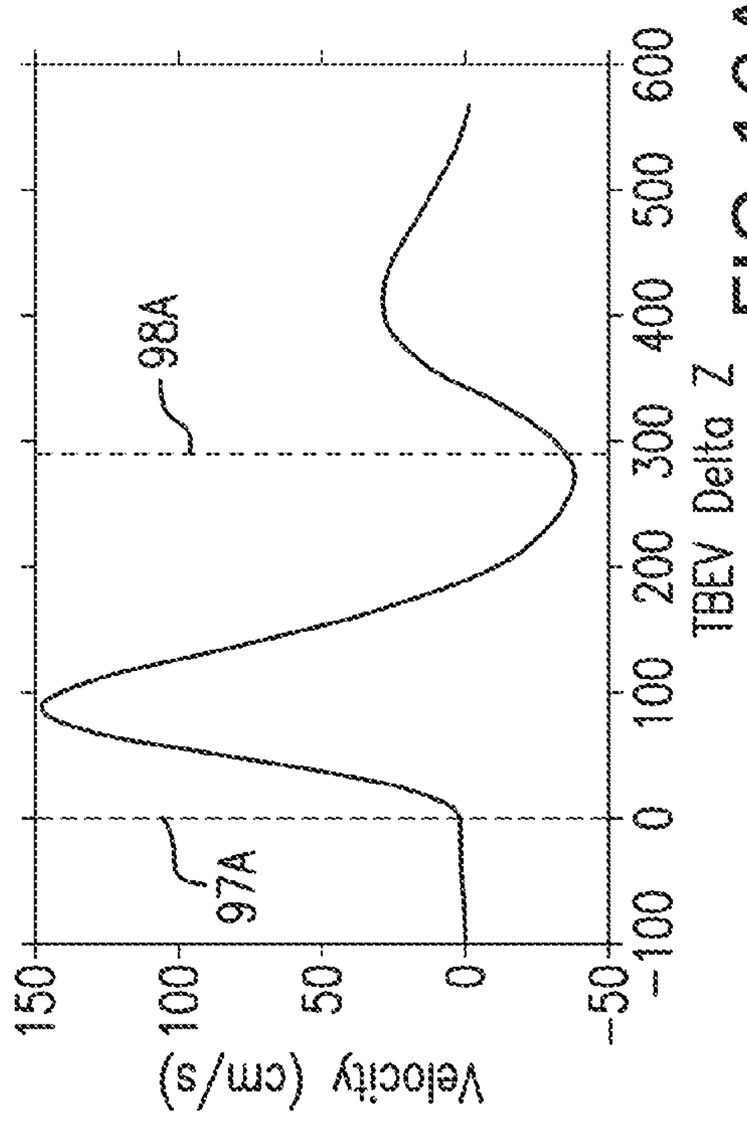

FIG. 16A

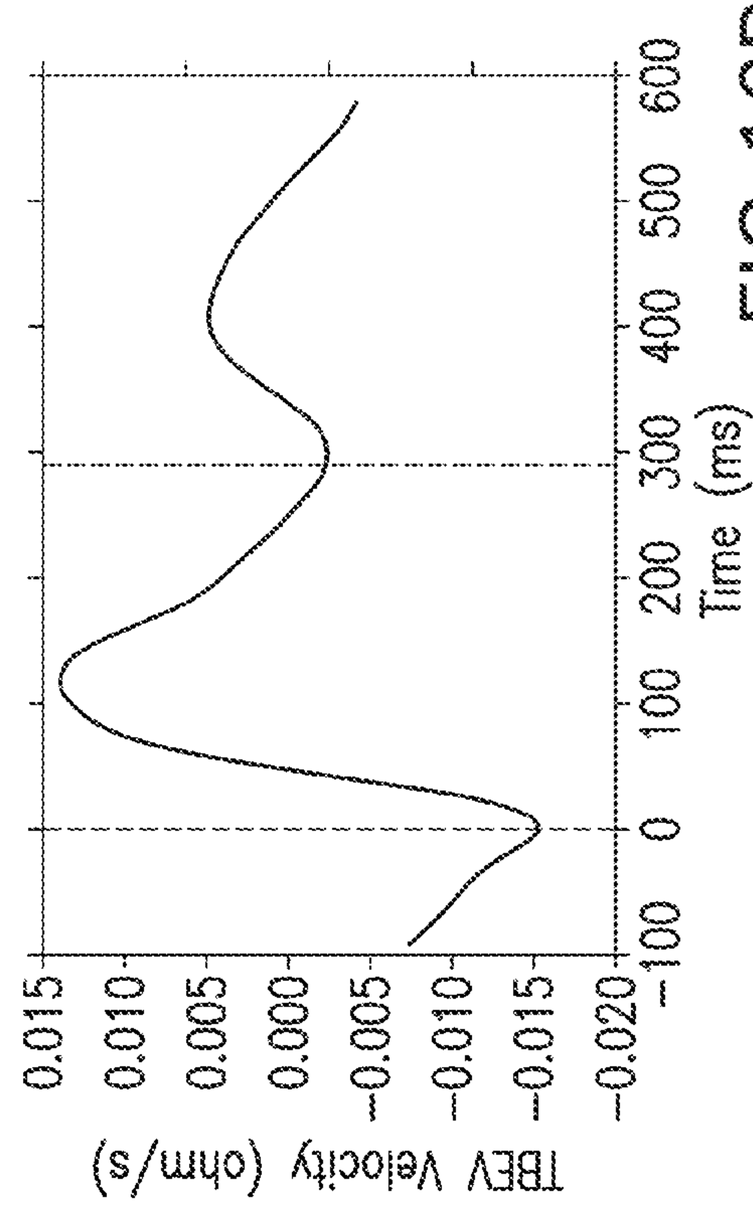

FIG. 16B

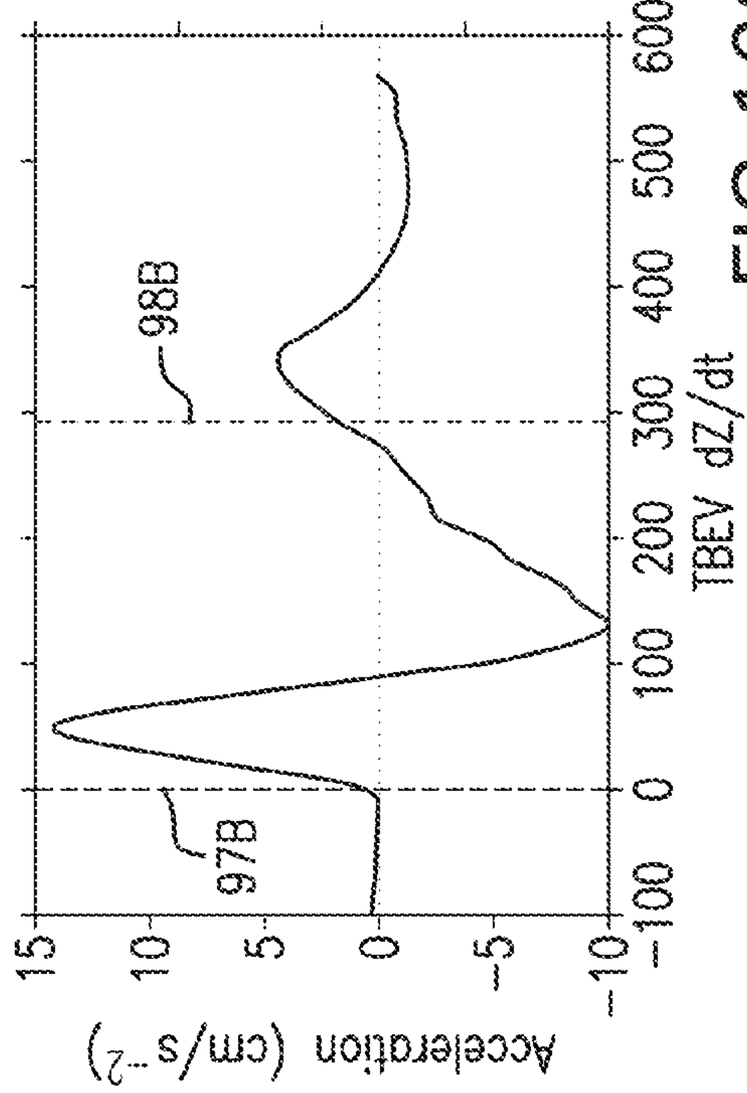

FIG. 16C

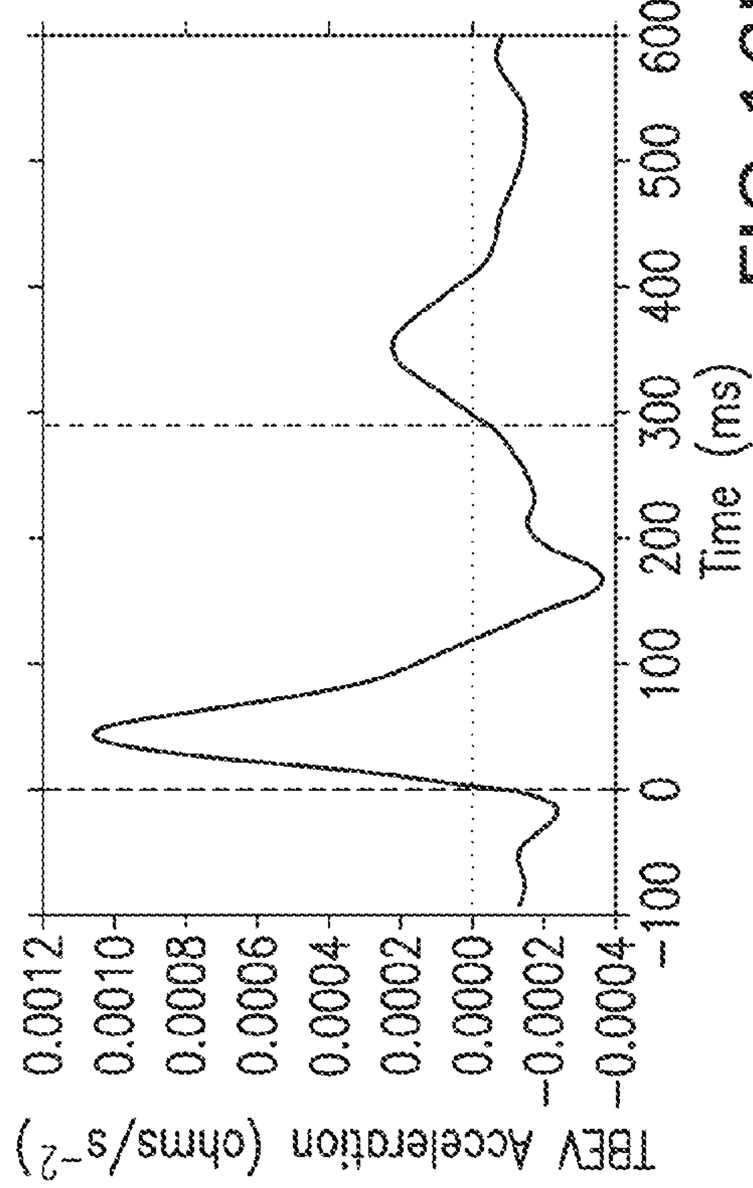

FIG. 16D

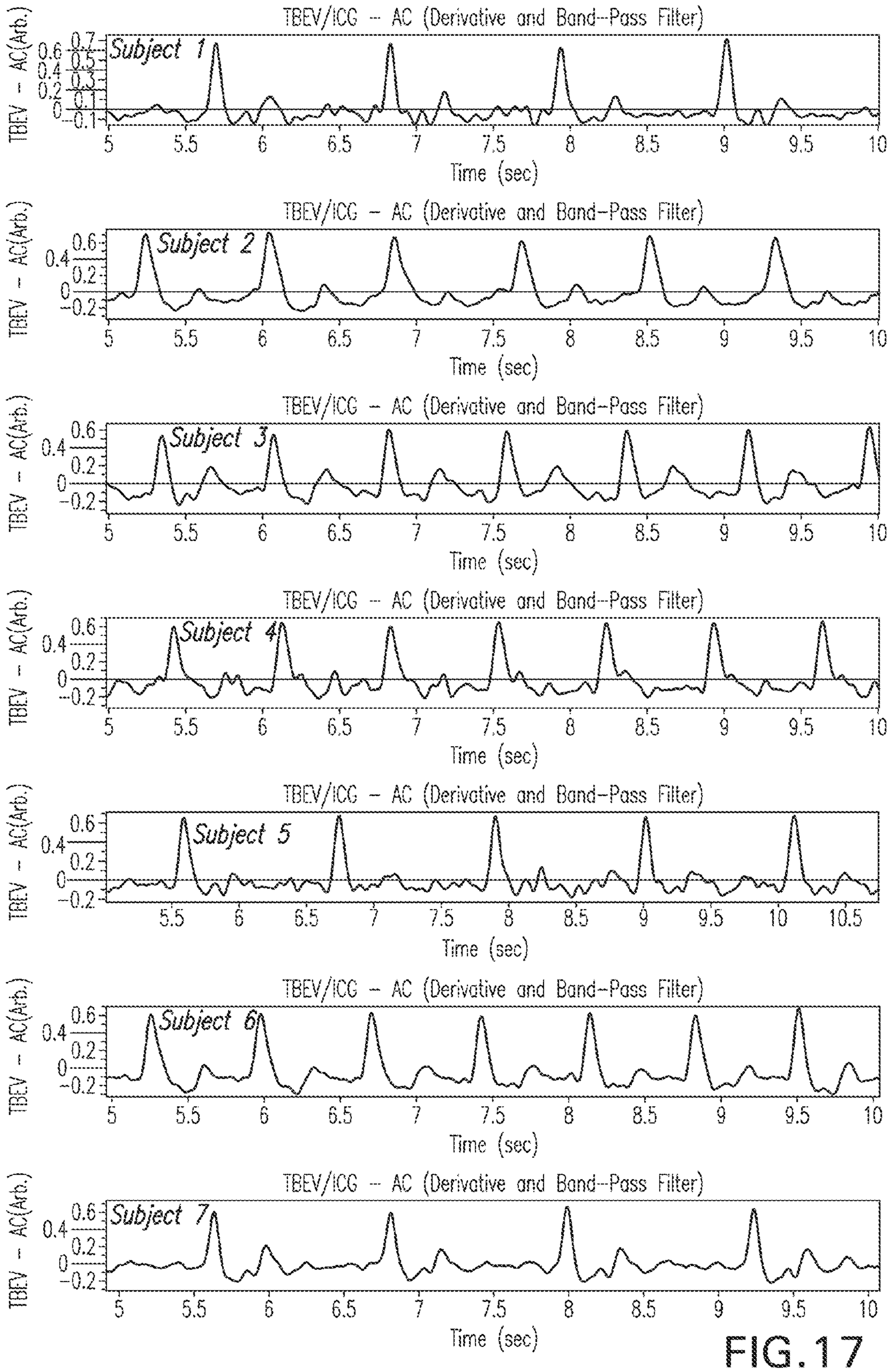
TBEV/ICG – AC (Derivative and Band-Pass Filter)
TBEV – AC(Arb.)
Subject 1
Subject 2
Subject 3
Subject 4
Subject 5
Subject 6
Subject 7
Time (sec)

FIG. 17

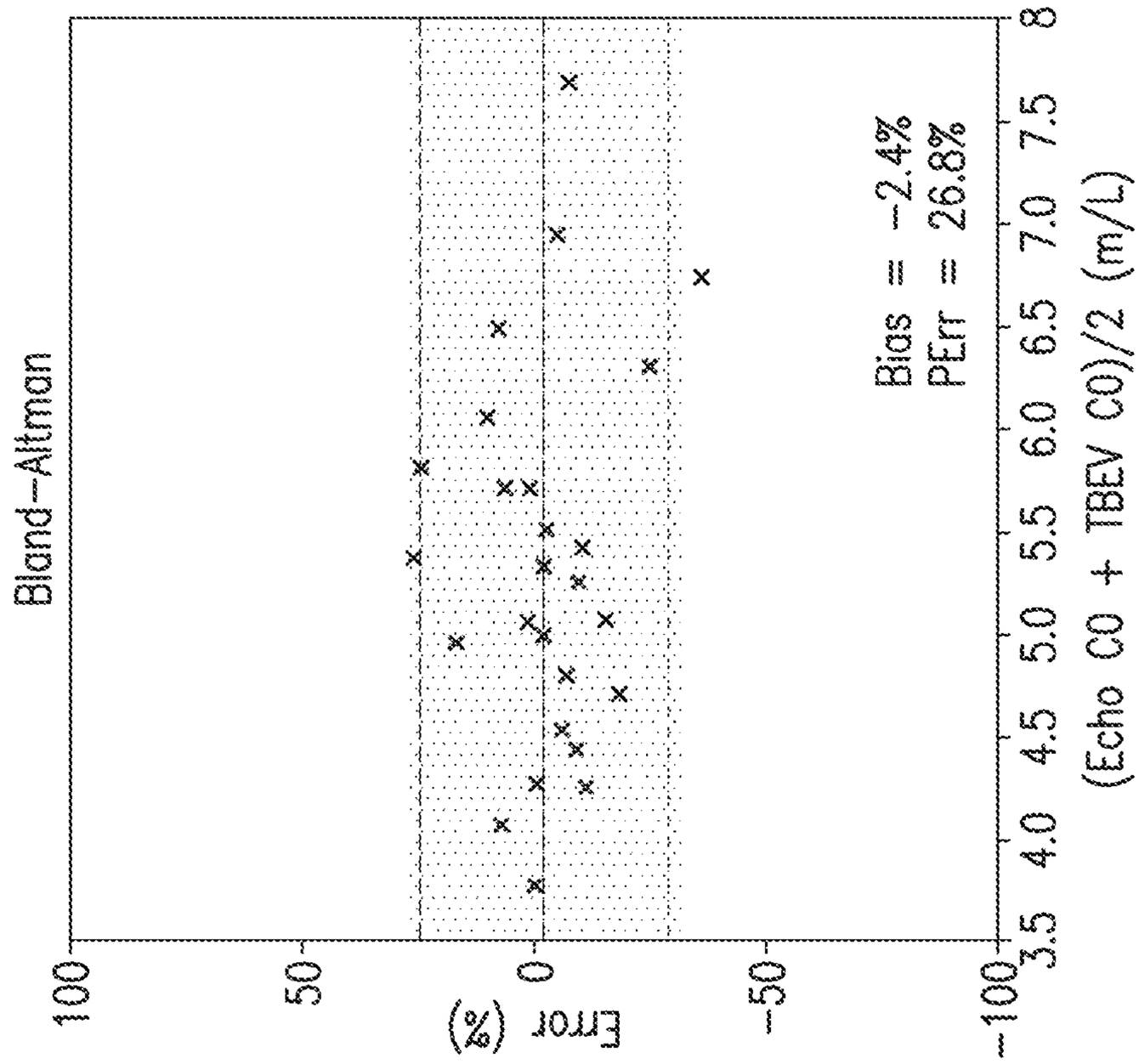

FIG. 18B

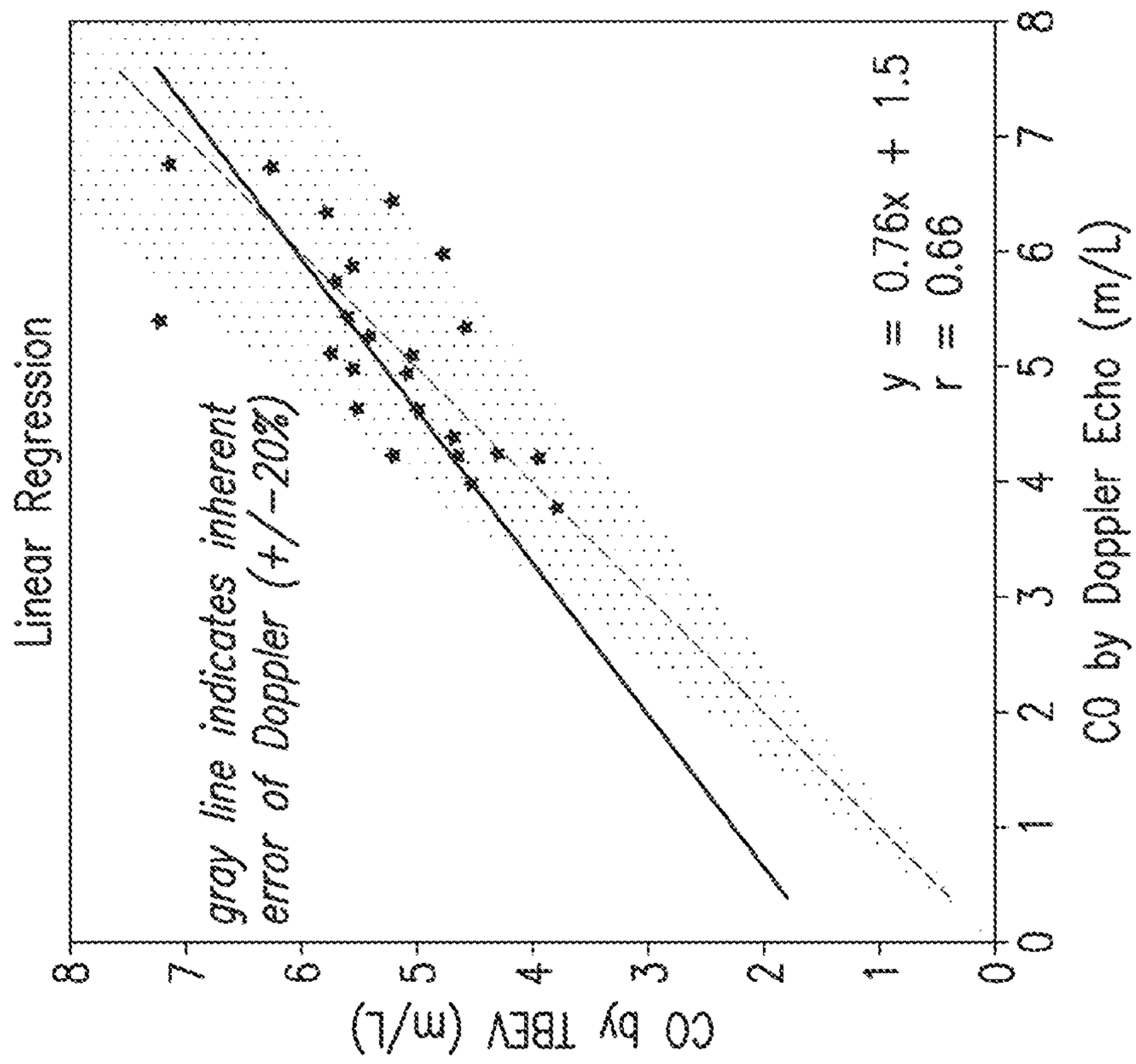

FIG. 18A

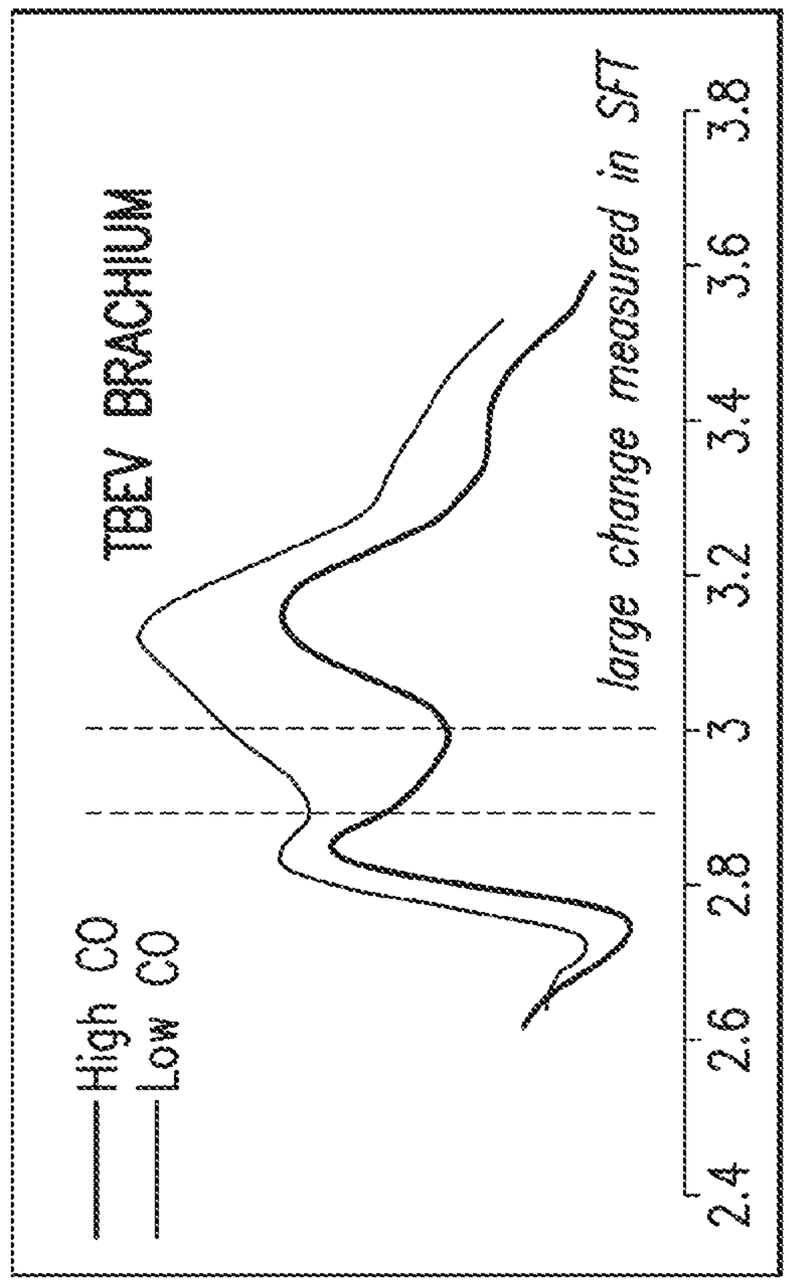

FIG. 19B

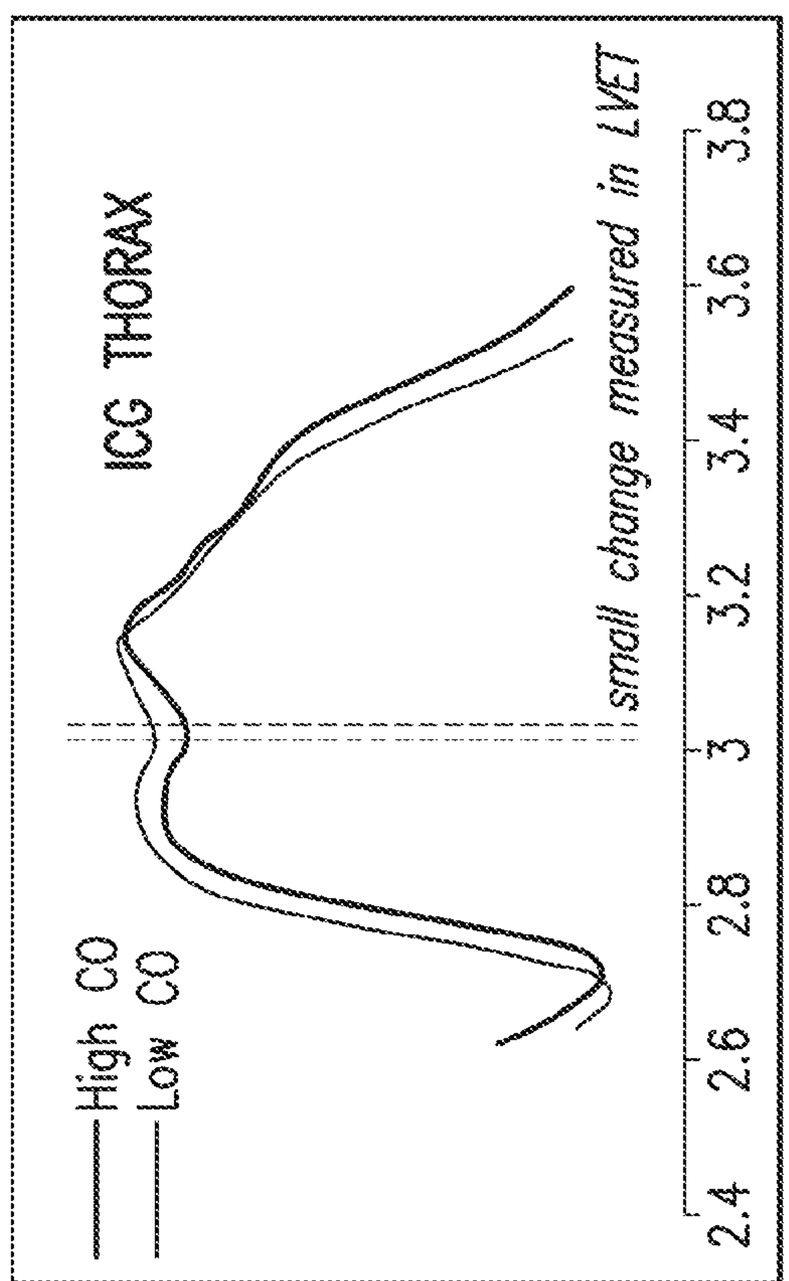

FIG. 19A

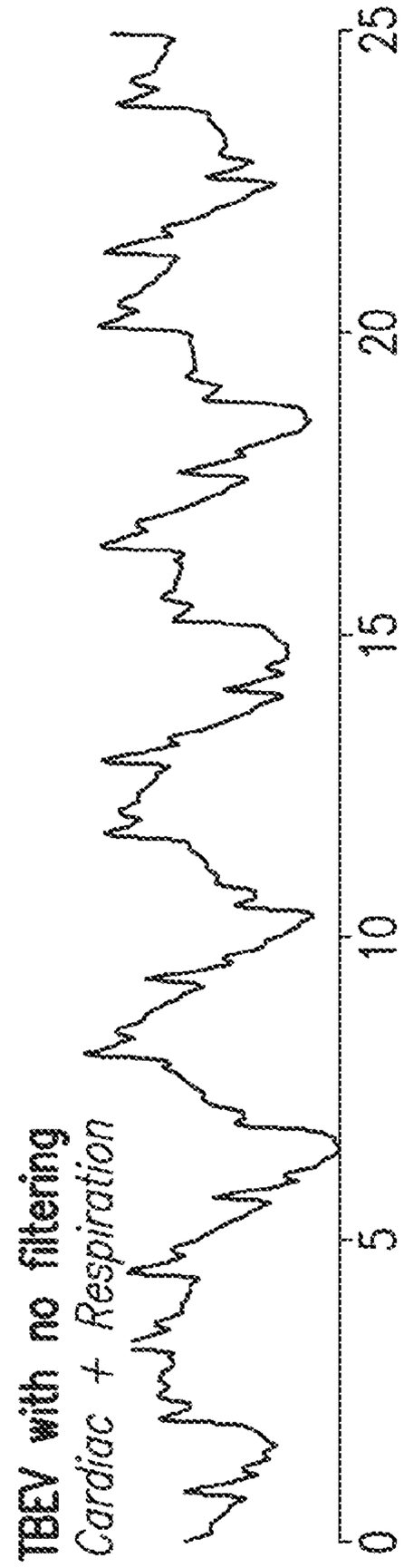

FIG.20A

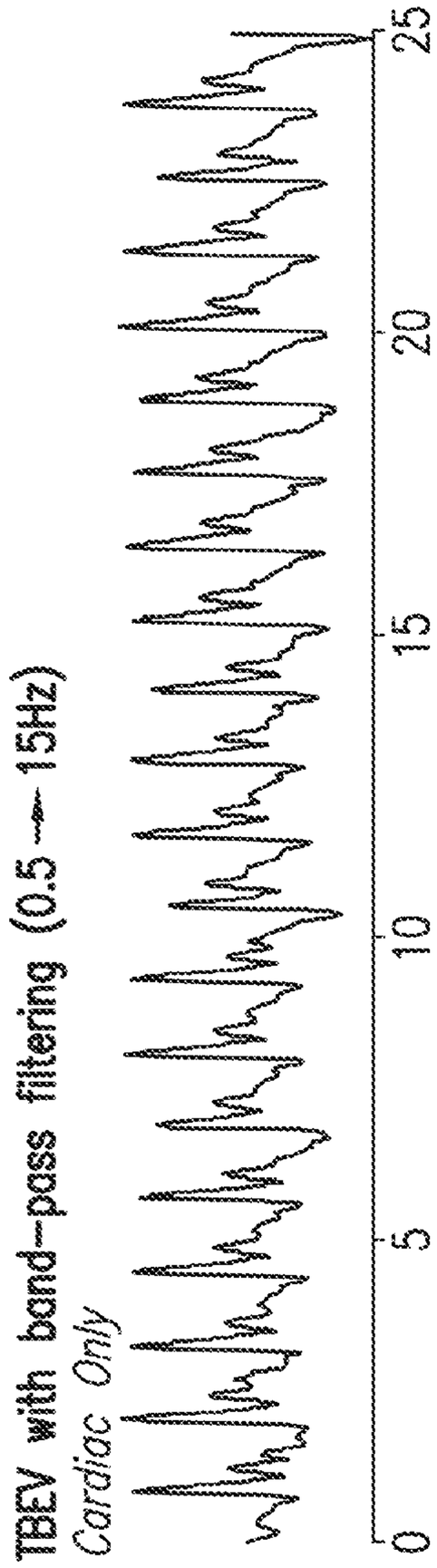

FIG.20B

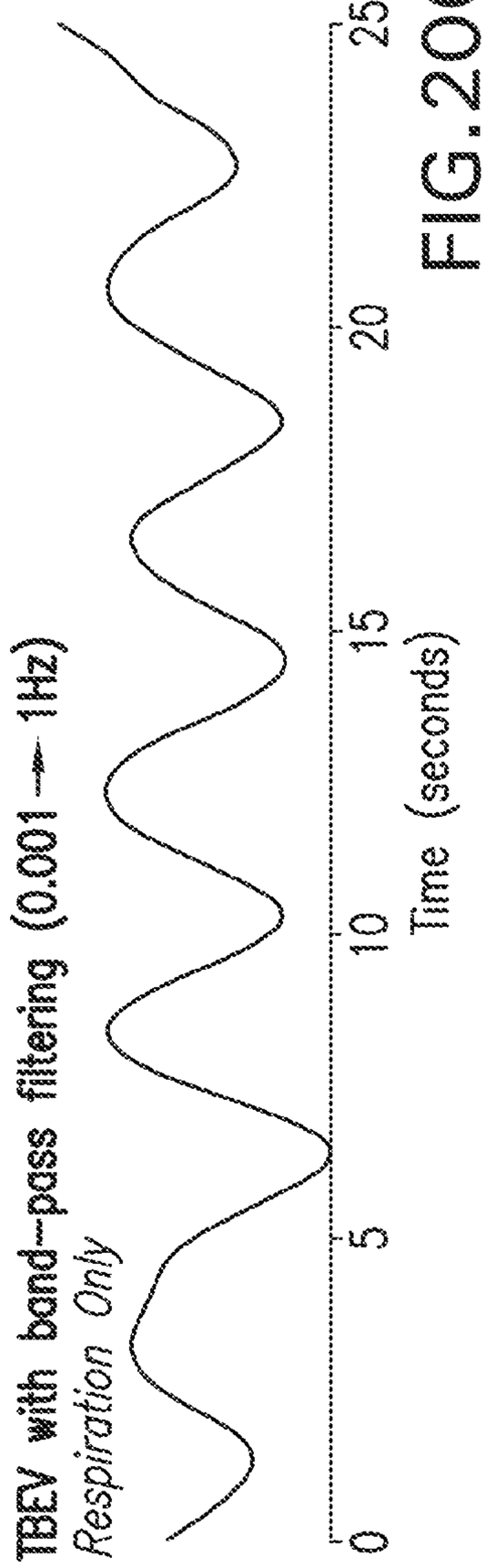

FIG.20C

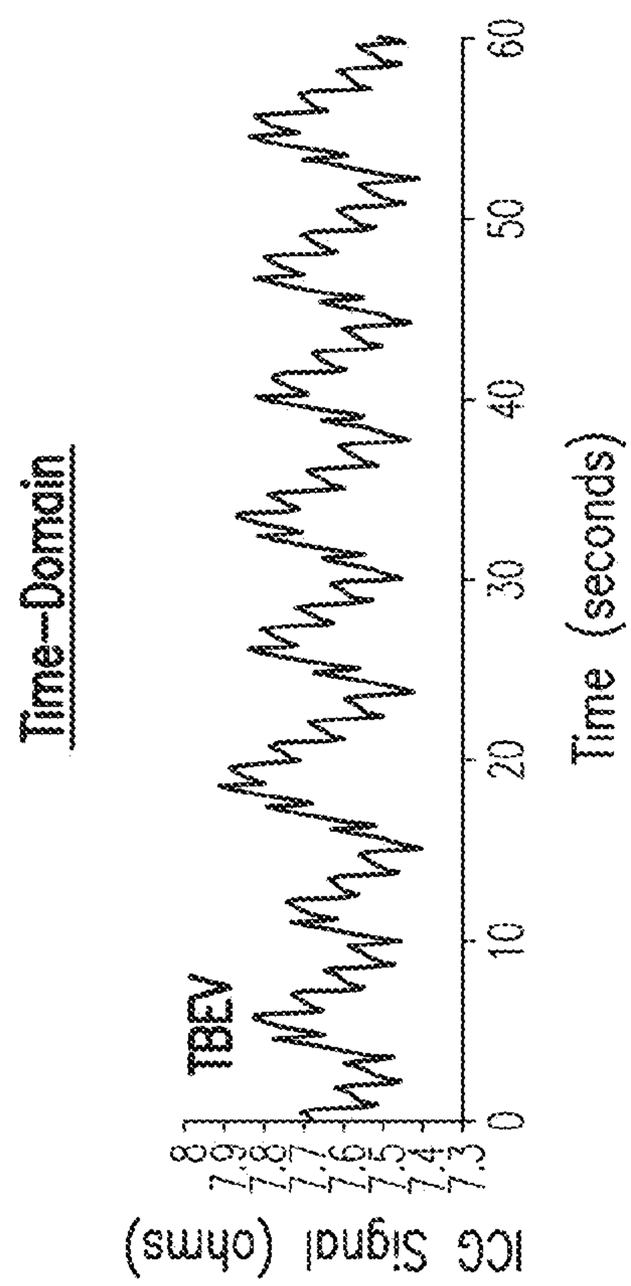

FIG.21A

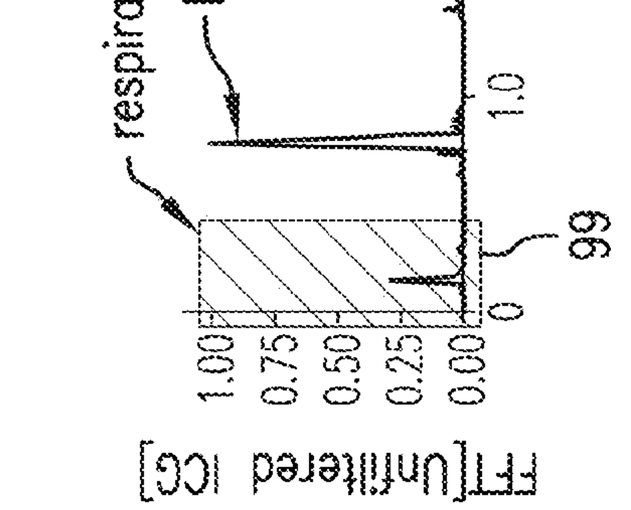

FIG.21C

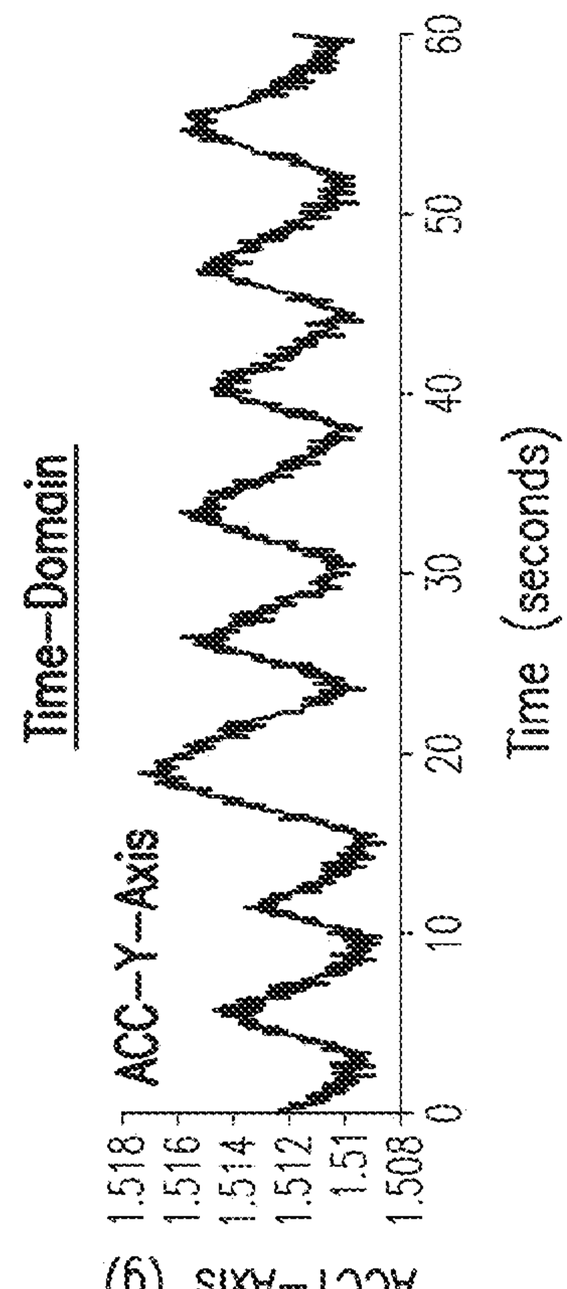

FIG.21B

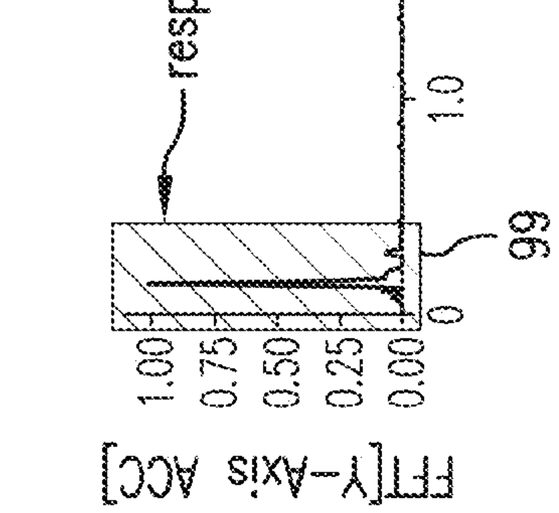

FIG.21D

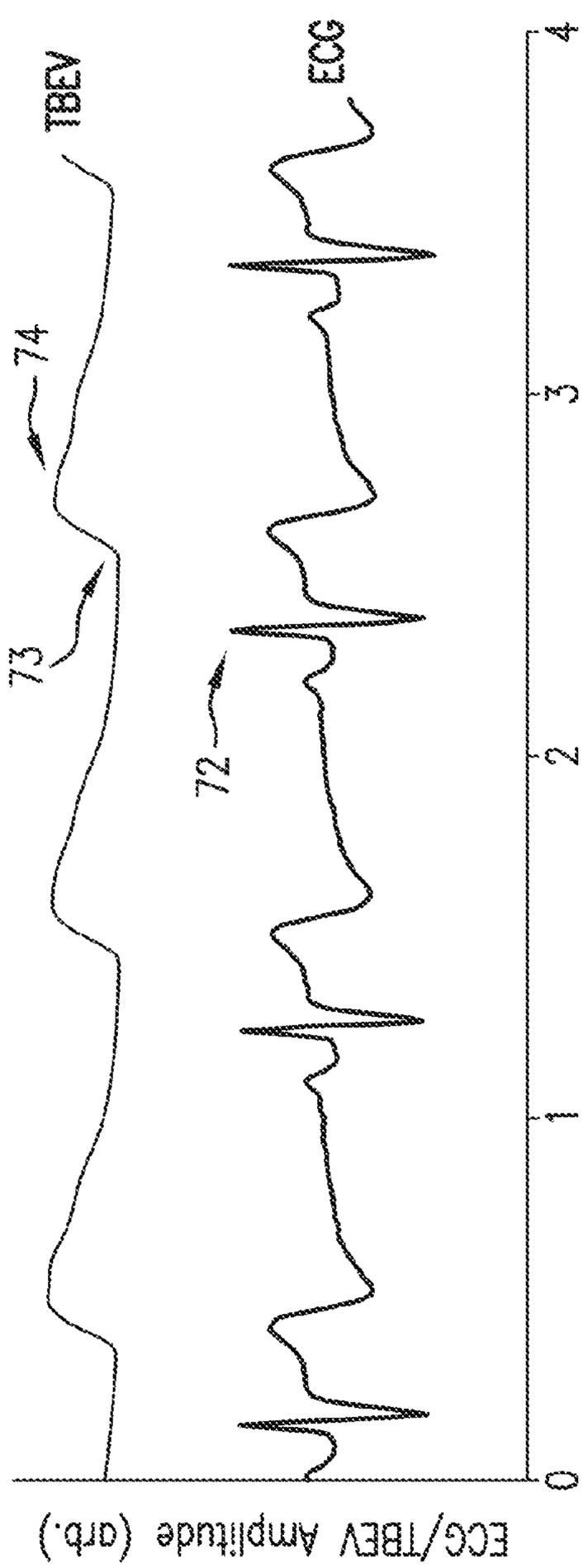

FIG.22A

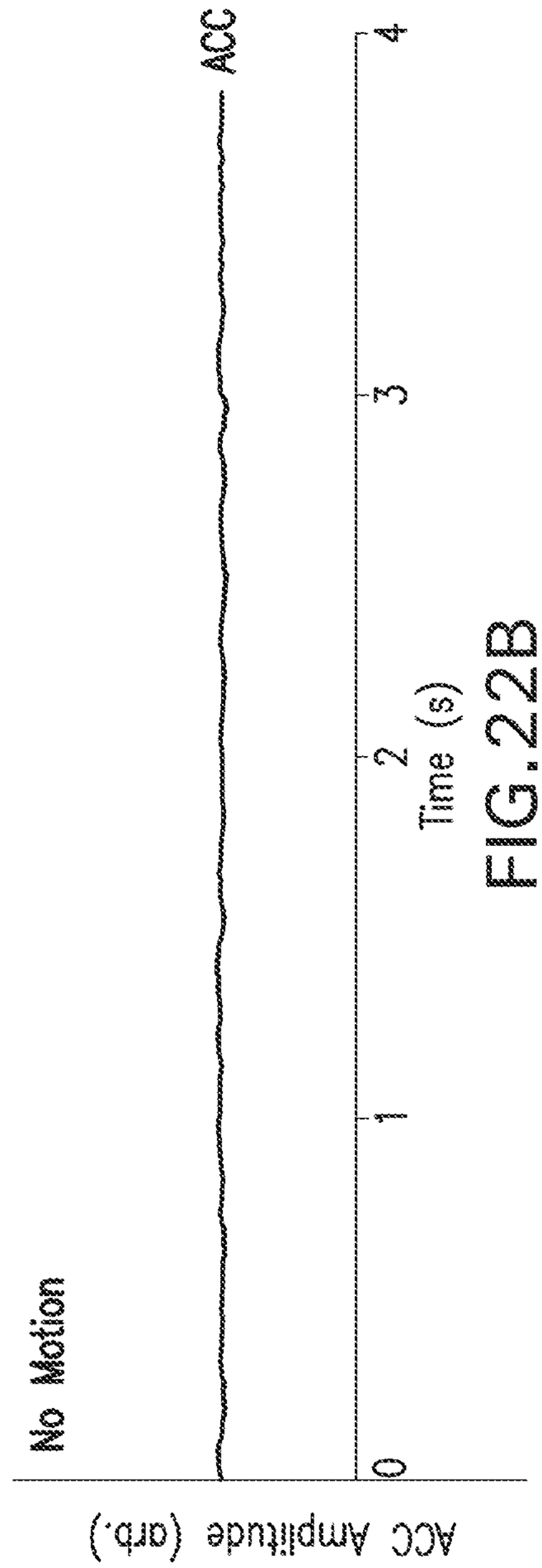

FIG.22B

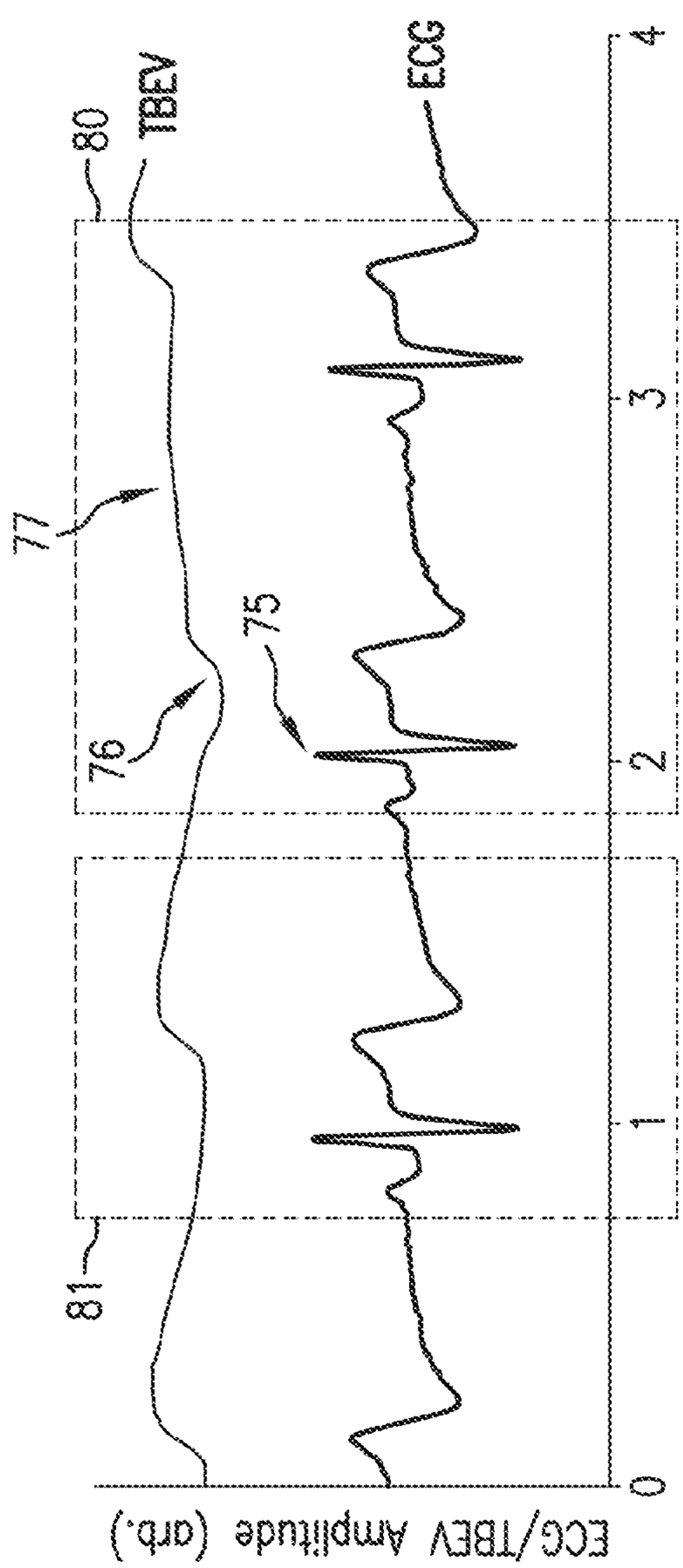

FIG. 23A

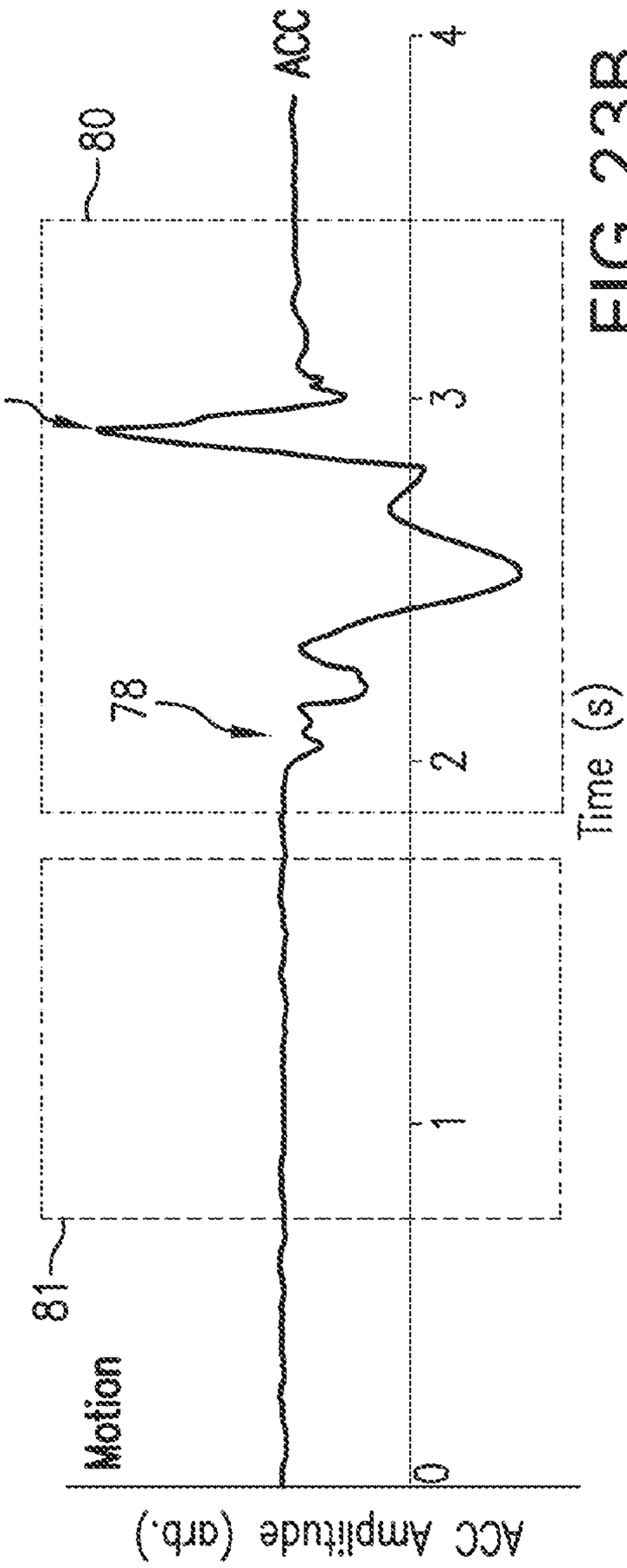

FIG. 23B

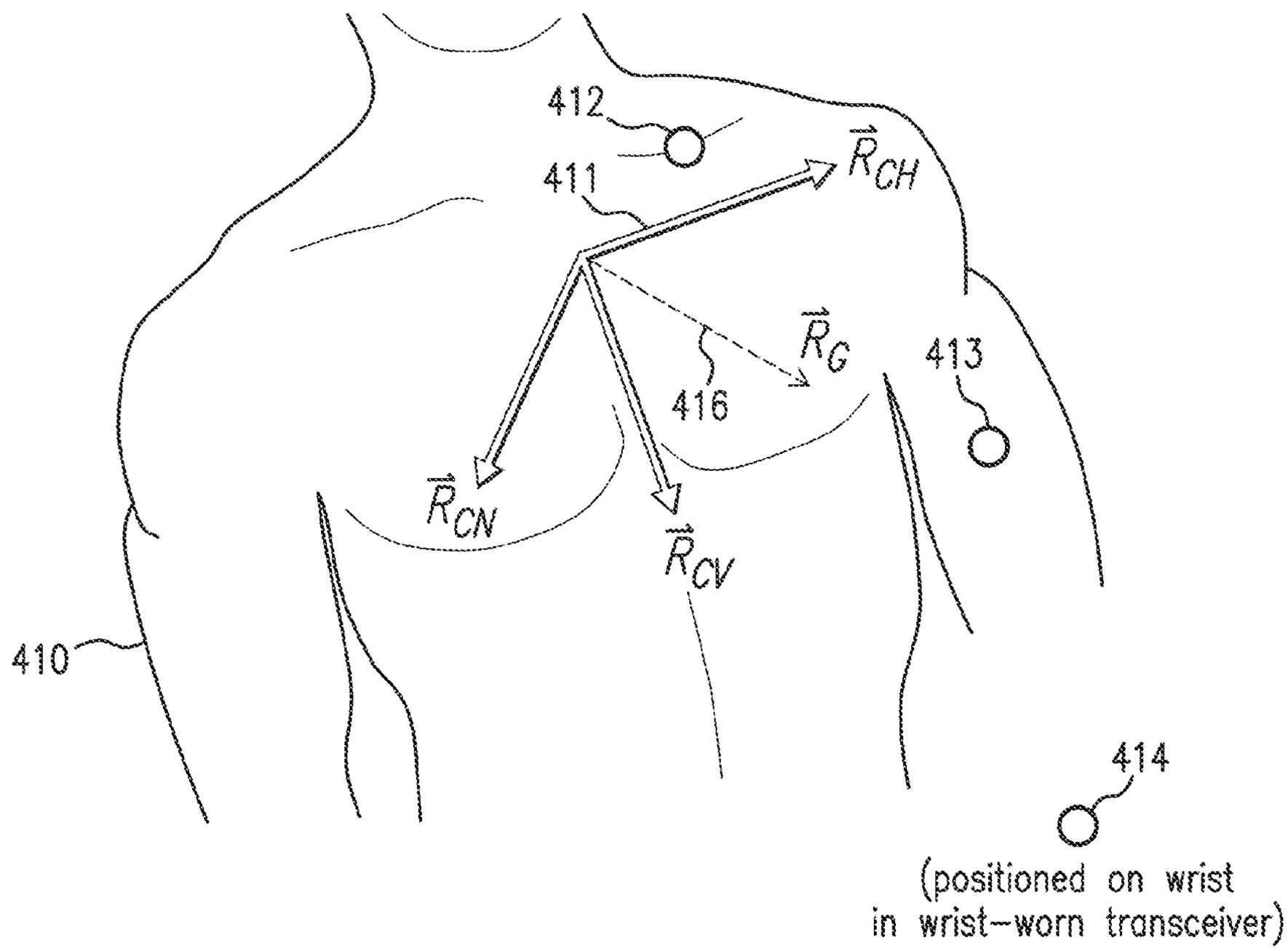
412
411
$\vec{R}_{CH}$
$\vec{R}_G$
413
416
$\vec{R}_{CN}$
$\vec{R}_{CV}$
410
414
(positioned on wrist
in wrist-worn transceiver)

FIG.24

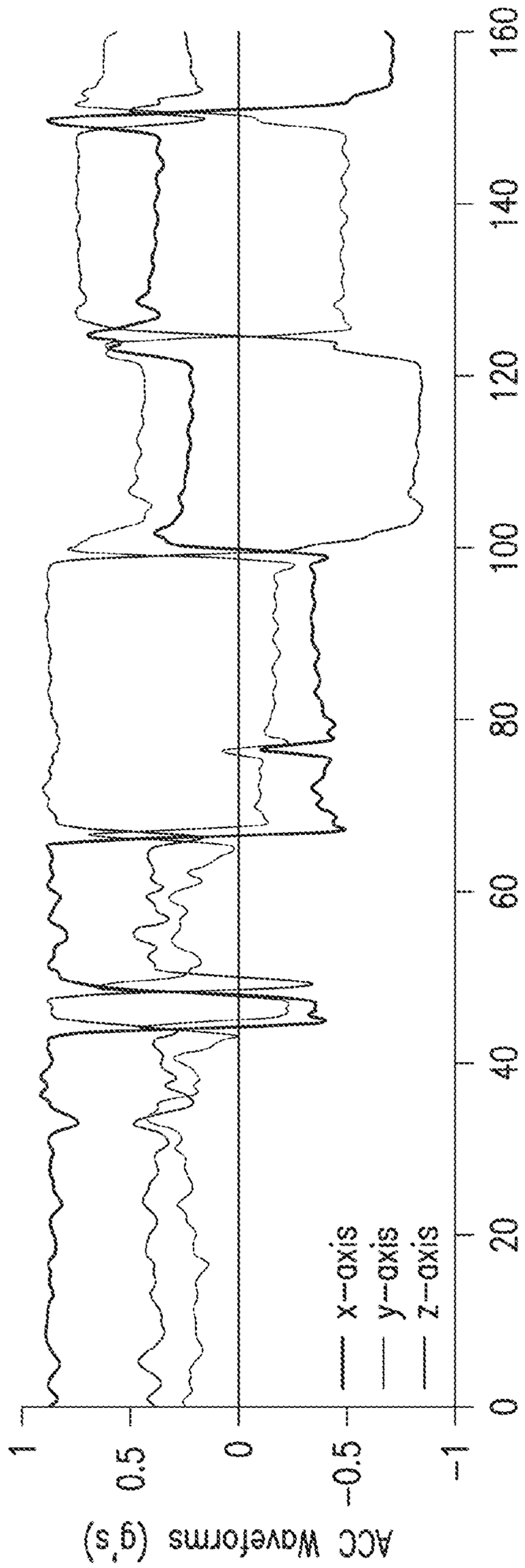

FIG.25A

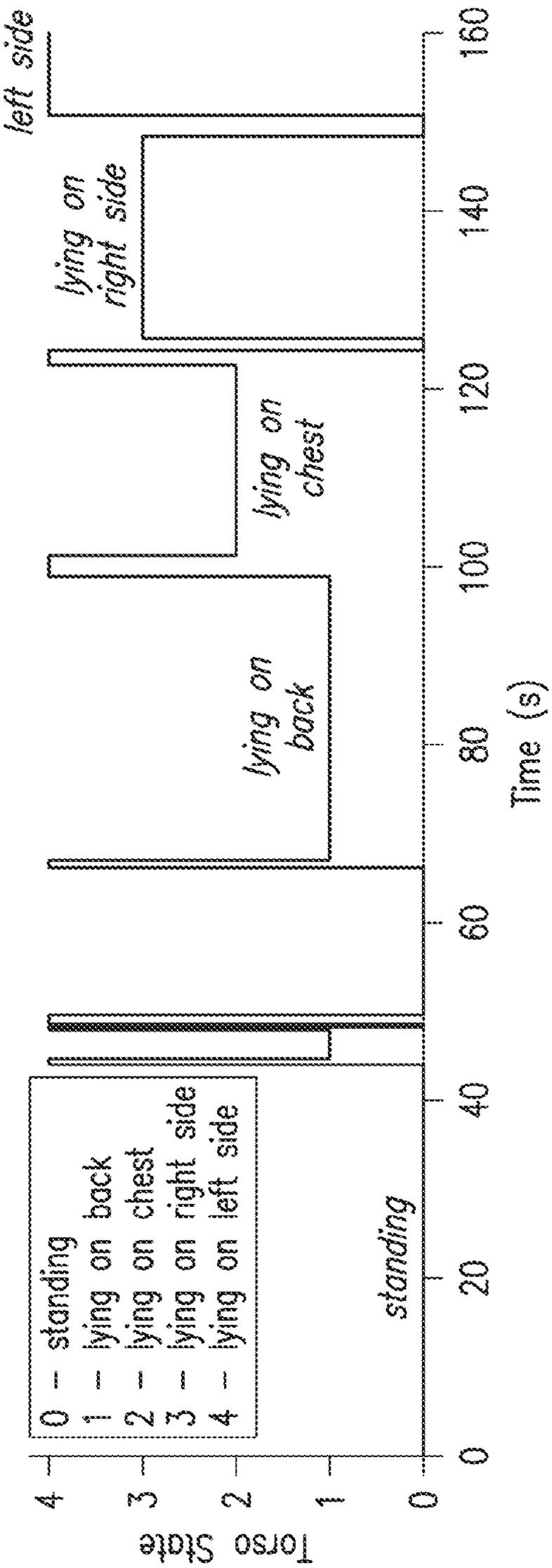

FIG.25B

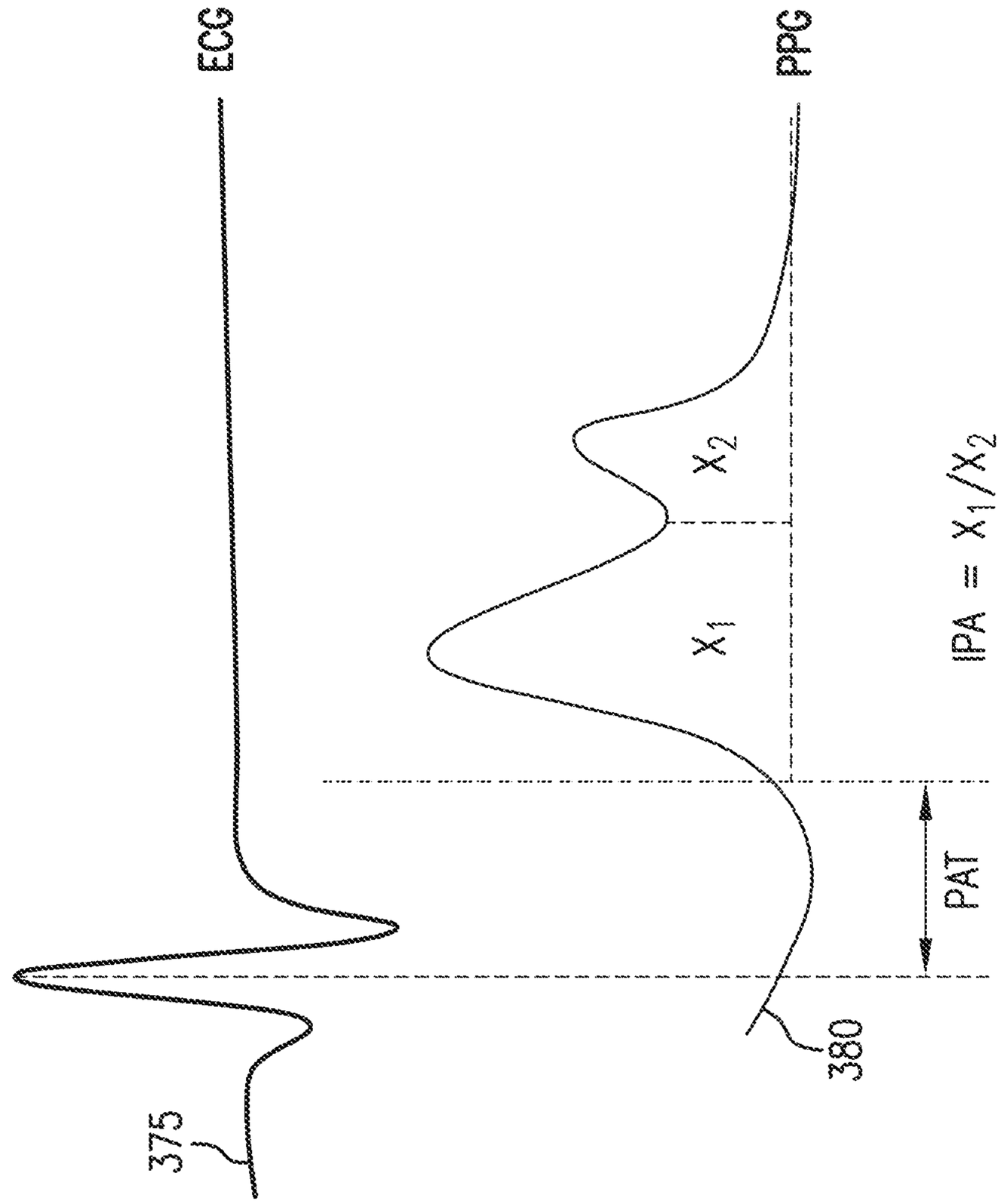

FIG. 26
Prior Art

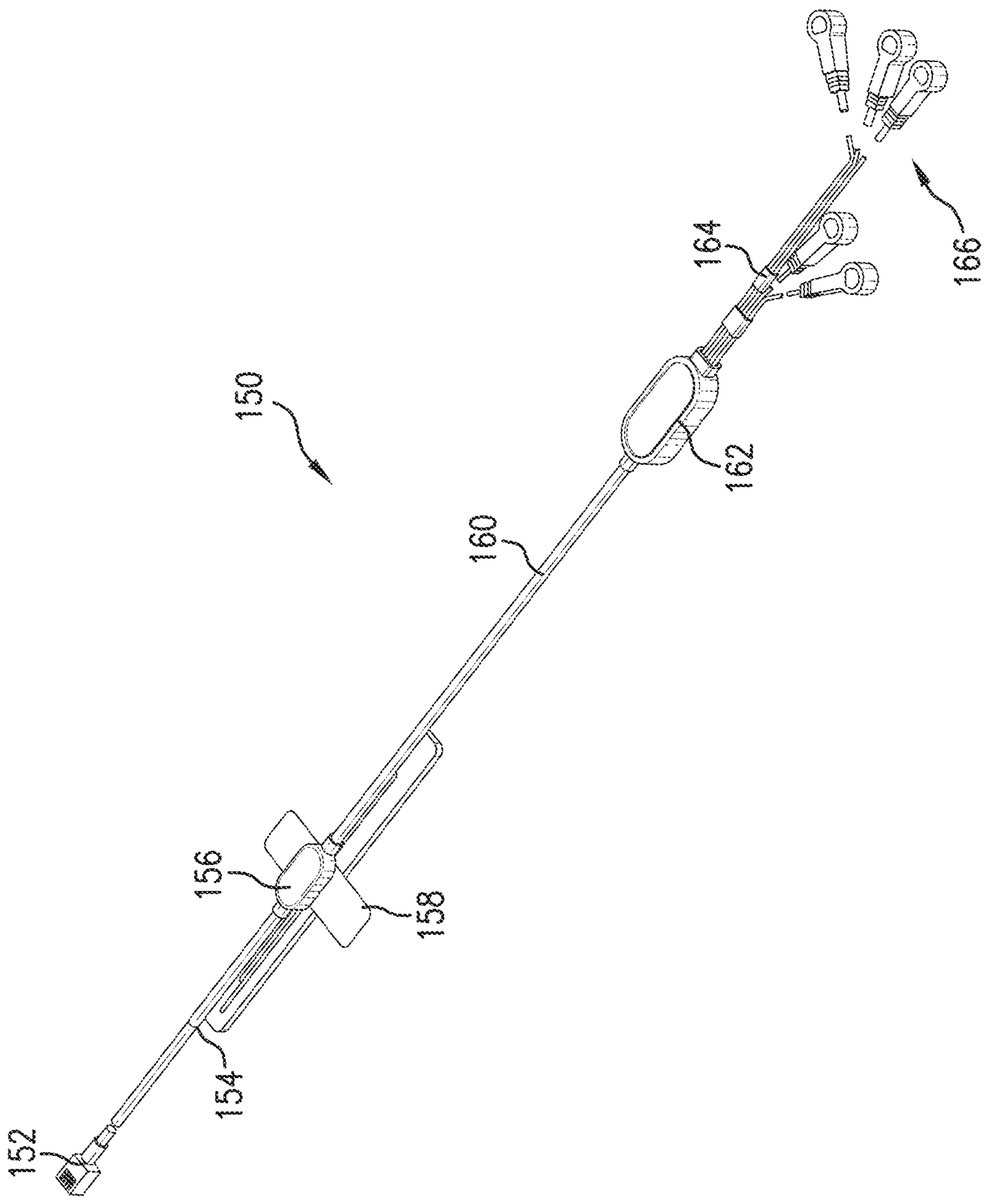

FIG. 27

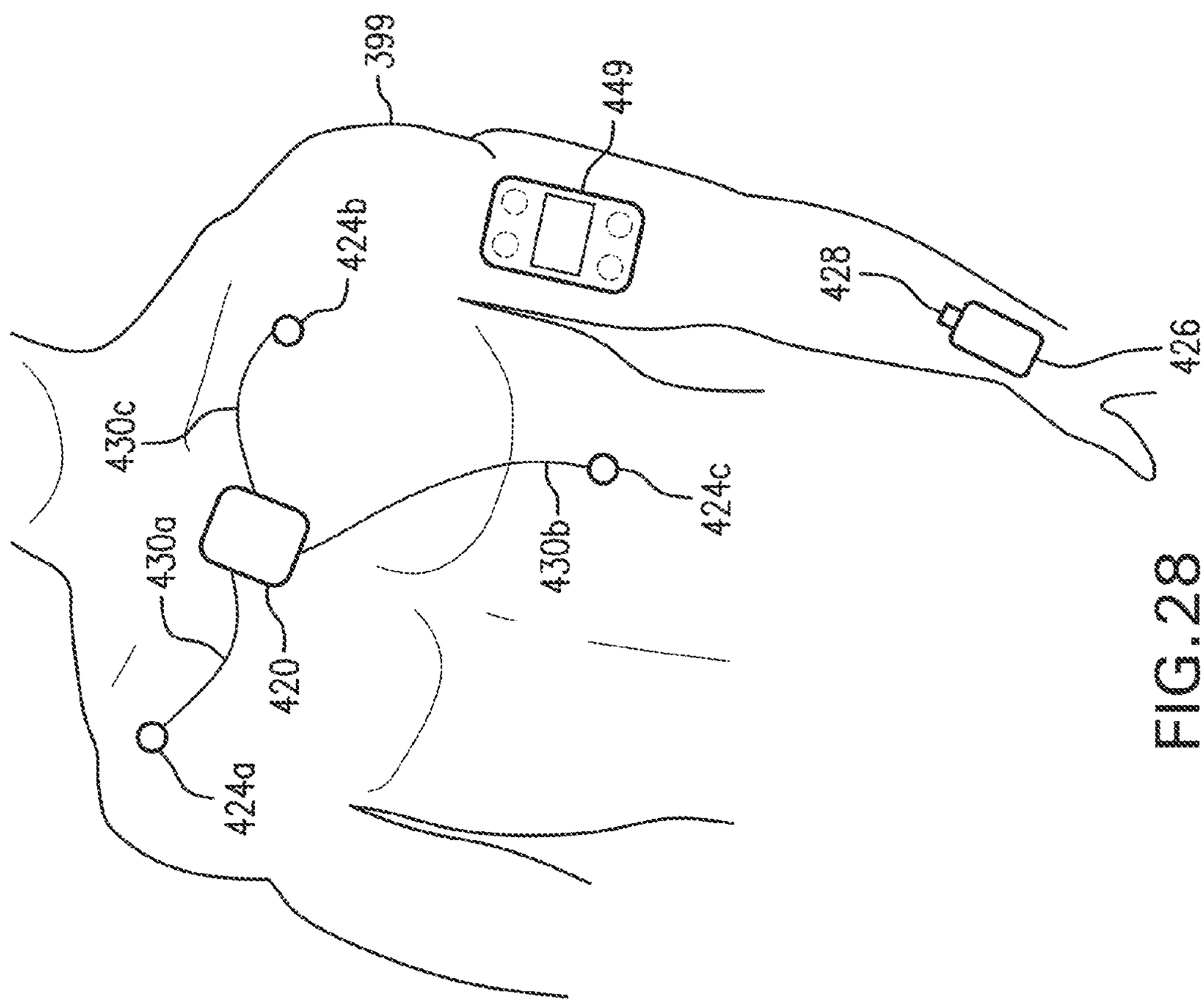

FIG. 28

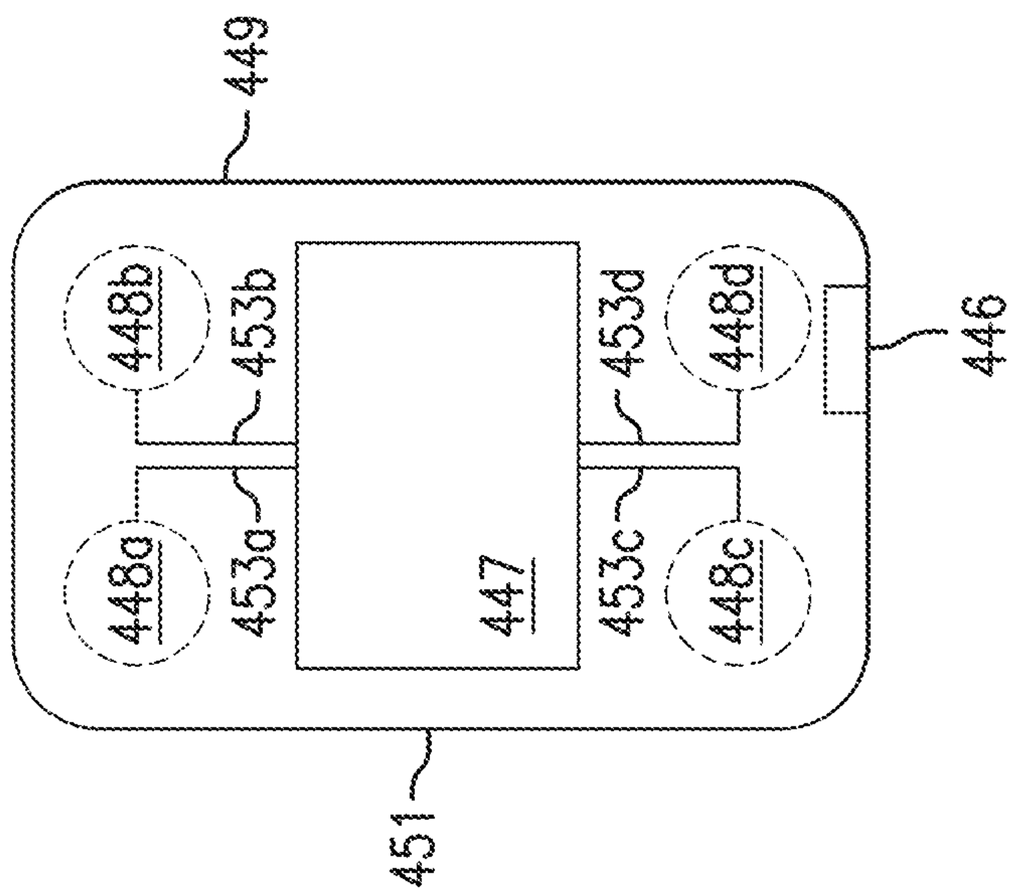

FIG. 29

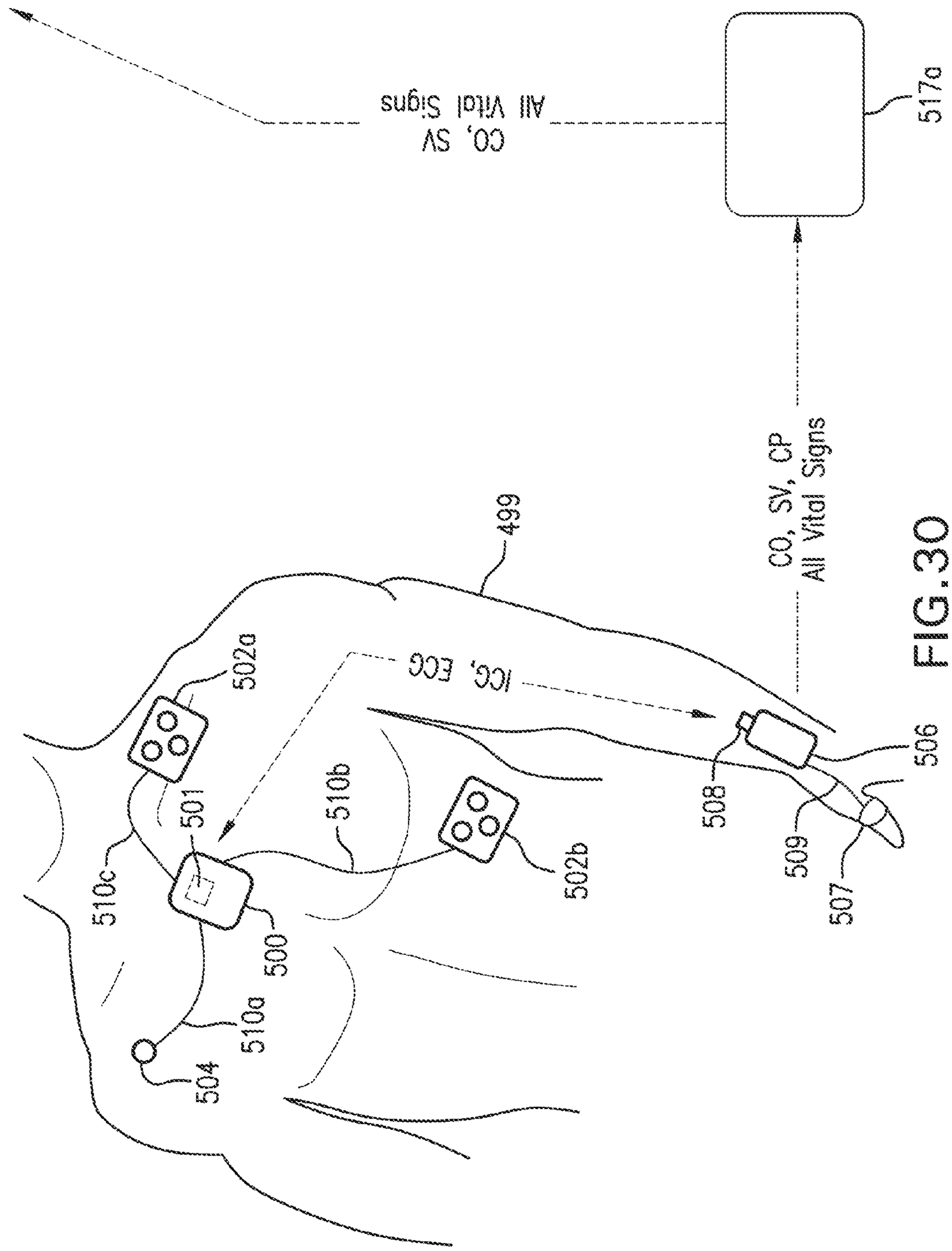
CO, SV
All Vital Signs
517a
CO, SV, CP
All Vital Signs
499
ICG, ECG
502a
501
510c
510b
502b
500
510a
504
508
506
509
507

FIG. 30

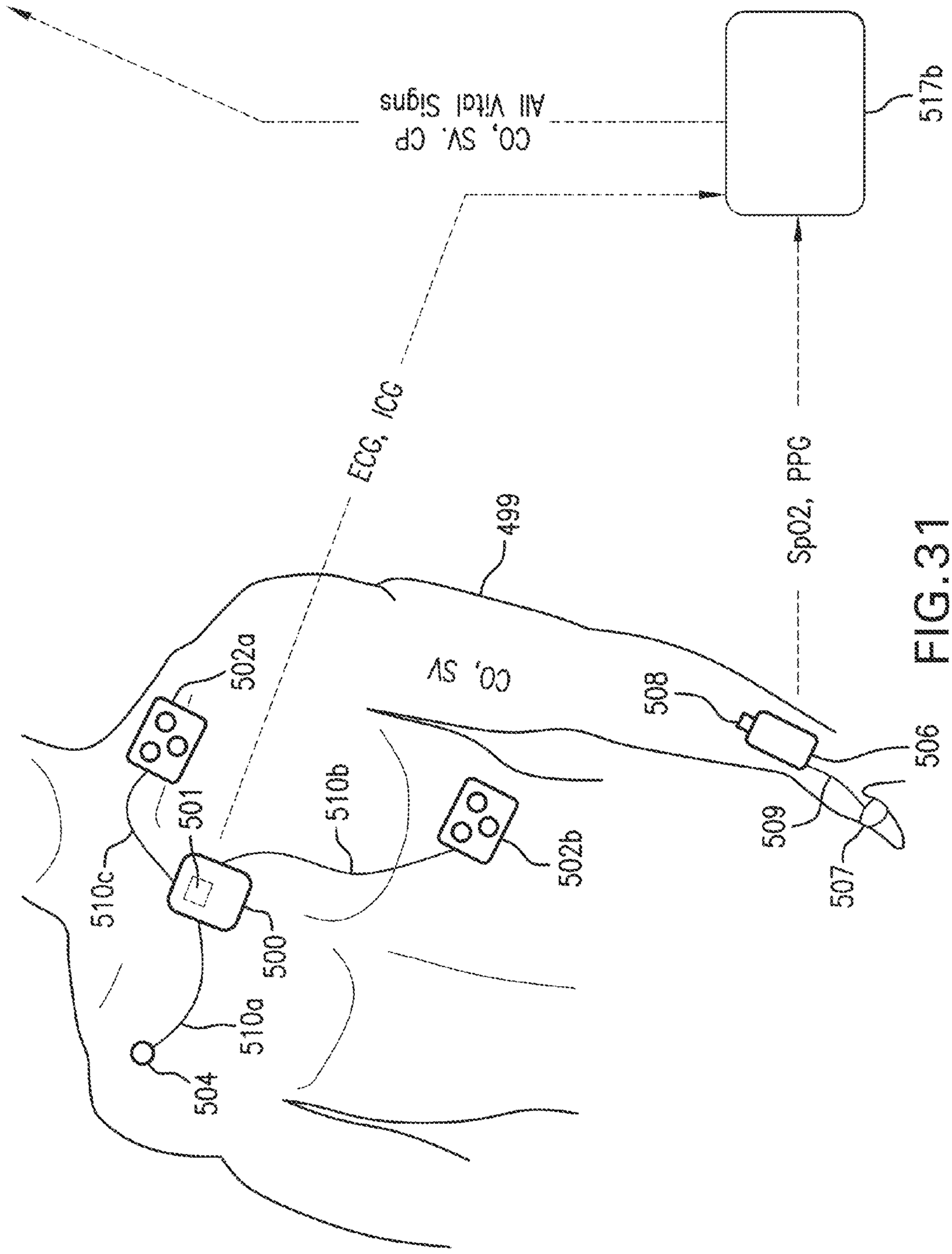
CO, SV, CP
All Vital Signs
517b
ECG, ICG
SpO2, PPG
499
CO, SV
502a
508
506
510c
501
510b
502b
509
507
500
510a
504

FIG. 31

BODY-WORN SYSTEM FOR CONTINUOUS, NONINVASIVE MEASUREMENT OF CARDIAC OUTPUT, STROKE VOLUME, CARDIAC POWER, AND BLOOD PRESSURE

CROSS REFERENCES TO RELATED APPLICATIONS

This application claims priority from a Provisional Application entitled 'BODY-WORN SYSTEM FOR CONTINUOUS, NONINVASIVE MEASUREMENT OF CARDIAC OUTPUT, STROKE VOLUME, AND BLOOD PRESSURE', U.S. Ser. No. 61/427,756, filed Dec. 28, 2010, which is hereby incorporated by reference in its entirety.

STATEMENT REGARDING FEDERALLY SPONSORED RESEARCH OR DEVELOPMENT

Work for some of the components described in this patent application was sponsored by the Department of Defense under contract W81XWH-11-2-0085.

BACKGROUND OF THE INVENTION

Field of the Invention

The present invention relates to medical devices for monitoring cardiovascular properties, e.g. cardiac output (CO), stroke volume (SV), and continuous non-invasive blood pressure (cNIBP).

Description of the Related Art

CO is typically measured in a hospital setting and, informally, indicates how efficiently a patient's heart pumps blood through their arterial tree. More specifically, CO, with units of liters/minute, describes the time-dependent volume of blood ejected from the left ventricle into the aorta; it indicates how well the patient's heart delivers blood-borne oxygen, nutrients, and other substances to the cells in the body. CO is the product of heart rate (HR) and SV, where SV is defined as the mathematical difference between left ventricular end diastolic volume (EDV) and end systolic volume (ESV), i.e.:

$$CO=SV\times HR \tag{1}$$

Combining CO and mean arterial blood pressure (MAP) into a single value, called 'cardiac power' (CP), provides a particularly valuable prognostic variable for monitoring patients suffering from cardiac conditions such as congestive heart failure (CHF), and is an independent predictor of mortality that can be measured non-invasively using cardiopulmonary exercise testing. Specifically, CP is defined as:

$$CP=CO\times MAP \tag{2}$$

Measuring CO and SV in a continuous, non-invasive manner with high clinical accuracy has often been considered a 'holy grail' of medical-device monitoring. Most existing techniques in this field require in-dwelling catheters, which in turn can harm the patient, are inherently inaccurate in the critically, and require a specially trained operator. For example, current 'gold standards' for this measurement are thermodilution cardiac output (TDCO) and the Fick Oxygen Principal (Fick). However both TDCO and Fick are highly invasive techniques that can cause infection and other complications, even in carefully controlled hospital environments. In TDCO, a pulmonary artery catheter (PAC), also known as a Swan-Ganz catheter, is typically inserted into the right portion of the patient's heart. Procedurally a bolus (typically 10 ml) of glucose or saline that is

cooled to a known temperature is injected through the PAC. A temperature-measuring device within the PAC, located a known distance away (typically 6-10 cm) from where fluid is injected, measures the progressively increasing temperature of the diluted blood. CO is then estimated from a measured time-temperature curve, called the 'thermodilution curve'. The larger the area under this curve, the lower the cardiac output. Likewise, a smaller the area under the curve implies a shorter transit time for the cold bolus to dissipate, hence a higher CO.

Fick involves calculating oxygen consumed and disseminated throughout the patient's blood over a given time period. An algorithm associated with the technique incorporates consumption of oxygen as measured with a spirometer with the difference in oxygen content of centralized blood measured from a PAC and oxygen content of peripheral arterial blood measured from an in-dwelling cannula.

Both TD and Fick typically measure CO with accuracies between about 0.5-1.0 l/min, or about +/−20% in the critically ill.

Several non-invasive techniques for measuring SV/CO/CP have been developed with the hope of curing the deficiencies of Fick and TD. For example, Doppler-based ultrasonic echo (Doppler/ultrasound) measures blood velocity using the well-known Doppler shift, and has shown reasonable accuracy compared to more invasive methods. But both two and three-dimensional versions of this technique require a specially trained human operator, and are thus, with the exception of the esophageal Doppler technique, impractical for continuous measurements. CO/SV can also be measured with techniques that rely on electrodes placed on the patient's torso that inject and then collect a low-amperage, high-frequency modulated electrical current. These techniques, based on electrical bioimpedance and called 'impedance cardiography' (ICG), 'electrical cardiometry velocimetry' (ECV), and 'bioreactance' (BR), measure a time-dependent electrical waveform that is modulated by the flow of blood through the patient's thorax. Blood is a good electrical conductor, and when pumped by the heart can further modulate the current injected by these techniques in a manner sensitive to the patient's CO. During a measurement, ICG, ECV, and BR each extract properties called left ventricular ejection time (LVET) and pre-injection period (PEP) from time-dependent ICG and ECG waveforms. A processer then analyzes the waveform with an empirical mathematical equation, shown below in Eq. 2, to estimate SV. CO is then determined from the product of SV and HR, as described above in Eq. 1.

ICG, ECV, and BR all represent a continuous, non-invasive alternative for measuring CO/SV, and in theory can be conducted with an inexpensive system and no specially trained operator. But the medical community has not embraced such methods, despite the fact that clinical studies have shown them to be effective with some patient populations. In 1992, for example, an analysis by Fuller et al. analyzed data from 75 published studies describing the correlation between ICG and TD/Fick (Fuller et al., *The validity of cardiac output measurement by thoracic impedance: a meta-analysis*; Clinical Investigative Medicine; 15: 103-112 (1992)). The study concluded using a meta analysis wherein, in 28 of these studies, ICG displayed a correlation of between r=0.80-0.83 against TDCO, dye dilution and Fick CO. Patients classified as critically ill, e.g. those suffering from acute myocardial infarction, sepsis, and excessive lung fluids, yielded worse results. Further impeding commercial acceptance of these techniques is the tendency of ICG monitors to be relatively bulky and similar in

both size and complexity to conventional vital signs monitors. This means two large and expensive pieces of monitoring equipment may need to be located bedside in order to monitor a patient's vital signs and CO/SV. For this and other reasons, impedance-based measurements of CO have not achieved widespread commercial success.

ICG-based methodologies for measuring CO/SV have evolved since Fuller's analysis. For example, it has recently been shown that the dimensionless peak rate of change of the trans-thoracic electrical impedance pulse variation, which is defined as the maximum value of the derivative of the ICG waveform $(dZ/dt)_{max}$ divided by the base impedance (Z_o), is an acceleration analog (with units of $1/s^2$). When subjected to square root transformation this yields ohmic mean velocity $[(dZ/dt)_{max}/Zo)]^{0.5}$. These parameters are described in detail in U.S. Pat. Nos. 7,740,590 and 7,261,697, the contents of which are fully incorporated herein by reference. Reasonable facsimiles of SV can be obtained when this value is multiplied by LVET and a volume conductor (V_c) allometrically related by body mass to the intrathoracic blood volume. As compared to CO measured with TDCO and transesophageal echocardiography, good to high correlation and limits of agreement within +/−30% are reported.

While most ICG measurements are conducted on the thorax, there is good evidence in the literature implying that left ventricular SV can be obtained from the upper extremity, and specifically the brachium. For example, Chemla et al. showed that peak aortic blood acceleration is highly correlated with peak brachial artery blood acceleration (r=0.79) (see, e.g., Chemla et al., *Blood flow acceleration in the carotid and brachial arteries of healthy volunteers: respective contributions of cardiac performance and local resistance*; Fundam Clin Pharmacol; 10: 393-399 (1996)). This study also demonstrated that, while brachial blood velocity is affected by downstream vasoactivity, peak brachial blood acceleration is solely affected by the upstream β-adrenergic influences of cardiac impulse formation. This suggests that square root transformation of brachial $(dZ/dt)_{max}/Z_o$ may yield accurate estimations of SV when multiplied by LVET and a Vc of appropriate magnitude. Stanley et al. showed that the maximum early systolic upslope of the transthoracic and brachial impedance changes (ΔZ) are identical, indicating that they are linearly correlated (see, e.g. Stanley et al., *Multi-channel electrical bioimpedance: a new noninvasive method to simultaneously measure cardiac and peripheral blood flow*; J Clin Monit Comput; 21: 345-51 (2007)). This implies that, despite being of different magnitudes, the peak rate of change of the trans-thoracic and trans-brachial impedance changes can both be used to calculate SV. Finally, Wang et al. demonstrated that impedance changes (ΔZ(t)) in the forearm are highly correlated with Doppler-derived SV, showing a correlation coefficient of r=0.86 (see, e.g. Wang et al., *Evaluation of changes in cardiac output from the electrical impedance waveform in the forearm*; Physiol Meas; 28: 989-999 (2007)).

CO/SV can also be estimated from a time-dependent arterial blood pressure waveform measured, e.g., with a tonometer or in-dwelling arterial catheter. Algorithms can be used to extract pulse pressure (PP) and other contour-related features from these waveforms, which are then processed to estimate CO/SV. Unfortunately both the heart and its associated vessels can function independently and sometimes paradoxically, so changes in parameters like PP may both reflect and mask changes in CO/SV. In other words, measurements of CO using time-dependent arterial waveforms represent a combination of cardiac and vascular function.

Pulse arrival time (PAT), defined as the transit time for a pressure pulse launched by a heartbeat in a patient's arterial system, has been shown in a number of studies to correlate to both systolic (SYS) and diastolic (DIA) blood pressures. In these studies, PAT is typically measured with a conventional vital signs monitor that includes separate modules to determine both an electrocardiogram (ECG) and a value for pulse oximetry (SpO2). During a PAT measurement, multiple electrodes typically attach to a patient's chest to determine a time-dependent component of the ECG waveform characterized by a sharp spike called the 'QRS complex'. The QRS complex indicates an initial depolarization of ventricles within the heart and, informally, marks the beginning of the heartbeat and a pressure pulse that follows. SpO2 is typically measured with a bandage or clothespin-shaped sensor that attaches to a patient's finger, and includes optical systems operating in both red and infrared spectral regions. A photodetector measures radiation emitted from the optical systems that transmits through the patient's finger. Other body sites, e.g., the ear, forehead, and nose, can also be used in place of the finger. During a measurement, a microprocessor analyses both red and infrared radiation measured by the photodetector to determine time-dependent waveforms corresponding to the different wavelengths, each called a photoplethysmogram waveform (PPG). From these a SpO2 value is calculated Time-dependent features of the PPG waveform indicate both pulse rate and a volumetric absorbance change in an underlying artery (e.g., in the finger) caused by the propagating pressure pulse.

Typical PAT measurements determine the time separating a maximum point on the QRS complex (indicating the peak of ventricular depolarization) and a portion of the PPG waveform (indicating the arrival of the pressure pulse). PAT depends primarily on arterial compliance, the propagation distance of the pressure pulse (which is closely approximated by the patient's arm length), and blood pressure. To account for patient-specific properties, such as arterial compliance, PAT-based measurements of blood pressure are typically 'calibrated' using a conventional blood pressure cuff. Typically during the calibration process the blood pressure cuff is applied to the patient, used to make one or more blood pressure measurements, and then removed. Going forward, the calibration measurements are used, along with a change in PAT, to determine the patient's blood pressure and blood pressure variability. PAT typically relates inversely to blood pressure, i.e., a decrease in PAT indicates an increase in blood pressure.

A number of issued U.S. Patents describe the relationship between PAT and blood pressure. For example, U.S. Pat. Nos. 5,316,008; 5,857,975; 5,865,755; and 5,649,543 each describe an apparatus that includes conventional sensors that measure ECG and PPG waveforms, which are then processed to determine PAT.

SUMMARY OF THE INVENTION

The invention provides a small-scale, body-worn monitor for measuring SV/CO/CP, along with cNIBP, HR, respiratory rate (RR), SpO2, and body temperature (TEMP), motion, and posture. Measurements of CO/SV are based on a measurement technique called 'transbrachial electro-velocimetry' (TBEV), which is described in detail below. TBEV measurements yield two time-dependent waveforms: Zo, which represents a base impedance in the brachial region, and is sensitive to slowly varying properties such as blood volume; and ΔZ(t), which features heartbeat-induced pulses that vary in contour as blood flows through the

brachium during both systole and diastole. These waveforms are measured from the patient's brachium, a region that is somewhat immune to pulmonary ventilatory affects that can complicate conventional ICG measurements obtained from the thorax. Collectively, an algorithm running on a microprocessor within the body-worn monitor analyzes features analysis of both Zo and $\Delta Z(t)$ to determine values for each TBEV measurement. More specifically, to determine SV/CO/CP values, the monitor relies on a 'hybrid measurement' that collectively processes combinations of time-dependent PPG, ECG, and TBEV waveforms, along with physiological parameters (e.g. blood pressure values) extracted from these waveforms, measured by the body-worn monitor. From these waveforms parameters such as LVET and PEP can be estimated and used in a mathematical relationship to continuously and accurately estimate SV/CO/CP values, as described in detail below. Once determined, they are combined with conventional vital signs, and wirelessly transmitted by the body-worn monitor to a central station to effectively monitor the patient.

The TBEV waveform is measured with a small module that connects to a first set of adhesive electrodes worn in the patient's clavicle/brachial (CB) region. This region roughly extends from areas near the tip of the shoulder (proximal to the axilla) to the elbow (proximal to the antecubital fossa). ECG waveforms are measured with a small module that connects to second set of adhesive electrodes that are typically worn on the patient's thorax in a conventional Einthoven's triangle configuration. Both the TBEV and ECG modules also include a 3-axis accelerometer that measures acceleration waveforms (ACC) that are sensitive to motion. Both accelerometers measure, for example, breathing-induced chest wall excursions that can be processed to estimate RR, as well as larger scale motion that can be processed to determine motion-related properties such as activity level, posture, degree/magnitude of motion, and frequency of motion.

During a measurement, the TBEV and ECG modules transmit waveforms and numerical information through either a wired or wireless connection to a wrist-worn transceiver. The transceiver also connects to an optical sensor, worn on the patient's thumb, that measures PPG waveforms generated with optical systems featuring red (~600 nm) and infrared (~900 nm) light-emitting diodes (LEDs). These waveforms can be processed to determine values of SpO2. The wrist-worn transceiver also includes an internal accelerometer that measures ACC waveforms associated with hand motions. Both PPG waveforms, along with the ECG waveforms, can be processed to determine cNIBP values.

The TBEV component of the hybrid measurement is measured by injecting a high-frequency, low-amperage alternating current (AC) field along the course of the brachial artery in the CB region, followed by simultaneously sensing and signal processing voltage changes produced within the current field. The fundamental rational for TBEV derives from the direct proportionality and high correlation observed between peak ascending aortic and peak brachial artery blood flow acceleration. This technique is in diametric opposition to the generally accepted volumetric theory, an alternative approach that suggests it is the velocity-induced peak rate of change in the specific resistance of axially-directed flowing blood that causes a time-dependent change in the measured impedance. Computationally, TBEV-determined SV is obtained by taking the square root of the peak rate of change of electrical impedance pulse variation divided by the base impedance as measured in the CB region, i.e. $[(dZ/dt)_{max}/Zo]^{0.5}$. This parameter is then multiplied by LVET and a constant V_c to yield SV.

The body-worn monitor simultaneously provides a technique for measuring cNIBP, based on either PAT, pulse transit time (PTT) or vascular transit time (VTT), as described in more detail in the above-referenced patent applications. These documents describe cNIBP measurements made using the 'Composite Method', described in detail below, which features a number of improvements over conventional PAT and PTT measurements.

Upon completion of a measurement, the body-worn monitor wirelessly transmits waveforms, vital signs, and SV/CO/CP values to a remote monitor, such as a personal computer (PC), workstation at a nursing station, tablet computer, personal digital assistant (PDA), or cellular telephone. Typically the wireless transmitter is within the wrist-worn transceiver, which also displays and further analyzes this information. Both the remote monitor and the wrist-worn transceiver can additionally include a barcode scanner, touch screen display, camera, voice and speaker system, and wireless systems that operate with both local-area networks (e.g. 802.11 or 'WiFi' networks) and wide-area networks (e.g. the Sprint network).

In one aspect, for example, the invention provides a system for measuring both SV and CO from a patient. The system features an impedance sensor, connected to at least two patient-worn electrodes, and featuring an impedance circuit that processes signals from the at least two electrodes to measure an impedance signal from the patient. An optical sensor within the system connects to an optical probe, and features an optical circuit that measures at least one optical signal from the patient. A body-worn processing system operably connects to both the impedance sensor and the optical sensor and receives and processes the impedance signal to determine a first value of SV and CO. It then receives the optical signal and processes it to determine a second value of these parameters. Finally, the processing system collectively processes both the first and second values of SV and CO to determine a third value of these parameters, which it then reports to a display device.

In another aspect, the invention provides a similar system that also features an ECG sensor, connected to at least two body-worn electrodes, and featuring an ECG circuit. The ECG circuit is configured to process signals from the electrodes to measure an ECG waveform and HR value. A processing system connects to the impedance, optical, and ECG sensors, and receives time-dependent waveforms from each of these systems. It then collectively processes the ECG and optical signals to determine a blood pressure value, and then processes the blood pressure value to estimate SV and CO.

In another aspect, the invention provides a similar system that features ECG, impedance, and optical sensors. Collectively these sensors generate signals that are processed to determine a collection of SV 'estimators'. The various estimators are then processed with a variety of algorithms to estimate stroke volume.

In another aspect the invention provides a method for determining SV that features the following steps: (a) measuring an impedance signal with an impedance sensor operably connected to the body-worn monitor; (b) measuring an optical signal with an optical sensor; (c) processing the impedance signal to determine a value of $(dZ/dt)_{max}$; (d) processing the optical signal to determine a value of SFT; and (e) collectively processing Z_0, $(dZ/dt)_{max}$ and SFT to determine the SV.

In another aspect, the invention provides a method of determining cardiac power, which as described in detail below is the product of CO and MAP. Here, CO is determined by processing an ECG waveform to determine a heart rate value, and a combination of impedance and optical waveforms to determine SV. MAP is then calculated from a PAT value determined from PPG and ECG waveforms. Alternatively, MAP is calculated from a VTT value determined from TBEV and PPG waveforms. In both cases, the Composite Method processes either PAT or PTT to determine MAP.

In another aspect, the invention provides a body-worn system for measuring a SV value from a patient. The body-worn system features a TBEV module that includes an electrical circuit configured to inject a current proximal to the patient's brachium. The circuit's bottom portion includes a pair of electrical connectors that are configured to snap into a pair of mated connectors disposed on a first electrode, with a first connector configured to inject the current into a first portion of the electrode, and a second connector configured to measure signals from a second portion of the electrode that relate to a voltage. An analog circuit then processes the signals from the second connector to generate a voltage value. A processor interfaced to the analog circuit converts the voltage value, or a value calculated therefrom, into a time-dependent resistance value, and then converts the time-dependent resistance value into a SV value.

In yet another aspect, the invention provides a method for determining SV from a patient that includes the following steps: (a) measuring a motion waveform with a first motion sensor; (b) processing the motion waveform with a motion algorithm to determine a motion-related parameter; (c) comparing the motion-related parameter to a pre-determined threshold parameter to determine if the patient's motion exceeds an acceptable level; (d) measuring an impedance waveform from the patient with an impedance sensor if the patient's motion does not exceed an acceptable level; and (e) calculating a SV value from the impedance waveform if the patient's motion does not exceed an acceptable level.

The Composite Method for cNIBP is described in detail in the following patent application, the contents of which are fully incorporated herein by reference: BODY-WORN SYSTEM FOR MEASURING CONTINUOUS NON-INVASIVE BLOOD PRESSURE (cNIBP), U.S. Ser. No. 12/650,354, filed Nov. 15, 2009. It includes both pressure-dependent and pressure-free measurements, and is based on the discovery that PAT and the PPG waveform used to determine it are strongly modulated by an applied pressure. During a pressure-dependent measurement, also referred to herein as an 'indexing measurement', two events occur as the pressure gradually increases to the patient's systolic pressure: 1) PAT increases, typically in a non-linear manner, once the applied pressure exceeds diastolic pressure; and 2) the magnitude of the PPG's amplitude systematically decreases, typically in a linear manner, as the applied pressure approaches systolic pressure. The applied pressure gradually decreases blood flow and consequent blood pressure in the patient's arm, and therefore induces the pressure-dependent increase in PAT. Each of the resulting pairs of PAT/blood pressure readings measured during the period of applied pressure can be used as a calibration point. Moreover, when the applied pressure equals SYS, the amplitude of the PPG waveform is completely eliminated, and PAT is no longer measurable. Collectively analyzing both PAT and the PPG waveform's amplitude over a suitable range, along with the pressure waveform using techniques borrowed from conventional oscillometry, yields the patient's SYS, DIA, and MAP, along with a patient-specific slope relating PAT and MAP. From these parameters the patient's cNIBP can be determined without using a conventional cuff.

A combination of several algorithmic features improves the efficacy of the Composite Method over conventional PAT measurements of cNIBP. For example, sophisticated, real-time digital filtering removes high-frequency noise from the PPG waveform, allowing its onset point to be accurately detected. When processed along with the ECG waveform, this ensures measurement of an accurate PAT and, ultimately, cNIBP value. The pressure-dependent indexing method, which is made during inflation of the arm-worn cuff, yields multiple data points relating PAT and blood pressure during a short (~60 second) measurement. Processing of these data points yields an accurate patient-specific slope relating PAT to cNIBP. Inclusion of multiple accelerometers yields a variety of signals that can determine features like arm height, motion, activity level, and posture that can be further processed to improve accuracy of the cNIBP calculation, and additionally allow it to be performed in the presence of motion artifacts. And a model based on femoral blood pressure, which is more representative of pressure in the patient's core, can reduce effects such as 'pulse pressure amplification' that can elevate blood pressure measured at a patient's extremities.

The Composite Method can also include an 'intermediate' pressure-dependent measurement wherein the cuff is partially inflated. This partially decreases the amplitude of the PPG waveform in a time-dependent manner. The amplitude's pressure-dependent decrease can then be 'fit' with a numerical function to estimate the pressure at which the amplitude completely disappears, indicating systolic pressure.

For the pressure-dependent measurement, a small pneumatic system attached to the cuff inflates the bladder to apply pressure to an underlying artery according to the pressure waveform. The cuff is typically located on the patient's upper arm, proximal to the brachial artery, and time-dependent pressure is measured by an internal pressure sensor, such as an in-line Wheatstone bridge or strain gauge, within the pneumatic system. The pressure waveform gradually ramps up in a mostly linear manner during inflation, and then slowly rapidly deflates through a 'bleeder valve' during deflation. During inflation, mechanical pulsations corresponding to the patient's heartbeats couple into the bladder as the applied pressure approaches DIA. The mechanical pulsations modulate the pressure waveform so that it includes a series of time-dependent oscillations. The oscillations are similar to those measured with an automated blood pressure cuff using oscillometry, only they are measured during inflation rather than deflation. They are processed as described below to determine a 'processed pressure waveform', from which MAP is determined directly, and SYS and DIA are determined indirectly.

Pressure-dependent measurements performed on inflation have several advantages to similar measurements performed on deflation, which are convention. For example, inflation-based measurements are relatively fast and comfortable compared to those made on deflation. Most conventional cuff-based systems using deflation-based oscillometry take roughly four times longer than the Composite Method's pressure-dependent measurement. Inflation-based measurements are possible because of the Composite Method's relatively slow inflation speed (typically 5-10 mmHg/second) and high sensitivity of the pressure sensor used within the body-worn monitor. Moreover, measurements made during inflation can be immediately terminated once systolic

blood pressure is calculated. In contrast, conventional cuff-based measurements made during deflation typically apply a pressure that far exceeds the patient's systolic blood pressure; pressure within the cuff then slowly bleeds down below DIA to complete the measurement.

Pressure-free measurements immediately follow the pressure-dependent measurements, and are typically made by determining PAT with the same optical and electrical sensors used in the pressure-dependent measurements. Specifically, the body-worn monitor processes PAT and other properties of the PPG waveform, along with the patient-specific slope and measurements of SYS, DIA, and MAP made during the pressure-dependent measurement, to determine cNIBP.

The invention in general, and particularly the hybrid measurement for SV/CO/CP, features many advantages over conventional techniques used to measure these properties. Compared to TDCO and Fick, for example, the body-worn monitor facilitates continuous, noninvasive measurement of these values that is highly accurate and has a low-risk of detrimental complications, such as infection and pulmonary artery vessel perforation. And unlike measurements based on TDCO, Fick, and Doppler, the hybrid measurement does not require a specially trained observer. TBEV measurements are performed at the brachium, which by itself has several advantages over conventional ICG measurements made from the thorax. For example, complications in the pulmonary system, i.e. intra-thoracic liquids and pulmonary edema, do not affect SV/CO/CP values measured from this region. Similarly, the baseline trans-brachial quasi-static impedance, Zo is not affected by medical equipment sometimes present in the thorax, such as chest tubes, external pacemaker wires, and central venous lines. Typically thoracic ICG measurements require 8 separate electrodes, whereas the TBEV measurement described herein only requires 2 separate electrodes. Finally, without the influence of pulmonary ventilation and pulmonary artery pulsations, the signal-to-noise ratio of waveforms measured from the brachium is relatively high.

These and other advantages of the invention will be apparent for the following detailed description, and from the claims.

BRIEF DESCRIPTION OF THE DRAWINGS

FIG. **1** shows a schematic drawing of an algorithm that performs the hybrid measurement for determining SV/CO/CP values according to the invention;

FIG. **2** shows a schematic drawing of the custom electrode patch used to perform TBEV measurements described in FIG. **1**;

FIG. **3** shows a schematic drawing of the human body's circulatory system indicating regions where both conventional ICG and TBEV measurements are made;

FIG. **4** shows a schematic diagram showing the body-worn monitor of the invention positioned relative to both the aorta and brachial arteries, and how these vessels change in diameter during systole and diastole;

FIG. **5** shows a schematic drawing of a body-worn monitor that performs the hybrid measurement shown in FIG. **1**;

FIG. **6**A shows a schematic drawing of an alternate embodiment of the body-worn monitor that performs the hybrid measurement shown in FIG. **1**;

FIG. **6**B shows a three-dimensional drawing of the TBEV module and custom electrode used in the alternate embodiment shown in FIG. **6**A;

FIG. **7**A shows a schematic diagram of analog and digital circuits used to make a TBEV measurement according to the invention; FIG. **7**B shows a TBEV waveform and a highpass filtered portion thereof;

FIG. **8** shows a flow chart of an algorithm for calculating SV where systolic flow time (SFT) is determined using Weissler's regression;

FIG. **9** shows a flow chart of an algorithm for calculating SV using the SV estimators shown in FIG. **1**;

FIG. **10** shows a three-dimensional image of a wrist-worn transceiver, which is part of the body-worn monitor shown in FIGS. **5** and **6**A;

FIGS. **11**A-E show time-dependent plots of, respectively, ECG, ICG, TBEV, d(ICG)/dt, and d(TBEV)/dt waveforms measured with the body-worn monitor of FIG. **5**;

FIGS. **12**A-B show time-dependent plots of dZ/dt waveform measured from, respectively, the thorax and brachium;

FIGS. **13**A-**13**D show time-dependent plots of, respectively, a TBEV waveform, a derivative of the TBEV waveform showing fiducial points near a pulse maximum used to determine the pulse's onset, a derivative of the TBEV waveform showing a shaded region indicating where Weissler's regression is used to estimate LVET, and a derivative of the TBEV waveform where SFT is determined;

FIG. **14** shows a correlation plot comparing SFT measured using a 'fused' approach that relies partially on HR, pulse rate (PR) and Weissler's regression, and LVET measured with Doppler/ultrasound;

FIGS. **15**A-E show two-dimensional Doppler/ultrasound images of the brachial artery measured during systole (FIGS. **15**A-C), and diastole (FIGS. **15**D, E);

FIG. **15**F shows a time-dependent plot of an ECG waveform and a TBEV waveform that corresponds to the two-dimensional images shown in FIGS. **15**A-E;

FIGS. **16**A, B show time-dependent plots of, respectively, a waveform extracted from Doppler/ultrasound images taken from the brachium, similar to those shown in FIGS. **15**A-E, and a simultaneously measured TBEV waveform;

FIG. **16**C, D show plots of, respectively, the time-dependent derivatives of the waveforms shown in FIGS. **16**A, B;

FIG. **17** shows derivatized TBEV waveforms measured from 7 unique subjects;

FIG. **18**A, B show, respectively, correlation and Bland-Altman plots comparing CO measured from of 23 subjects using Doppler/ultrasound and TBEV;

FIGS. **19**A, B show time-dependent plots of, respectively, ICG and TBEV waveforms corresponding to high and low values of CO measured while a subject is wearing military anti-shock trousers (MAST);

FIGS. **20**A-C show time-dependent plots of, respectively, an unfiltered TBEV waveform showing both cardiac and respiratory events, a TBEV waveform filtered with a 0.5 to 15 Hz band-pass filter showing only cardiac events, and a TBEV waveform filtered with a 0.001 to 1 Hz band-pass filter showing only respiration events;

FIGS. **21**A, B show time-dependent plots of, respectively, TBEV and ACC waveforms modulated by respiration events;

FIGS. **21**C, D show frequency-domain power spectra of the time-dependent plots shown, respectively, in FIGS. **21**A, B;

FIG. **22**A shows a time-dependent plot of TBEV and ECG waveforms measured during a period of no motion;

FIG. **22**B shows a time-dependent plot of ACC waveforms, measured simultaneously with the TBEV and ECG waveforms of FIG. **22**A, during the period of no motion;

FIG. **23**A shows time-dependent plots of TBEV and ECG waveforms measured during a period of motion;

FIG. **23**B shows a time-dependent plot showing ACC waveforms, measured simultaneously with the TBEV and ECG waveforms of FIG. **22**A, during the period of motion;

FIG. **24** shows a schematic drawing of a patient and an overlying coordinate axis used with an algorithm and ACC waveforms to determine the patient's posture;

FIG. **25**A shows a plot of time-dependent ACC waveforms measured from a patient's chest during different postures;

FIG. **25**B shows a plot of time-dependent postures determined by processing the ACC waveforms of FIG. **25**A with an algorithm and coordinate axis shown in FIG. **24**;

FIG. **26** shows a schematic drawing of ECG and PPG waveforms, and how the PAT determined from these waveforms and the contours of the PPG waveforms can be collectively analyzed to determine an estimator for SV;

FIG. **27** shows a three-dimensional drawing of a harness used to make a TBEV measurement according to an alternate embodiment of the invention;

FIG. **28** shows a schematic drawing of an alternate embodiment of the invention wherein the TBEV circuit is contained within a module attached directly to the brachium and detached from the ECG circuit, which is worn on the chest;

FIG. **29** shows a schematic drawing of the TBEV module shown in FIG. **28**;

FIG. **30** shows a schematic drawing of an alternate embodiment of the invention wherein the body-worn monitor wirelessly transmits information between a chest-worn module and the wrist-worn transceiver, and from there to a remote monitor; and,

FIG. **31** shows a schematic drawing of the body-worn monitor, similar to that shown in FIG. **30**, that wirelessly transmits information between both a chest-worn module and the wrist-worn transceiver to the remote monitor.

DETAILED DESCRIPTION OF THE INVENTION

Measurement Overview

Referring to FIG. **1**, the invention described herein features a body-worn monitor that continuously and non-invasively determines SV from TBEV measurements **7** collected from a patient's CB region, along with a series of SV 'estimators' **1-6** made calculated from cNIBP measurements. The body-worn monitor is described, for example, in the following patent applications, the contents of which are incorporated herein by reference: BODY-WORN VITAL SIGN MONITOR, U.S. Ser. No. 12/560,077, filed Sep. 15, 2009; and BODY-WORN VITAL SIGN MONITOR, U.S. Ser. No. 12/762,726, filed Apr. 19, 2009. SV measurements made using TBEV **7** and the estimators **1-6** can be incorporated into a 'hybrid measurement' **10**, operating on a microprocessor within the body-worn monitor, that determines SV and ultimately CO and CP.

TBEV is a variation of conventional bioimpedance techniques, such as ICG, and measures waveforms from the CB region to determine time-dependent parameters such as systolic flow time (SFT), $(dZ/dt)_{max}$, and Zo. These parameters feed into Eq. 3, below, where they are coupled with a static parameter V_c to determine SV.

$$SV = V_C\sqrt{\frac{(dZ/dt)_{max}}{Z_0}}\,SFT \tag{3}$$

Here, SV is obtained by taking the square root of the peak rate of change of each TBEV pulse divided by the transbrachial base impedance, Zo. This parameter is then multiplied by SFT and a constant-magnitude V_c to yield SV. The derivation of Eq. 3 is described in detail in U.S. Pat. No. 6,511,438 and in the following reference, the contents of which are fully incorporated herein by reference: Bernstein et al., *Stroke Volume Obtained By Electrical Interrogation of the Brachial Artery: Transbrachial Electrical Bioimpedance Velocimetry*. Unpublished manuscript, submitted 2012. Eq. 3 assumes that $(dZ/dt)_{max}/Z_o$ represents a dimensionless acceleration of blood (with units of $1/s^2$), which is the ohmic analog of peak aortic blood acceleration (cm/s^2). Forceful systolic ejection of blood from the left ventricle of the heart aligns the erythrocytes in parallel during systolic flow to generate a pulsatile increase in conductivity. For this model, V_c is estimated entirely from weight, and is independent of any factors that depend on electrode separation.

Along with SV, the body-worn monitor simultaneously measures cNIBP values (SYS, DIA, MAP, and PP) using a cuffless technique called the 'Composite Method', which is described in detail above. According to the hybrid method, SV is determined explicitly from the TBEV waveforms, and can be estimated from the cNIBP values. From these parameters multiple estimators **1-7** are determined which the algorithm **10** collectively processes to determine SV. Additionally, the body-worn monitor features multiple accelerometers that generate time-dependent ACC waveforms, which are then further processed by a motion algorithm **11** to estimate the patient's level of motion. A function for filtering and rejecting bad data **8** processes information from both the estimators **1-7** and the motion algorithm **11** to determine a collection of valid data points, which are then linearly combined with another function **9** to determine final values of SV. The valid data points, for example, are relatively uncorrupted by motion artifacts; they are determined when the motion algorithm **11** compares a parameter extracted from an ACC waveform to a pre-determined 'motion threshold' value. If the parameter exceeds the pre-determined threshold value, the function **8** rejects the corresponding SV values. On the other hand, if the parameter is lower than the pre-determined threshold value, the function **8** approves the corresponding SV value, and it is passed into the linear combination algorithm **9**, where it will be processed to determine a final value for SV.

Different threshold values can be applied for SV calculated from TBEV **7**, a measurement that is particularly sensitive to motion, and SV estimated from estimators related to blood pressure **1-6**, which are less sensitive to motion. For example, the motion algorithm **11** may determine that a small amount of motion is present, and thus the linear combination algorithm **9** relies completely on SV values determined from the estimators related to blood pressure **1-6**. Or it may determine that a large amount of motion is present, and in response the linear combination algorithm **9** will not report an SV value. If the motion algorithm **11** determines that no motion is present, the linear combination algorithm **9** typically reports a SV value determined entirely from TBEV **7**.

In embodiments, the linear combination algorithm **9** combines different estimators using a simple average or

weighted average to determine a single value of SV. More sophisticated approaches can also be used to process the estimators. For example, specific estimators can be selected based on a patient's physiological condition or biometric parameters, e.g. their age, gender, weight, or height.

Once SV is determined, it can be further processed as defined in Eqs. 1, 2 to determine both CO and CP.

Upon completion of a measurement, the body-worn monitor wirelessly transmits SV/CO/CP values, along with conventional vital signs, to a remote processing system. For example, these data may flow through a hospital-based wireless network to a central computer interfaced to an electronic medical records system. From there, medical professionals, such as doctors, nurses, and first responders, can evaluate a constellation of physiological values corresponding to the patient to make a diagnosis. Typically, patients wear the body-worn monitor as they transition from the ambulance, into the hospital, and ultimately to the home.

A TBEV measurement, described in detail below, injects a low-amperage, high-frequency current into the patient's CB region, and monitors a voltage which relates to the time-dependent resistance encountered by the current through Ohm's Law (V=I×R). It is based on the assumption that the brachial artery, which is the only major artery in the CB region, undergoes little volumetric expansion during systole, and thus changes in resistance are due exclusively to acceleration-induced alignment of erythrocytes within this artery. Stated another way, as blood flows through the artery with each heartbeat, the diameter of the brachial artery stays relatively constant, but acceleration of the blood causes the erythrocytes to align. This physiological process consequently increases conductivity, and decreases resistance, in the artery. The time-dependent resistance in the artery is manifested as a first waveform, called ΔZ(t), which features a series of pulses, each corresponding to a unique heartbeat. A second TBEV waveform, Zo, is filtered to only reflect the baseline impedance of the artery, and is sensitive to relatively low-frequency processes, such as blood volume, interstitial fluids, and occasionally respiration rate.

Estimators for determining SV from blood pressure values include the Lilijestrand **1**, Wesseling **2**, MAP **3**, and Herd **4** estimators. These depend linearly on blood pressure values, and are shown below in Table 1. In this table SYS_{area} refers to the area under the PPG waveform during systole, ΔP_n is the beat-to-beat blood pressure change, is the duration of the cardiac cycle, and τ_n is a time constant that governs the intra-cycle dynamics of the Windkessel model.

These estimators are summarized in detail in the following reference, among other places, the contents of which are incorporated herein by reference: Chen, *Cardiac Output Estimation from Arterial Blood Pressure Waveforms using the MIMIC II Database*; Thesis for Masters Degree submitted to the Massachusetts Institute of Technology; (2009); and Parlikar et al., *Model-Based Estimation of Cardiac Output and Total Peripheral Resistance*, Computers in Cardiology 34: 379-382 (2007). Estimators based on blood pressure can be determined using the Composite Method, or alternatively with a conventional cuff-based method, such as oscillometry or auscultation.

TABLE 1

Estimators for CO

CO ESTIMATOR	CO FORMULA (CO = k*equation below)
Lilijestrand	[(PP/(SYS + DIA)] *HR
Wesseling	(163 + HR − 0.48*MAP)*SYS_{area} * HR
MAP	MAP
SYS	SYS_{area} * HR
ParlikarHeldt	($\Delta P_n/T_n$ + MAP/τ_n)
Herd	(MAP − DIA) * HR
Windkessel	PP * HR

Other SV estimators that can be processed by the algorithm include those based on PAT **5**, which is determined using PPG and ECG waveforms measured by the body-worn monitor, and is described in the following reference, the contents of which are incorporated by reference: Wang et al., *The non-invasive and continuous estimation of cardiac output using a photoplethysmogram and electrocardiogram during incremental exercise*; Physiol. Meas.; 31: 715-726 (2010). FIG. **26** and Eq. 4, below, indicate Wang's methodology for analyzing PAT, ECG **375**, and PPG **380** waveforms to determine a relative value of CO.

$$CO=D\times[C-\ln(PAT)]\times(1-IPA)\times(1+IPA)^{-1} \quad (4)$$

In the equation D and C are constants defined in the Wang reference, and IPA is shown schematically in FIG. **26**. This theory assumes that the PPG waveform **380** includes a well-defined dichrotic notch allowing the parameters X_1, X_2, and ultimately IPA to be determined. Integration of an area under the PPG before the notch yields X_1, while integration of an area under the PPG after the notch yields X_2. IPA is defined as the ratio of X_1 to X_2. Once determined, PAT and IPA are used in Eq. 4 to yield another estimator of SV/CO/CP.

The PPG waveform, taken by itself, can be analyzed and used as an 'other' estimator **6** for algorithm **10**. This waveform represents a time-dependent volumetric expansion of the underlying artery from which it is measured, and is thus different than a traditional cNIBP waveform, such as that measured using an in-dwelling arterial catheter, which represents the time-dependent pressure in the artery. However, PPG and cNIBP waveforms share a similar morphology, particularly over relatively long time periods, and can be analyzed to estimate both blood flow dynamics and hence SV. The following reference, the contents of which are incorporated herein by reference, describes an analysis method for processing waveforms to extract these parameters: Lu et al., *Continuous cardiac output monitoring in humans by invasive and noninvasive peripheral blood pressure waveform analysis*; J Appl Physiol 101: 598-608 (2006).

In still other embodiments, an 'other' estimator **6** for the SV/CO/CP measurement can be based on a measurement technique performed by an external sensor that connects to the body-worn monitor. Such a connection can be made using either wired or wireless means. For example, a technique such as near-infrared spectroscopy (NIRS) can be used to estimate SV as described in the following references, the contents of which are incorporated herein by reference: Soller et al., *Noninvasively determined muscle oxygen saturation is an early indicator of central hypovolemia in humans*; J Appl Physiol 104: 475-481 (2008). A sensor incorporating a NIRS measurement can thus be integrated with the body-worn monitor and attached to the patient's body during a measurement. Values for SV calculated with this sensor are sent to the monitor through the wired or wireless connection, and can be incorporated in the algo-

rithm **10** to further improve the accuracy of the continuous, non-invasive determination of SV. In all cases, the collection of estimators **1-6** relate to CO through a calibration factor (k in Table 1) determined from an absolute measurement of SV, which in the algorithm **10** is provided by the TBEV measurement **7**. Typically TBEV determines SV to within about +/−20%. Perhaps more importantly, the estimators **1-6** and TBEV measurement **7** determine SV with completely different methodologies and from different locations on the body. Thus it is possible that combining the measurements into a single algorithm **10** may reduce error caused by well-known physiological effects that are typically isolated to these locations.

As shown in FIG. **2**, TBEV measurements are typically made with a pair of custom electrodes **24**, each featuring two conductive regions **45**, **47**. The outer conductive region **45** (i.e. the region furthest removed from the CB region) of each electrode **24** injects a low-amperage (<5 mA), high frequency (50-100 kHz) current into the patient's CB region. The inner conductive region **47** then measures the time-dependent voltage across the artery. As described above, variations in this voltage are due to resistance changes caused by blood flowing through the brachial artery, and more specifically due to acceleration-induced alignment of erythrocytes occurring with each heartbeat. This physiology provides a basis for the mathematical model shown above in Eq. 3.

Each conductive region **45** and **47** typically consists of a conductive 'liquid gel' material that roughly matches the impedance properties of human skin. The liquid gel is deposited on top of a conductive substrate coated with a large-area Ag:AgCl film that, in turn, is deposited on top of a flexible substrate **23**. The liquid gel, for example, can be a sponge-like material saturated with a conductive gel or fluid. The neighboring conductive regions **45**, **47** are electrically isolated from each other, and individually connect through a pair of individual conductive traces **54**A, B to a pair of electrical leads **52**A, B adhered to the flexible substrate **23**. The electrical leads **52**A, B, for example, can be metal rivets or posts that easily snap into a corresponding female connector. An insulating adhesive layer (not shown in the figure) dispersed between the conductive regions **45** and **47** electrically isolates these portions of the electrode **24**, and is coated with an adhesive that enables it to be securely attached to the patient during a measurement.

FIGS. **3** and **4** indicate some of the advantages of TBEV measurements, which are made in the CB region **58** of the patient **20**, as compared to conventional ICG measurements, which are made in the thorax **59**. As is clear from FIG. **3** (with the underlying image borrowed from Gray's Anatomy), the thorax **59** features a vast and complicated collection of arteries and veins, as well as most of the patient's vital organs, such as their lungs, heart, kidneys, liver, stomach, and gastro-intestinal track. Each of these systems, and most particularly the lungs and large arteries stemming from the left side of the heart, contain conductive fluids (e.g. blood and lung fluids) that will influence conventional ICG waveforms. For example, physiological processes such as excess lung fluids, pulmonary edema, and pulmonary injury can alter the time-dependent impedance characteristics of the patient's thorax. Thus, the resulting waveforms measured therefrom are no longer reflective of the true hemodynamic state. In stark contrast is the brachium **58**, which is physically removed from pulmonary affects and features only one large artery—the brachial artery—which influences the TBEV measurement. Ultimately this simplifies the morphology of the TBEV waveform and lessens its patient-to-patient variability, thereby simplifying the calculation of SV.

Importantly, previous studies have indicated a strong correlation between peak blood acceleration in the aorta, where the SV is first manifested, and peak blood acceleration in the brachium, where TBEV measures a signal used to estimate SV by square root transformation. Insofar as velocities are concerned, peak aortic blood velocity is roughly 80-124 cm/s (mean ~100 cm/s), while that in the brachial artery is roughly 30-70 cm/s (mean ~50 cm/s). Experiments that measured these parameters are described in the following references, the contents of which are incorporated herein by reference: Gardin J M et al., *Evaluation of blood flow velocity in the ascending aorta and main pulmonary artery of normal subjects by Doppler echocardiograpy*. Am. Heart J. 1984; 107:310; Wilson S et al., *Normal intracardiac and great artery blood velocity measurements by pulsed Doppler echocardiography*. Br. Heart J. 1985; 53:451; Fronek A., *Non invasive diagnostics in vascular disease*. McGraw-Hill, N.Y. 1989, pp 117; Green D, et al., *Assessment of brachial artery blood flow across the cardiac cycle: retrograde flows during bicycle ergometry*. J. Appl. Physiol 2002; 93:361. These references indicate that, to a first approximation, the average blood velocity in the aorta is roughly twice that in the brachial artery.

FIG. **4** indicates how TBEV signals are further reduced in complexity as compared to ICG signals. Without being bound to any theory, this is likely because of the relatively complex time-dependent properties of vasculature in the thorax (e.g. the aorta **66**A, **66**B), as compared to those in the CB region (e.g. the brachium **68**A, **68**B). More specifically, the figure shows the location of the body-worn monitor **19** on a patient, along with schematic drawings of the patient's aorta **66**A, **66**B and brachial artery **68**A, **68**B. During systole, the left ventricle contracts to force blood into the aorta **66**A, with the volume of ejection defined as the SV. This process creates two simultaneous processes in the aorta as the cardiac cycle moves from diastole to systole: 1) a volumetric increase as the aorta's arterial walls, which are highly elastic and expand to an enlarged state **66**A during systole and then recoil to a relaxed state **66**B during diastole; and 2) an acceleration-induced alignment of erythrocytes within the arterial lumen, causing these cells to move from a random orientation during diastole to an aligned parallel orientation during systole. Without being bound by any theory, it is likely that both the volumetric and acceleration-induced alignment processes take place in the aorta during the cardiac cycle. Both processes affect the conductivity of blood in the aorta in a patient-specific manner, thereby complicating the pulsatile component of the ICG signal, and making it difficult for a single mathematical equation to characterize a large set of patients. Historically parameters extracted from ICG signals are fed into the well-known Sramek-Bernstein equation, shown below in Eq. 5, is based on the volumetric expansion model:

$$SV = \delta \frac{L^3}{4.25} \frac{(dZ/dt)_{max}}{Z_0} LVET \tag{6}$$

In Eq. 5 δ represents compensation for body mass index, Zo is the base impedance, and L is estimated from the distance separating the current-injecting and voltage-measuring electrodes on the thorax. This equation and several mathematical derivatives are described in detail in the following reference,

the contents of which are incorporated herein by reference: Bernstein, *Impedance cardiography: Pulsatile blood flow and the biophysical and electrodynamic basis for the stroke volume equations*; J Electr Bioimp; 1: 2-17 (2010). Eq. 5 depends on LVET, which is estimated from each pulse in the ICG waveform, as is described in more detail below. Both the Sramek-Bernstein Equation and an earlier derivative of this, called the Kubicek Equation, feature a 'static component', Z_0, and a 'dynamic component', $\Delta Z(t)$, which relates to LVET and a $(dZ/dt)_{max}/Z_o$ value, calculated from the derivative of the raw ICG signal, $\Delta Z(t)$. These equations assume that $(dZ/dt)_{max}/Z_o$ represents a radial velocity (with units of Ω/s) of blood due to volume expansion of the aorta.

In contrast to the aorta, the brachial artery is a relatively muscular vessel that undergoes little expansion during systole **68**A and recoil during diastole **68**B; its arterial volume, as shown in FIG. **4**, thus remains relatively constant during the cardiac cycle. Time-dependent changes in the arterial waveform are thus due nearly exclusively to periodic, sinusoidal, heartbeat-induced parallel alignment of the erythrocytes within the artery. Ultimately this means that, to develop an underlying mathematical model for the brachial artery, it is not necessary to estimate the relative contributions of volumetric expansion and erythrocyte alignment, which as described above may vary with each patient.

Sensor Configurations

Referring to FIGS. **5** and **6**, in a preferred embodiment the body-worn monitor **19** is distributed on a patient **20** to measure SV/CO/CP. The monitor features a TBEV module **22**, worn near the CB region, which is attached to the patient **20** using a first two-part electrode **24** shown in FIG. **2**. A second two-part electrode **28** attaches to the patient **20** near the elbow. As described above, the outer conductive area in the first two-part electrode injects a high-frequency, low-amperage current into the patient's CB region, while the outer conductive area in the second two-part electrode serves as a sink for this current. Simultaneously, the inner electrodes measure a voltage that describes resistance encountered by the propagating current according to Ohm's Law. Each electrode in the first two-part electrode **24** features a rivet or post that snaps into a mated female component in the TBEV module, thereby connecting these components directly to analog circuitry therein. Similarly, electrodes in the second two-part electrode **28** connect to snaps embedded in a cable **26** that connects the first **24** and second **28** electrodes. The cable **26** includes conductors for transmitting digital data through the control area network (CAN) protocol. Use of this protocol is described in detailed in the following patent application, the contents of which have been previously incorporated herein by reference: BODY-WORN VITAL SIGN MONITOR, U.S. Ser. No. 12/560,077, filed Sep. 15, 2009. The cable **26** additionally includes conductors for transmitting analog signals to the TBEV module **22** to measure the above-described voltage. An analog-to-digital converter (not shown in the figure) within the module digitizes the TBEV waveforms to form $\Delta Z(t)$ and Zo, which are then analyzed with a microprocessor (also not shown in the figure) as described above to determine a value for SV.

An ECG module **40** worn on the patient's thorax connects to the TBEV module **22** through a similar cable **27** that only includes conductors for transmitting digital signals according to the CAN protocol. The ECG module **40** connects to a trio of disposable ECG electrodes **42**A-C, disposed on the patient's thorax in a conventional 'Einthoven's triangle' configuration, through a corresponding trio of ECG leads **44**A-C. During a measurement, the ECG module **40** measures analog signals from each electrode **42**A-C and lead **44**A-C, and performs a differential amplification of these signals according to known techniques in the art to generate an ECG waveform. An analog-to-digital converter (not shown in the figure) digitizes the ECG waveform, and a microprocessor (also not shown in the figure) analyzes the well-known QRS complex within this waveform with a beat-picking algorithm to determine a HR value. Digital representations of these data are sent within CAN-formatted packets through the cable **27** to a CAN transceiver (not shown in the figure) within the TBEV module **22**. There, the packets are combined with corresponding packets that include the TBEV waveform and SV values, which are calculated as described above. These packets pass through CAN conductors in the cable **26**, past the second two-part electrode **28**, and then through a third cable **29** to a wrist-worn transceiver **30** that connects to the patient's wrist using a plastic cradle **32** and Velcro strap **34**. These components are described in more detail in the following co-pending patent applications, the contents of which have been previously incorporated by reference: BODY-WORN VITAL SIGN MONITOR, U.S. Ser. No. 12/560,077, filed Sep. 15, 2009; and BODY-WORN VITAL SIGN MONITOR, U.S. Ser. No. 12/762,726, filed Apr. 19, 2009. The wrist-worn transceiver **30** additionally connects through a short cable **38** that carries only analog signals measured by a thumb-worn optical sensor **36**. Within the wrist-worn transceiver is a pulse oximetry circuit (not shown in the figure) that converts signals measured by the optical sensor **36** to generate PPG waveforms and corresponding values of SpO2. A microprocessor within the wrist-worn transceiver **30** processes PPG and ECG waveforms to generate a value of PAT, or alternatively TBEV and PPG waveforms to generate a value of VTT. These transit times are converted into cNIBP values using the Composite Method, as described above. The cNIBP values, in turn, are converted into SV estimators using the algorithm shown in FIG. **1**. From there, corresponding values of CO are determined using SV and ECG-determined values of HR, while values of CP are determined using MAP and CO.

Technically, TBEV-based measurements of SV only require an isolated TBEV waveform, and can be performed without an ECG waveform. However, this signal, which is relatively easy to measure and denotes the beginning of the cardiac cycle associated with each heartbeat, can be used to 'gate' the relatively weak TBEV signal to make it easier to extract the properties described above in Eq. 3. More specifically, the above-described software beat picker can detect the QRS complex within the ECG waveform, which is associated with the onset of an individual heartbeat. Relevant portions of the TBEV waveform typically follow the QRS complex by a few hundred milliseconds. Analysis of these portions of the TBEV waveforms yields properties such as SFT, $(dZ/dt)_{max}$, and Zo that are used to calculate SV as described above. Gating the TBEV waveform in this manner can be particularly effective in analyzing these properties when noise is present in the TBEV waveform, e.g. during periods of motion.

HR, determined from the ECG waveform, is used to convert SV into CO and CO into CP, as described in Eqs. 1 and 2, above. Typically HR is determined from the time period separating neighboring QRS complexes in the ECG waveform; alternatively it can be estimated from neighboring pulses in either the PPG or TBEV waveform.

The ECG module **40** can additionally connect to 5 leads, and alternatively 12 leads. It is typically hard-wired into the TBEV module **22**. The third cable **29** plugs into the wrist-

worn transceiver **30** using a detachable connector **31** that allows it to be easily removed. In other embodiments the order of the ECG module **40** and TBEV module **22** can be reversed so that the TBEV module **22** is closer to the thorax, and the ECG module **40** is closer to the CB region. In still other embodiments, the TBEV module **22** can be disposed on the third cable **29** and attach directly to the second electrode **28**, and the ECG module **40** can be disposed in the original location of the TBEV module **22**, and be encapsulated by a housing that attaches to the first electrode **24** and feeds analog signals into the TBEV module **22**. In general, multiple configurations of the various modules, cables, and electrodes shown in FIG. **6** are within the scope of the invention.

An alternate embodiment of the invention is shown in FIGS. **6**A, B. Here, the ECG module **40** is worn on the patient's CB region, and the TBEV module **22** is worn near the elbow. Both the ECG **40** and TBEV **22** modules are attached to the patient with two-part electrodes **24**, **28**, with the TBEV electrode **24** shown in more detail in FIG. **6**B. The two-part electrode **24** features a pair of female snaps **62**A, B disposed on a flexible substrate **64** that connects to underlying conductive regions **63**A, B. Each conductive region **63**A, B features a solid gel material, chosen to match the electrical impedance characteristics of human skin, deposited on a thin Ag/AgCl film. The flexible substrate **64** features an underlying adhesive layer that during use securely attaches the electrode **24** to the patient's CB region. The female snaps **62**A, B are chosen to geometrically match a pair of metal rivets **61**A, B that attach to a bottom portion of a TBEV circuit board **60**. During use the rivets **61**A, B snap into the female snaps **62**A, B, thus securing the TBEV module **22** to the patient. The rivet **61**B furthest away from the CB region connects to the TBEV circuit and injects a current through the corresponding conducting region **63**B, while the rivet **61**A closest to the region measures a corresponding voltage. A plastic housing **65** covers the TBEV circuit board **60** and shields it from liquids and other materials present in the hospital. Note that in the figure the female snaps **62**A, B are disposed on the electrode **28**, and the metal rivets **61**A, B are disposed on the circuit board **60**. However in an alternate embodiment these components can be reversed, i.e. the female snaps **62**A, B can be disposed on the bottom of the circuit board and the metal rivets **61**A, B can be disposed on the top of the electrode **28**.

The ECG module **40** is attached to a second electrode **24** with a geometry similar to that shown in FIG. **6**B. Here, however, the electrode **24** is not electrically connected to an internal ECG circuit, but rather is used exclusively to hold the ECG module **40** in place. The electrode's conductive regions connect through electrical leads within the module **40** that are not connected to the ECG circuit, and then through a cable **68** to the TBEV module **22**. There, the module **22** receives and collectively processes signals from the first **28** and second **24** electrode to measure a time-dependent voltage as described above. This voltage is then converted into a time-dependent resistance to form the TBEV waveform, which is then processed to determine SV and ultimately CO. The cable **68** also includes conductors for sending packets containing digitized ECG waveforms and HR according to the CAN protocol. These packets pass through CAN transceivers in the TBEV module **22**, through the third cable **29**, and ultimately to the wrist-worn transceiver **30** for further processing and display.

In FIG. **6**A the individual ECG electrodes **42**A-C are disposed on a single chest-worn patch **67** that attaches near the middle of the patient's thorax. The patch **67** connects to the ECG module **40** through a single cable **69** that includes individual conductors corresponding to each electrode **42**A-C. These conductors port analog signals to the ECG module **40**, where they are analyzed as described above to determine ECG waveforms and HR.

Within the body-worn monitor **19** are three three-axis accelerometers that measure ACC waveforms corresponding to x, y, and z-axes. The accelerometers, which are not shown in the figure, are disposed within the ECG module **40**, the TBEV module **22**, and the wrist-worn transceiver **30**. During a measurement, ACC waveforms generated by the accelerometers are processed by microprocessors within each of the above-mentioned components to determine a motion-related parameter. Measurements of SV (or any vital sign, for that matter) are rejected if the parameter, or a secondary parameter derived therefrom, is lower than the pre-determined threshold value. Algorithms for such calculations are described, for example, in the following co-pending patent application, the contents of which are incorporated herein by reference: VITAL SIGN MONITORING SYSTEM FEATURING 3 ACCELEROMETERS, U.S. Ser. No. 12/469,094 (filed May 20, 2009).

Within the TBEV module is an analog circuit **100**, shown in FIG. **7**, that performs the TBEV measurement according to the invention. The figure shows just one embodiment of the circuit **100**; similar electrical results can be achieved using a design and collection of electrical components that differ from those shown in the figure.

The circuit **100** features a first electrode **105**B that injects a high-frequency, low-amperage current (I_{in}) into the patient's brachium. This serves as the current source. Typically a current pump **102** provides the modulated current, with the modulation frequency typically being between 50-100 KHz, and the current magnitude being between 0.1 and 10 mA. Preferably the current pump **102** supplies current with a magnitude of 4 mA that is modulated at 70 kHz through the first electrode **105**B. A second electrode **104**A serves as the current drain (I_{out}).

A pair of electrodes **104**B, **105**A measure the time-dependent voltage encountered by the propagating current. These electrodes are indicated in the figure as V+ and V−. As described above, using Ohm's law (V=I×R), the measured voltage divided by the magnitude of the injected current yields a time-dependent resistance to ac (i.e. impedance) that relates to blood flow in the brachial artery. As shown by the waveform **128** in the figure, the time-dependent resistance features a slowly varying dc offset, characterized by Zo, that indicates the baseline impedance encountered by the injected current; for TBEV this will depend, for example, on the amount of fat, bone, muscle, and blood volume in the brachium of a given patient. Zo, which typically has a value between about 10 and 150Ω, is also influenced by low-frequency, time-dependent processes such as respiration. Such processes affect the inherent capacitance near the brachial region that TBEV measures, and are manifested in the waveform by low-frequency undulations, such as those shown in the waveform **128**. A relatively small (typically 0.1-0.5Ω) ac component, ΔZ(t), lies on top of Zo and is attributed to changes in resistance caused by the heartbeat-induced blood that propagates in the brachial artery, as described in detail above. ΔZ(t) is processed with a high-pass filter to form a TBEV signal that features a collection of individual pulses **130** that are ultimately processed to ultimately determine stroke volume and cardiac output.

Voltage signals measured by the first electrode **104**B (V+) and the second electrode **105**A (V−) feed into a differential

amplifier **107** to form a single, differential voltage signal which is modulated according to the modulation frequency (e.g. 70 kHz) of the current pump **102**. From there, the signal flows to a demodulator **106**, which also receives a carrier frequency from the current pump **102** to selectively extract signal components that only correspond to the TBEV measurement. The collective function of the differential amplifier **107** and demodulator **106** can be accomplished with many different circuits aimed at extracting weak signals, like the TBEV signal, from noise. For example, these components can be combined to form a 'lock-in amplifier' that selectively amplifies signal components occurring at a well-defined carrier frequency. Or the signal and carrier frequencies can be deconvoluted in much the same way as that used in conventional AM radio using a circuit features one or more diodes. The phase of the demodulated signal may also be adjusted with a phase-adjusting component **108** during the amplification process. In one embodiment, the ADS **1298** family of chipsets marketed by Texas Instruments may be used for this application. This chipset features fully integrated analog front ends for both ECG and impedance pneumography. The latter measurement is performed with components for digital differential amplification, demodulation, and phase adjustment, such as those used for the TBEV measurement, that are integrated directly into the chipset.

Once the TBEV signal is extracted, it flows to a series of analog filters **110**, **112**, **114** within the circuit **100** that remove extraneous noise from the Zo and ΔZ(t) signals. The first low-pass filter **1010** (30 Hz) removes any high-frequency noise components (e.g. power line components at 60 Hz) that may corrupt the signal. Part of this signal that passes through this filter **110**, which represents Zo, is ported directly to a channel in an analog-to-digital converter **120**. The remaining part of the signal feeds into a high-pass filter **112** (0.1 Hz) that passes high-frequency signal components responsible for the shape of individual TBEV pulses **130**. This signal then passes through a final low-pass filter **114** (10 Hz) to further remove any high-frequency noise. Finally, the filtered signal passes through a programmable gain amplifier (PGA) **116**, which, using a 1.65V reference, amplifies the resultant signal with a computer-controlled gain. The amplified signal represents ΔZ(t), and is ported to a separate channel of the analog-to-digital converter **120**, where it is digitized alongside of Zo. The analog-to-digital converter and PGA are integrated directly into the ADS **1298** chipset described above. The chipset can simultaneously digitize waveforms such as Zo and ΔZ(t) with 24-bit resolution and sampling rates (e.g. 500 Hz) that are suitable for physiological waveforms. Thus, in theory, this one chipset can perform the function of the differential amplifier **107**, demodulator **108**, PGA **116**, and analog-to-digital converter **120**. Reliance of just a single chipset to perform these multiple functions ultimately reduces both size and power consumption of the TBEV circuit **100**.

Digitized Zo and ΔZ(t) waveforms are received by a microprocessor **124** through a conventional digital interface, such as a SPI or I2C interface. Algorithms for converting the waveforms into actual measurements of SV and CO are performed by the microprocessor **124**. The microprocessor **124** also receives digital motion-related waveforms from an on-board accelerometer **122**, and processes these to determine parameters such as the degree/magnitude of motion, frequency of motion, posture, and activity level.

FIGS. **8** and **9** show flow charts of algorithms **133**A, B that function using compiled computer code that operates, e.g., on the microprocessor **124** shown in FIG. **7**. The compiled computer code is loaded in memory associated with the microprocessor, and is run each time a TBEV measurement is converted into a numerical value for CO and SV. The microprocessor typically runs an embedded real-time operating system. The compiled computer code is typically written in a language such as C, C++, or assembly language. Each step **135-151** in the different algorithms **133**A, B is typically carried out by a function or calculation included in the compiled computer code.

Wrist-Worn Transceiver

The wrist-worn transceiver **272** used to perform the hybrid measurement method of SV according to the invention is shown in more detail in FIG. **10**. It features an embedded microprocessor (not shown in the figure) for making these calculations, and a touch panel interface **273** that displays CO/SV along with other properties described above. A flexible wrist strap **290** affixes the transceiver **272** to the patient's wrist like a conventional wristwatch. Connected to the transceiver **272** is an analog cable **292** that terminates with an optical sensor (not shown in the figure) that wraps around the base of the patient's thumb to measure PPG waveforms. During the measurement, the optical sensor generates a series of time-dependent PPG waveforms (measured with both red and infrared wavelengths) that a microprocessor in the transceiver processes along with a TBEV and ECG to measure cNIBP, SpO2, and provide waveforms to the hybrid measurement for SV/CO/CP.

As described above, the wrist-worn transceiver attaches to the patient's wrist using a flexible strap **290** which threads through two D-ring openings in a plastic housing **206**. The transceiver **272** features a touch panel display **220** that renders a GUI **273** that is altered depending on the viewer (typically the patient or a medical professional). Specifically, the transceiver **272** includes a small-scale infrared barcode scanner **202** that, during use, can scan a barcode worn on a badge of a medical professional. The barcode indicates to the transceiver's software that, for example, a nurse or doctor is viewing the user interface. In response, the GUI **273** displays vital sign data and other medical diagnostic information appropriate for medical professionals. Using this GUI **273**, the nurse, doctor, or medical professional, for example, can view the vital sign information, set alarm parameters, and enter information about the patient (e.g. their demographic information, medication, or medical condition). For example, for the SV/CO/CP measurement described above, the clinician can enter the patient's gender, height, weight, and age. These parameters may be used in the calculations described in Eq. 3, above, to estimate the Vc used in Eq. 3 to calculate SV. Once entered, the clinician can press a button on the GUI **273** indicating that these operations are complete and that the appropriate data for the SV measurement has been entered. At this point, the display **220** renders an interface that is more appropriate to the patient, such as one that simply displays the time of day and battery power.

The transceiver **272** features three CAN connectors **204***a-c* on the side of its upper portion, each which supports the CAN protocol and wiring schematics, and relays digitized data to the transceiver's internal CPU. Digital signals that pass through the CAN connectors include a header that indicates the specific signal (e.g. TBEV, ECG, ACC, or numerical values calculated from these waveforms) and the sensor from which the signal originated. In alternative embodiments some of these are sent from the chest-worn module through Bluetooth, which maintains the CAN structure of the packets. This allows the CPU to easily interpret signals that arrive through the CAN connectors **204***a-c*, such

as those described above corresponding to TBEB and ECG waveforms, and means that these connectors are not associated with a specific cable. Any cable connecting to the transceiver can be plugged into any connector **204***a-c*.

As shown in FIG. **10**, one embodiment of the invention features a first connector **204***a* that receives a Bluetooth 'dongle' **208** that features an embedded antenna **213** and a connector **209** which snaps into and mates with any one of the CAN connectors **204***a-c*. During operation the dongle **208** is automatically paired with the Bluetooth transceiver in the chest-worn sensor, and then receives a digital data stream over Bluetooth with the antenna **213**. An internal CAN transceiver formats the data stream into CAN-compliant packets, and then passes these through the connector **209** into the wrist-worn transceiver, where it is processed as described above.

The second CAN connector **204***b* receives the cable **295** that connects to another sensor, e.g. a pneumatic cuff-based system used to measure blood pressure values used in the Composite Method. This connector **204***b* receives a time-dependent pressure waveform delivered by the pneumatic system to the patient's arm, along with values for SYS, DIA, and MAP values determined during the Composite Method's indexing measurement. The cable **295** unplugs from the connector **204***b* once the indexing measurement is complete, and is plugged back in after approximately four hours for another indexing measurement.

The final CAN connector **204***c* can be used for an ancillary device, e.g. a glucometer, infusion pump, body-worn insulin pump, NIRS system, ventilator, or et-CO2 measurement system. As described above, digital information generated by these systems will include a header that indicates their origin so that the CPU can process them accordingly.

The transceiver **272** includes a speaker **201** that allows a medical professional to communicate with the patient using a voice over Internet protocol (VOIP). For example, using the speaker **201** the medical professional could query the patient from a central nursing station or mobile phone connected to a wireless, Internet-based network within the hospital. Or the medical professional could wear a separate transceiver similar to the shown in the figure, and use this as a communication device. In this application, the transceiver **272** worn by the patient functions much like a conventional cellular telephone or 'walkie-talkie': it can be used for voice communications with the medical professional and can additionally relay information describing the patient's vital signs and motion. The speaker can also enunciate pre-programmed messages to the patient, such as those used to calibrate the chest-worn accelerometers for a posture calculation, as described above.

Clinical Data from CO/SV Measurements

FIGS. **11**A-E shows examples of ECG, ICG, and TBEV waveforms, along with time-dependent derivatives of the both ICG (d(ICG)/dt) and TBEV (d(TBEV)/dt) waveforms. These data were simultaneously measured from a human subject over a 5-second period with a body-worn monitor similar to that shown in FIG. **5**. Each waveform features a heartbeat-induced 'pulse' indicating a unique physiologic process. For example, the ECG waveform shown in FIG. **11**A is measured with conventional ECG electrodes and circuitry described above. It features a conventional QRS complex indicating rapid depolarization of the heart's right and left ventricles. Informally, the ECG waveform denotes the onset of the cardiac cycle. The ICG waveform (FIG. **11**B) is measured from the thorax using a conventional ICG monitor and configuration of chest-worn electrodes as described above, and its derivatized form (FIG. **11**D) yields parameters used above in Eq. 5 to calculate SV. Specifically, from the derivatized waveform a computer program calculates parameters such as $(dZ/dt)_{max}$ and SFT, which as described above corresponds to the time period from opening of the aortic valve, heralding the onset of ejection, to closure of the aortic valve, signifying the end of ejection. The TBEV waveform (FIG. **11**C) and its time-dependent derivative (FIG. **11**E) are measured from the brachium using a configuration of arm-worn electrodes similar to that shown in FIG. **5**. The derivatized TBEV waveform, like the derivatized ICG waveform, yields similar impedance parameters such as $(dZ/dt)_{max}$ and SFT, and features a signal-to-noise ratio similar to that shown for the ICG waveform, despite the fact that its genesis is the much smaller brachial artery.

FIGS. **12**A, **12**B indicate how LVET and SFT are extracted, respectively, from both the derivatized ICG and TBEV waveforms. As shown in FIG. **12**A, the derivatized ICG waveform features consecutive pulses, each characterized by three points: a 'B' point on the pulse's upswing indicating opening of the aortic valve; an X point on the pulse's nadir indicating closing of the aortic valve; and a 'C' point on its maximum value indicating the maximum slope of the $\Delta Z(t)$ pulse's upswing, which is equivalent to $(dZ/dt)_{max}$. LVET is typically calculated from the time differential between the B and X points. However, due to the subtle nature of these fiducial markers, even low levels of noise in the waveforms can make them difficult to determine. Ultimately such noise adds errors to the calculated LVET and resulting SV.

Determining SFT from the derivatized TBEV waveform shown in FIG. **12**B is relatively easier. Here, there are no complicated B and X points. The initial upswing, or onset of the pulse, indicates the onset of flow, corresponding to opening of the aortic valve. And the second zero crossing point after dZ/dt_{max}, occurring later in time, indicates when acceleration of the erythrocytes is temporarily ceased. The second zero crossing indicates the end of systolic forward flow, corresponding to closing of the valve. Computationally, using a computer algorithm, such a determination of SFT can be easily done by following the progression of the pulse and recording the appropriate zero-point crossings.

FIGS. **13**A-D indicate a technique for determining both an onset **90** and dichrotic notch **91**, **95** in a pulse contained in a TBEV waveform. As described above, such fiducial markers can sometimes be obscured by baseline noise (caused, e.g., by motion or low signal levels), making them difficult to determine. In the derivatized waveform in FIG. **13**B, a pair of data points **92** near the peak of the pulse can be selected and fit with a simple line **96**, with the point at which the line **96** intersects a zero value (shown in the figure by the dashed line **90**) indicating the pulse's onset. Once this point is determined, the zero-point crossing indicating the dichrotic notch can be first initially estimated using an approximation for SFT, which is the time separating the pulse's onset and dichrotic notch. This is done using an equation known as 'Weissler' s Regression', shown below in Eq. 6, that estimates LVET from HR.

$$LVET=-0.0017\times HR+0.413 \quad (6)$$

Weissler's Regression allows LVET, equivalent to SFT **94**, **95**, to be estimated from HR determined from either the ECG waveform, or alternatively from PR determined from the PPG waveform. FIG. **13**C depicts a derivative of the TBEV waveform showing a shaded region **93** indicating where Weissler's regression is used to estimate LVET. LVET determined from Weissler's relationship is also shown as a vertical line in FIGS. **13**A and **13**D. FIG. **14** shows a

correlation plot of a 'fused' SFT determined from HR and PR and compared to LVET from the Doppler/ultrasound for a 38-subject study. Here, Doppler/ultrasound represents a gold standard for determining LVET. As is clear from these data, strong correlation (r=0.8) exists between these two methods, indicating that Eq. 6 is a reasonable way to determine SFT. This method can thus be used along with parameters extracted from TBEV signals measured at the brachium to estimate SV.

To further support this point, FIGS. **15**A-E show Doppler/ultrasound images measured from the brachial artery, and FIG. **15**F shows concurrently measured TBEV and ECG waveforms. These data indicate two important aspects of the TBEV measurement. First, the Doppler/ultrasound images confirm that, during a typical cardiac cycle, volumetric expansion in the brachial artery is minimal. The artery's diameter undergoes little to no measurable change during the cycle, meaning that heartbeat-induced changes in blood conductivity, as measured by TBEV, are mostly due to acceleration of blood and the consequent parallel alignment of erythrocytes. Second, the images also indicate that the dichrotic notch in the TBEV waveform does indeed correspond to a point in time when the acceleration of blood is temporarily zero, and thus SFT can be accurately calculated from this fiducial marker.

More specifically, the figures show Doppler/ultrasound images indicating forward blood velocity is zero prior to systole (FIG. **15**A), thereby reducing conductivity and the corresponding amplitude of the TBEV waveform. This point marks the onset of the TBEV pulse. Opening of the aortic valve induces systole (FIG. **15**B) and increases acceleration of blood and thus conductivity in the brachium, causing the TBEV waveform to rapidly increase in amplitude. Closure of the aortic valve, as characterized by SFT, marks the end of the systole (FIG. **15**C) a temporary lull in acceleration, and consequently the appearance of the dichrotic notch. During diastole (FIG. **15**D) flow is once again increased due to reflected waves, as well as blood remaining in the aorta, which is injected into the brachium, and eventually decays away until the cycle is repeated with a new heartbeat (FIG. **15**E). This relatively simple physiology contrasts the complex, underlying physiological processes that take place in the thorax as mentioned above, which are the basis for ICG-based determination of SV.

FIGS. **16**A-D further illustrates how TBEV waveforms yield SFT in much the same way as Doppler/ultrasound yields LVET, which as described above represents a gold standard for this measurement. Here, FIG. **16**A shows a time-dependent waveform extracted from a collection of two-dimensional Doppler/ultrasound images, such as those shown in FIGS. **15**A-E. The waveform indicates time-dependent blood velocity, and its derivatized form is shown in FIG. **16**C. Shown below these waveforms in FIGS. **16**B and **16**D are simultaneously measured TBEV waveforms (FIG. **16**B) and its derivatized form (FIG. **16**D). Dashed lines **97**A, B, **98**A, B in the figures show, respectively, the pulse onset (determined, e.g., as shown in FIG. **13**) and the dichrotic notch from the two sets of waveforms. As is clear from the figure, these points coincide exactly, indicating that LVET determined explicitly from Doppler/ultrasound waveforms is nearly identical to SFT determined from TBEV waveforms.

Another advantage of TBEV waveforms compared to those measured with conventional ICG is that they undergo little patient-to-patient variation, thus making their computer-based analysis relatively easy. FIG. **17** demonstrates this point by showing derivatized waveforms from 7 different subjects. Each waveform has roughly the same morphology, and in all cases the relevant fiducial makers (pulse onset, pulse maximum, zero-point crossing) are clear. This indicates that a simple computer algorithm can be used to extract $(dZ/dt)_{max}$ and SFT, which is then used as described above to calculate SV.

The analysis described above was used in a formal clinical study to test accuracy of determining CO using TBEV and Eq. 3 above, compared to CO determined using Doppler/ultrasound. Correlation and Bland-Altman plots are shown, respectively, in FIGS. **18**A and **18**B. The shaded gray area in the plots indicates the inherent errors associated with conventional Doppler/ultrasound measurements, which are about +/−20%. In total 23 subjects (11M, 12W) with ages ranging from 21-80 were measured for this study, and correlations for all but two of these subjects fell within the error of the Doppler/ultrasound measurements.

FIGS. **19**A-B indicate that TBEV waveforms measured from the brachium may be a better determinant of CO than ICG waveforms measured from the thorax. Here, both waveforms were measured while a subject wore a 'MAST' suit, which is a pair of pressurized trousers used to force blood from the lower extremities toward the torso and the heart. A MAST suit thus simulates the reverse of hemorrhage, and thus causes CO/SV to increase. As shown in the figures by the dashed lines, LVET was determined from ICG, while SFT was determined using TBEV. Waveforms from these techniques were measured simultaneously from the thorax and brachium during period of high and low SV measurements. Increased SV is achieved when the MAST suit forces blood into the thorax. An increase in both LVET and SFT indicate an increase in SV. In the ICG waveforms (FIG. **19**A) only a small increase in LVET was detected. In contrast, in the TBEV waveforms (FIG. **19**B), a large increase in SFT was detected, indicating measurements made in this region of the body may be more sensitive to small changes in SV and CO.

Measuring Respiration Rate with TBEV

TBEV, like techniques such as impedance pneumography, injects small amounts of current into the patient's body, and measures resistance (i.e. impedance) encountered by the current to calculate a parameter of interest. During a TBEV measurement, heartbeat-induced blood flow results in the pulsatile component of $\Delta Z(t)$. Additionally, changes in capacitance due to breathing may also affect the impedance as measured by TBEV. FIGS. **20**A-C illustrate this point. In FIG. **20**A, for example, a TBEV waveform with no digital filtering shows both high-frequency cardiac components due to blood flow, as well as low-frequency undulations due to respiration rate. Both features can be extracted and analyzed using digital filtering. For example, as shown in FIG. **20**B, processing the TBEV waveform shown in FIG. **20**A with a first band-pass filter (0.5→15 Hz) removes the respiratory component, leaving only the cardiac component. Similarly, as shown in FIG. **20**C, processing the TBEV waveform shown in FIG. **20**A with a second band-pass filter (0.001→1 Hz) removes the cardiac component, leaving on the undulations due to respiration. In this latter case, the peaks in the waveform can be counted with a conventional breath-picking algorithm to determine respiration rate.

The algorithm for calculating respiration rate can be expanded to include processing of signal from the accelerometer within the TBEV module. For example, as shown in FIGS. **21**A-D, these signals can be collectively processed to accurately determine respiration rate, even in the presence of motion. A similar technique is described in the following co-pending application, the contents of which are incorpo-

rated herein by reference: BODY-WORN MONITOR FOR MEASURING RESPIRATION RATE, U.S. Ser. No. 12/762,874, filed Apr. 14, 2010. More specifically, FIGS. **21**A and **21**B show time-domain TBEV and ACC waveforms measured simultaneously from a patient with the system similar to that described above. In the TBEV waveform, the slowly varying pulses occurring approximately every 7 seconds correspond to individual breaths, while the sharp peaks in the waveform correspond to heartbeat-induced pulses. FIGS. **21**C and **21**D show, respectively, frequency-domain power spectra of both the TBEV and ACC waveforms. Clearly shown in the power spectra of the TBEV waveform is a dominant peak near 0.8 Hz corresponding to the heartbeat-induced pulses. A much weaker peak corresponding to the patient's breathing rate is also evident near 0.15 Hz. As shown in the gray shaded region **99**, the power spectra corresponding to the ACC waveform features only one well-defined peak near 1.5 Hz that includes nearly the exact same frequency components as the corresponding peak in the TBEV waveform. Further processing of these two spectra with a simple peak-finding algorithm yields the patient's actual RR, which corresponds to about 8 breaths/minute.

Measuring TBEV Waveforms in the Absence of Motion

FIGS. **22**A, B and **23**A, B indicate how different degrees of motion from a patient's arm can influence both ECG and TBEV waveforms, thereby affecting the accuracy of SV measurements. The ACC waveform is typically measured along the vertical axis of the accelerometer embedded in the TBEV module. The magnitude of the axes for ECG and TBEV waveforms are the same for all figures.

In FIG. **22**B, for example, the ACC waveform is relatively flat and lacks any significant time-dependent features, indicating that the patient is not moving and is relatively still. Consequently the TBEV waveform in FIG. **22**A, which is strongly affected by motion, features well-defined values for the pulse onset, indicated by marker **73**, and $(dZ/dt)_{max}$, indicated by marker **74**. Likewise the ECG waveform features a QRS complex, indicated by marker **72**, which is undistorted. The fidelity of these features indicate that both HR and SV values can typically be accurately determined during periods of little or no motion, as indicated by the ACC waveform in FIG. **22**B.

FIGS. **23**A, B show the affects of a major amount of arm motion on both the ECG and TBEV waveforms. Here, the period of motion is indicated in both figures by the dashed box **80**, which contrasts with the preceding period where motion is not present, as shown in the dashed box **81**. The ACC waveform in FIG. **23**B indicates that motion lasts for roughly one second, beginning and ending at times indicated, respectively, near markers **78** and **79**. The motion is complex and peaks in intensity at marker **79**. Even for major finger motion the ECG waveform and its QRS complex, indicated by marker **75**, are relatively undistorted. But the TBEV measured during the period of motion is strongly distorted to the point that its peak value, indicated by marker **77**, is relatively flat and basically immeasurable. This makes it difficult to accurately measure TBEV waveforms and the subsequent SV value calculated from this parameter. The peak onset, indicated by marker **76**, is also distorted, but to a lesser degree than the corresponding peak value.

Data shown in FIGS. **22**A, B and **22**A, B indicate that motion can be detected and accounted for during TBEV measurements to minimize the occurrence of false alarms and, additionally, make accurate readings in the presence of motion. For example, during periods of motion SFT can be calculated using Weissler's Regression, and then used to Eq. 3 above to estimate SV. Or during such motion one of the various estimators shown in FIG. **1** could be used to estimate SV.

Processing ACC Waveforms to Determine Posture

A patient's posture may influence their values of SV/CO/CP, and thus knowing this parameter may improve the measurement described herein. To make this measurement, the body-worn monitor described above includes three 3-axis accelerometers as well as the ECG and TBEV circuits. In addition to determining SV/CO/CP, these sensors can generate time-dependent waveforms that when analyzed yield RR and the patient's motion-related properties, e.g. degree of motion, posture, and activity level.

FIGS. **25**A-B show, for example, that the body-worn monitor can generate ACC waveforms that can be analyzed to accurately estimate the patient's posture. Specifically, FIG. **25**A shows that the 3-axis accelerometer in the torso accurately measures ACC waveforms which correlate directly to the patient's position (e.g. standing, lying on back, lying on chest, lying on side) as indicated in FIG. **25**B. This property, in turn, can be used along with the patient's SV/CO/CP value and a series of 'heuristic rules' to generate an alarm/alert value. For example, an alarm need not be sounded if the patient's SV/CO/CP value is low (e.g. below about 1.5 l/min. for CO), but analysis of the ACC waveforms indicates that the patient is standing or walking as shown in FIG. **25**B. The assumption here is that a patient in this posture/activity level is not in need of medical assistance. In contrast, a combination of a low SV/CO/CP value and a patient that is either supine or, worse yet, recently fallen should trigger an alarm.

FIG. **24** indicates how the body-worn monitor can determine motion-related parameters (e.g. degree of motion, posture, and activity level) from a patient **410** using time-dependent ACC waveforms continuously generated from the three accelerometers **412**, **413**, **414** worn, respectively, on the patient's chest, bicep, and wrist. Additionally, the height of the patient's arm can affect the cNIBP measurement, as blood pressure can vary significantly due to hydrostatic forces induced by changes in arm height. Moreover, this phenomenon can be detected and exploited to calibrate the cNIBP measurement, as described in detail in the above-referenced patent applications, the contents of which have been previously incorporated by reference. As described in these documents, arm height can be determined using DC signals from the accelerometers **413**, **414** disposed, respectively, on the patient's bicep and wrist. Posture, in contrast, can be exclusively determined by the accelerometer **412** worn on the patient's chest. An algorithm operating on the wrist-worn transceiver extracts DC values from waveforms measured from this accelerometer and processes them with an algorithm described below to determine posture.

Specifically, torso posture is determined for a patient **410** using angles determined between the measured gravitational vector and the axes of a torso coordinate space **411**. The axes of this space **411** are defined in a three-dimensional Euclidean space where $\vec{R}_{CV}$ is the vertical axis, $\vec{R}_{CH}$ is the horizontal axis, and $\vec{R}_{CN}$ is the normal axis. These axes must be identified relative to a 'chest accelerometer coordinate space' before the patient's posture can be determined.

The first step in determining a patient's posture is to identify alignment of $\vec{R}_{CV}$ in the chest accelerometer coordinate space. This can be determined in either of two

approaches. In the first approach, $\vec{R}_{CV}$ is assumed based on a typical alignment of the body-worn monitor relative to the patient. During a manufacturing process, these parameters are then preprogrammed into firmware operating on the wrist-worn transceiver. In this procedure it is assumed that accelerometers within the body-worn monitor are applied to each patient with essentially the same configuration. In the second approach, $\vec{R}_{CV}$ is identified on a patient-specific basis. Here, an algorithm operating on the wrist-worn transceiver prompts the patient (using, e.g., video instruction operating on the wrist-worn transceiver, or audio instructions transmitted through a speaker) to assume a known position with respect to gravity (e.g., standing upright with arms pointed straight down). The algorithm then calculates $\vec{R}_{CV}$ from DC values corresponding to the x, y, and z-axes of the chest accelerometer while the patient is in this position. This case, however, still requires knowledge of which arm (left or right) the monitor is worn on, as the chest accelerometer coordinate space can be rotated by 180 degrees depending on this orientation. A medical professional applying the monitor can enter this information using the GUI, described above. This potential for dual-arm attachment requires a set of two pre-determined vertical and normal vectors that are interchangeable depending on the monitor's location. Instead of manually entering this information, the arm on which the monitor is worn can be easily determined following attachment using measured values from the chest accelerometer values, with the assumption that $\vec{R}_{CV}$ is not orthogonal to the gravity vector.

The second step in the procedure is to identify the alignment of $\vec{R}_{CN}$ in the chest accelerometer coordinate space. The monitor determines this vector in the same way it determines $\vec{R}_{CV}$ using one of two approaches. In the first approach the monitor assumes a typical alignment of the chest-worn accelerometer on the patient. In the second approach, the patient is prompted to the alignment procedure and asked to assume a known position with respect to gravity. The monitor then calculates $\vec{R}_{CN}$ from the DC values of the time-dependent ACC waveform.

The third step in the procedure is to identify the alignment of $\vec{R}_{CH}$ in the chest accelerometer coordinate space. This vector is typically determined from the vector cross product of $\vec{R}_{CV}$ and $\vec{R}_{CN}$, or it can be assumed based on the typical alignment of the accelerometer on the patient, as described above.

A patient's posture is determined using the coordinate system described above and in FIG. **24**, along with a gravitational vector $\vec{R}_G$ **416** that extends normal from the patient's chest. The angle between $\vec{R}_{CV}$ and $\vec{R}_G$ is given by Eq. 7:

$$\theta_{VG}[n] = \arccos\left(\frac{\vec{R}_G[n]\cdot\vec{R}_{CV}}{\|\vec{R}_G[n]\|\|\vec{R}_{CV}\|}\right) \tag{7}$$

where the dot product of the two vectors is defined as:

$$\vec{R}_G[n]\cdot\vec{R}_{CV}=(y_{Cx}[n]\times r_{CVx})+(y_{Cy}[n]\times r_{CVy})+(y_{Cz}[n]\times r_{CVz}) \tag{8}$$

The definitions of the norms of $\vec{R}_G$ and $\vec{R}_{CV}$ are given by Eqs. 9 and 10:

$$\|\vec{R}_G[n]\|=\sqrt{(y_{Cx}[n])^2+(y_{Cy}[n])^2+(y_{Cz}[n])^2} \tag{9}$$

$$\|\vec{R}_{CV}\|=\sqrt{(r_{CVx})^2+(r_{CVy})^2+(r_{CVz})^2} \tag{10}$$

As indicated in Eq. 12, the monitor compares the vertical angle θ_{VG} to a threshold angle to determine whether the patient is vertical (i.e. standing upright) or lying down:

$$\text{if } \theta_{VG}\leq 45^\circ \text{ then Torso State=0, the patient is upright} \tag{11}$$

If the condition in Eq. 11 is met the patient is assumed to be upright, and their torso state, which is a numerical value equated to the patient's posture, is equal to 0. The patient is assumed to be lying down if $\theta_{VG}>45$ degrees. Their lying position is then determined from angles separating the two remaining vectors, as defined below.

The angle θ_{NG} between $\vec{R}_{CN}$ and $\vec{R}_G$ determines if the patient is lying in the supine position (chest up), prone position (chest down), or on their side. Based on either an assumed orientation or a patient-specific calibration procedure, as described above, the alignment of $\vec{R}_{CN}$ is given by Eq. 11, where i, j, k represent the unit vectors of the x, y, and z axes of the chest accelerometer coordinate space respectively:

$$\vec{R}_{CN}=r_{CNx}\hat{i}+r_{CNy}\hat{j}+r_{CNz}\hat{k} \tag{12}$$

The angle between $\vec{R}_{CN}$ and $\vec{R}_G$ determined from DC values extracted from the chest ACC waveform is given by Eq. 13:

$$\theta_{NG}[n] = \arccos\left(\frac{\vec{R}_G[n]\cdot\vec{R}_{CN}}{\|\vec{R}_G[n]\|\|\vec{R}_{CN}\|}\right) \tag{13}$$

The body-worn monitor determines the normal angle θ_{NG} and then compares it to a set of predetermined threshold angles to determine which position in which the patient is lying, as shown in Eq. 14:

$$\text{if } \theta_{NG}\leq 35^\circ \text{ then Torso State=1, the patient is supine}$$

$$\text{if } \theta_{NG}\geq 135^\circ \text{ then Torso State=2, the patient is prone} \tag{14}$$

If the conditions in Eq. 14 are not met then the patient is assumed to be lying on their side. Whether they are lying on their right or left side is determined from the angle calculated between the horizontal torso vector and measured gravitational vectors, as described above.

The alignment of $\vec{R}_{CH}$ is determined using either an assumed orientation, or from the vector cross-product of $\vec{R}_{CV}$ and $\vec{R}_{CN}$ as given by Eq. 15, where i, j, k represent the unit vectors of the x, y, and z axes of the accelerometer coordinate space respectively. Note that the orientation of the calculated vector is dependent on the order of the vectors in the operation. The order below defines the horizontal axis as positive towards the right side of the patient's body.

$$\vec{R}_{CH}=r_{CVx}\hat{i}+r_{CVy}\hat{j}+r_{CVz}\hat{k}=\vec{R}_{CV}\times\vec{R}_{CN} \tag{15}$$

The angle θ_{HG} between $\vec{R}_{CH}$ and $\vec{R}_G$ is determined using Eq. 16:

$$\theta_{HG}[n] = \arccos\left(\frac{\vec{R}_G[n]\cdot\vec{R}_{CH}}{\|\vec{R}_G[n]\|\|\vec{R}_{CH}\|}\right) \tag{16}$$

The monitor compares this angle to a set of predetermined threshold angles to determine if the patient is lying on their right or left side, as given by Eq. 17:

$$\text{if } \theta_{HG} \geq 90° \text{ then Torso State=3, the patient is on their right side}$$

$$\text{if } \theta_{NG} < 90° \text{ then Torso State=4, the patient is on their left side} \quad (17)$$

Table 1 describes each of the above-described postures, along with a corresponding numerical torso state used to render, e.g., a particular icon on a remote computer.

TABLE 2

postures and their corresponding torso states

Posture	Torso State
standing upright	0
supine: lying on back	1
prone: lying on chest	2
lying on right side	3
lying on left side	4
undetermined posture	5

Data shown in FIGS. **25**A, B were calculated using the above-mentioned approach. As the patient moves, the DC values of the ACC waveforms measured by the chest accelerometer vary accordingly, as shown in FIG. **25**A. The body-worn monitor processes these values as described above to continually determine $\vec{R}_G$ and the various quantized torso states for the patient, as shown in FIG. **25**B. The torso states yield the patient's posture as defined in Table 2. For this study the patient rapidly alternated between standing, lying on their back, chest, right side, and left side within a time period of about 160 seconds. Different alarm/alert conditions (e.g. threshold values) for vital signs can be assigned to each of these postures, or the specific posture itself may result in an alarm/alert. Additionally, the time-dependent properties of the graph can be analyzed (e.g. by counting changes in torso states) to determine, for example, how often the patient moves in their hospital bed. This number can then be equated to various metrics, such as a 'bed sore index' indicating a patient that is so stationary in their bed that lesions may result.

Alternate Embodiments

Other embodiments are within the scope of the invention. For example, the TBEV harness and its associated electrode can take on a variety of configurations. One of these is shown in FIG. **27**. Here, the TBEV harness **170** features a TBEV module **156** disposed directly on top of a single TBEV electrode **158**. The electrode **158** features four conductive regions (not shown in the figure): 1) a current source; 2) a current sink; and 3), 4) a pair of electrodes for measuring a voltage in the CB region. As described above, conductive regions for sourcing and draining the current are on an outer portion of the electrode **158**, while those for measuring voltage are on an inner portion of the electrode. Each conductive region connects to analog circuitry within the TBEV module **156** with a single connector (not shown in the figure). The TBEV module **156** also includes a CAN transceiver (not shown in the figure) that sends digitized waveforms and CO/SV values through a first cable **154** to a connector **152** which plugs into the back panel of the wrist worn transceiver, such as that shown in FIG. **10**. A second cable **160** connects to an ECG module **162**, which in turn connects through a short third cable **164** to a collection of ECG leads **166**. During a measurement, the ECG module **163** sends digitized versions of ECG waveforms, HR, and other information through the second cable **160** and to the TBEV module **156**. Data are sent according to the CAN protocol. From there, data are relayed with the module's internal CAN transceivers through the second cable **154** and to the connector **152**, which then passes the data onto the wrist transceiver.

FIG. **28** shows an alternate embodiment of the invention where TBEV **449** and ECG **420** modules are physically separated and connected through a wireless interface. Here, the ECG module **420** includes the ECG circuit, and attaches through cables **430***a-c* to ECG electrodes **424***a-c*. A second arm-worn module **449** includes four electrodes (two for injecting current; two for measuring voltage) dispersed on its upper and lower portions that connect to a central TBEV circuit to perform a measurement at the brachium as described above. Both the chest-worn module **420** and arm-worn module **449** include a unique Bluetooth transmitter that sends, respectively, ECG and TBEV waveforms to a paired Bluetooth transmitter **428** in the wrist-worn transceiver **426**.

FIG. **29** shows the arm-worn module **449** in more detail. As described above, it includes four electrodes **448***a-d* that snap on to the back surface of a flexible substrate **451** that holds an TBEV circuit **447**, located in the module's center in place. The electrodes **448***a-d* provide the current-injecting and voltage-measuring functions of the TBEV measurement as described above, and connect to the TBEV circuit **447** through a series of metal traces **453***a-d* embedded within the flexible substrate. The electrodes **448***a-d* also adhere to the patient's skin to hold the module **449** on the brachium. Once a TBEV waveform is measured, a Bluetooth transmitter **446** located at the bottom of the module sends it to the wrist-worn transceiver for processing, as described above.

FIGS. **30** and **31** show schematic drawings of an alternate embodiment of the invention, and indicate how data relating to SV/CP/CP can be wirelessly transmitted from the chest-worn sensor **500** and wrist-worn transceiver **506** to an external router (**517** *a* in FIG. **30**, **517** *b* in FIG. **31**), and from there to an external network (e.g. the Internet). Multiple strategies can be used for this data-transfer process, two of which are shown in the figures. In FIG. **30**, for example, the module **500** attaches through cables **510***a-c* to electrode patches **502** *a*, **502** *b*, and **504**. ICG and ECG waveforms are measured from analog signals collected by electrode patches **502** *a*, **502** *b*, **504**, and then wirelessly transmitted using Bluetooth module **501** from the chest-worn sensor **500** to the wrist-worn transceiver **506**, where they are received using Bluetooth module **508** and then analyzed as described above to determine SV/CO/CP, along with all other vital signs. The wrist-worn transceiver **506** additionally connects through a short cable **509** that carries only analog signals measured by a thumb-worn optical sensor **507**. These processed data are then sent from the transceiver **506** to the external router **517** *a* using Bluetooth, 802.11, or any other wireless protocol. Once the router **506** receives the data, it transmits it out using a wireless protocol (e.g. CDMA, GSM, iDEN) or wired protocol (e.g. Ethernet) to the external network. From there, for example, the data can be transferred to a hospital medical records systems, website, or sent through a web service to another application.

FIG. **31** shows an alternate approach where the external router **517***b* performs a higher degree of the computing load. In this case, the chest-worn sensor **500** processes analog signals measured by the electrode patches **502***a*, **502***b*, **504**

to determine ECG and ICG waveforms, and then wirelessly transmits these in a digital form to the router **517***b*. At around the same time, the wrist-worn transceiver measures SpO2 and PPG waveforms and wirelessly transmits these to the router **517***b*. There, an embedded processor analyzes ECG waveforms to determine HR; ECG and PPG waveforms to determine PAT and cNIBP; and ECG, ICG, PPG waveforms and PAT to determine SV/CO/CP. These data are then transmitted as described above to the external network, and from there to another system.

In addition to those methods described above, the body-worn monitor can use a number of additional methods to calculate blood pressure and other properties from the optical and electrical waveforms. These are described in the following co-pending patent applications, the contents of which are incorporated herein by reference: 1) CUFFLESS BLOOD-PRESSURE MONITOR AND ACCOMPANYING WIRELESS, INTERNET-BASED SYSTEM (U.S. Ser. No. 10/709,015; filed Apr. 7, 2004); 2) CUFFLESS SYSTEM FOR MEASURING BLOOD PRESSURE (U.S. Ser. No. 10/709,014; filed Apr. 7, 2004); 3) CUFFLESS BLOOD PRESSURE MONITOR AND ACCOMPANYING WEB SERVICES INTERFACE (U.S. Ser. No. 10/810,237; filed Mar. 26, 2004); 4) VITAL SIGN MONITOR FOR ATHLETIC APPLICATIONS (U.S. Ser. No.; filed Sep. 13, 2004); 5) CUFFLESS BLOOD PRESSURE MONITOR AND ACCOMPANYING WIRELESS MOBILE DEVICE (U.S. Ser. No. 10/967,511; filed Oct. 18, 2004); 6) BLOOD PRESSURE MONITORING DEVICE FEATURING A CALIBRATION-BASED ANALYSIS (U.S. Ser. No. 10/967,610; filed Oct. 18, 2004); 7) PERSONAL COMPUTER-BASED VITAL SIGN MONITOR (U.S. Ser. No. 10/906,342; filed Feb. 15, 2005); 8) PATCH SENSOR FOR MEASURING BLOOD PRESSURE WITHOUT A CUFF (U.S. Ser. No. 10/906,315; filed Feb. 14, 2005); 9) PATCH SENSOR FOR MEASURING VITAL SIGNS (U.S. Ser. No. 11/160,957; filed Jul. 18, 2005); 10) WIRELESS, INTERNET-BASED SYSTEM FOR MEASURING VITAL SIGNS FROM A PLURALITY OF PATIENTS IN A HOSPITAL OR MEDICAL CLINIC (U.S. Ser. No. 11/162,719; filed Sep. 9, 2005); 11) HAND-HELD MONITOR FOR MEASURING VITAL SIGNS (U.S. Ser. No. 11/162,742; filed Sep. 21, 2005); 12) CHEST STRAP FOR MEASURING VITAL SIGNS (U.S. Ser. No. 11/306,243; filed Dec. 20, 2005); 13) SYSTEM FOR MEASURING VITAL SIGNS USING AN OPTICAL MODULE FEATURING A GREEN LIGHT SOURCE (U.S. Ser. No. 11/307,375; filed Feb. 3, 2006); 14) BILATERAL DEVICE, SYSTEM AND METHOD FOR MONITORING VITAL SIGNS (U.S. Ser. No. 11/420,281; filed May 25, 2006); 15) SYSTEM FOR MEASURING VITAL SIGNS USING BILATERAL PULSE TRANSIT TIME (U.S. Ser. No. 11/420,652; filed May 26, 2006); 16) BLOOD PRESSURE MONITOR (U.S. Ser. No. 11/530,076; filed Sep. 8, 2006); 17) TWO-PART PATCH SENSOR FOR MONITORING VITAL SIGNS (U.S. Ser. No. 11/558,538; filed Nov. 10, 2006); and, 18) MONITOR FOR MEASURING VITAL SIGNS AND RENDERING VIDEO IMAGES (U.S. Ser. No. 11/682,177; filed Mar. 5, 2007).

Other embodiments are also within the scope of the invention. For example, other measurement techniques, such as conventional oscillometry measured during deflation, can be used to determine SYS for the above-described algorithms. Additionally, processing units and probes for measuring SpO2 similar to those described above can be modified and worn on other portions of the patient's body. For example, optical sensors with finger-ring configurations can be worn on fingers other than the thumb. Or they can be modified to attach to other conventional sites for measuring SpO2, such as the ear, forehead, and bridge of the nose. In these embodiments the processing unit can be worn in places other than the wrist, such as around the neck (and supported, e.g., by a lanyard) or on the patient's waist (supported, e.g., by a clip that attaches to the patient's belt). In still other embodiments the probe and processing unit are integrated into a single unit.

In other embodiments, a set of body-worn monitors can continuously monitor a group of patients, wherein each patient in the group wears a body-worn monitor similar to those described herein. Additionally, each body-worn monitor can be augmented with a location sensor. The location sensor includes a wireless component and a location-processing component that receives a signal from the wireless component and processes it to determine a physical location of the patient. A processing component (similar to that described above) determines from the time-dependent waveforms at least one vital sign, one motion parameter, and an alarm parameter calculated from the combination of this information. A wireless transceiver transmits the vital sign, motion parameter, location of the patient, and alarm parameter through a wireless system. A remote computer system featuring a display and an interface to the wireless system receives the information and displays it on a user interface for each patient in the group.

In embodiments, the interface rendered on the display at the central nursing station features a field that displays a map corresponding to an area with multiple sections. Each section corresponds to the location of the patient and includes, e.g., the patient's vital signs, motion parameter, and alarm parameter. For example, the field can display a map corresponding to an area of a hospital (e.g. a hospital bay or emergency room), with each section corresponding to a specific bed, chair, or general location in the area. Typically the display renders graphical icons corresponding to the motion and alarm parameters for each patient in the group. In other embodiments, the body-worn monitor includes a graphical display that renders these parameters directly on the patient.

Typically the location sensor and the wireless transceiver operate on a common wireless system, e.g. a wireless system based on 802.11 (i.e. 'WiFi'), 802.15.4 (i.e. 'Bluetooth'), or cellular (e.g. CDMA, GSM) protocols. In this case, a location is determined by processing the wireless signal with one or more algorithms known in the art. These include, for example, triangulating signals received from at least three different base stations, or simply estimating a location based on signal strength and proximity to a particular base station. In still other embodiments the location sensor includes a conventional global positioning system (GPS) that processes signals from orbiting satellites to determine patient's position.

The body-worn monitor can include a first voice interface, and the remote computer can include a second voice interface that integrates with the first voice interface. The location sensor, wireless transceiver, and first and second voice interfaces can all operate on a common wireless system, such as one of the above-described systems based on 802.11 or cellular protocols. The remote computer, for example, can be a monitor that is essentially identical to the monitor worn by the patient, and can be carried or worn by a medical professional. In this case the monitor associated with the medical professional features a GUI wherein the user can select to display information (e.g. vital signs, location, and alarms) corresponding to a particular patient. This monitor

can also include a voice interface so the medical professional can communicate directly with the patient.

Still other embodiments are within the scope of the following claims.

What is claimed is:

1. A method for determining stroke volume from a patient, comprising:

(a) measuring a motion waveform with a first motion sensor;

(b) processing the motion waveform with a motion algorithm to determine a motion-related parameter;

(c) comparing the motion-related parameter to a predetermined threshold parameter to determine if the patient's motion exceeds an acceptable level;

(d) measuring a transbrachial electro-velocimetry (TBEV) impedance waveform from the patient with an impedance sensor if the patient's motion does not exceed an acceptable level; and

(e) calculating a stroke volume value from the impedance waveform if the patient's motion does not exceed an acceptable level.

2. A method for determining stroke volume from a patient, comprising:

(a) measuring a motion waveform with a first motion sensor;

(b) processing the motion waveform with a motion algorithm to determine a motion-related parameter;

(c) comparing the motion-related parameter to a predetermined threshold parameter to determine if the patient's motion exceeds an acceptable level;

(d) measuring a transbrachial electro-velocimetry (TBEV) impedance waveform from the patient with an impedance sensor;

(e) calculating a stroke volume value from the impedance waveform; and

(f) reporting the stroke volume value if the patient's motion does not exceed an acceptable level.

3. A method for generating an alarm from a stroke volume value calculated from a patient, comprising:

(a) measuring a motion waveform with a first motion sensor;

(b) processing the motion waveform with a motion algorithm to determine a motion-related parameter;

(c) comparing the motion-related parameter to a predetermined threshold parameter to determine if the patient's motion exceeds an acceptable level;

(d) measuring a transbrachial electro-velocimetry (TBEV) impedance waveform from the patient with an impedance sensor;

(e) calculating a stroke volume value from the impedance waveform; and

(f) generating the alarm based on the stroke volume value if the patient's motion does not exceed an acceptable level.

4. A method for determining stroke volume from a patient, comprising:

(a) measuring a motion waveform with a first motion sensor;

(b) processing the motion waveform with a motion algorithm to determine a motion-related parameter;

(c) processing the motion-related parameter to determine the patient's posture;

(d) measuring a transbrachial electro-velocimetry (TBEV) impedance waveform from the patient with an impedance sensor;

(e) calculating a stroke volume value from the impedance waveform and the patient's posture.

5. A method for generating an alarm from a stroke volume value calculated from a patient, comprising:

(a) measuring a motion waveform with a first motion sensor;

(b) processing the motion waveform with a motion algorithm to determine a motion-related parameter;

(c) processing the motion-related parameter with an algorithm to determine the patient's posture;

(d) measuring a transbrachial electro-velocimetry (TBEV) impedance waveform from the patient with an impedance sensor;

(e) calculating a stroke volume value from the impedance waveform; and

(f) generating the alarm based on the stroke volume value and the patient's posture.

6. The method of claim **1**, wherein the first motion sensor is an accelerometer.

7. The method of claim **6**, wherein the first motion sensor is a three-axis accelerometer.

8. The method of claim **1**, where the first motion sensor and the impedance sensor are disposed on a common substrate.

9. The method of claim **8**, wherein the common substrate is attached to the patient's clavicle/brachial (CB) region.

10. The method of claim **1**, wherein the first motion sensor is disposed on a first sensor module, and the impedance sensor is disposed on a second sensor module.

11. The method of claim **10**, wherein the first sensor module is configured to attach to the patient's chest, and the second sensor module is configured to attach to the patient's CB region.

12. The method of claim **10**, wherein the first sensor module is configured to attach to the patient's wrist, and the second sensor module is configured to attach to the patient's CB region.

13. The method of claim **1**, wherein the motion-related parameter is a magnitude of motion.

14. The method of claim **1**, wherein the motion-related parameter is a frequency of motion.

15. The method of claim **1**, wherein the motion-related parameter is a specific type of motion.

16. The method of claim **15**, wherein the specific type of motion is one of walking, running, lying down, and being motionless.

17. The method of claim **1**, wherein the motion-related parameter is a posture.

18. The method of claim **17**, wherein the posture is one of standing up, sitting down, lying down, lying down on the right side, and lying down on the left side.

19. The method of claim **1**, wherein the impedance sensor is not powered on until after the comparing step.

20. The method of claim **1**, wherein the impedance sensor is only partially powered on until after the comparing step.

21. The method of claim **1**, wherein the impedance sensor is powered on after the comparing step indicates that the patient's motion does not exceed an acceptable level.

* * * * *